



Bond strength of cementitious screeds on concrete bearing floors

Master of Science Thesis
M. van Dooren



Bond strength of cementitious screeds on concrete bearing floors

Master of Science Thesis

By

Maikel van Dooren
October 16, 2017

For the degree of Master of Science in Structural Engineering at Delft University of Technology
to be defended publicly on Tuesday October 24, 2017 at 04:00 PM.

Faculty of Civil Engineering and Geosciences – Delft University of Technology

Author: Maikel van Dooren
Student number: 4399617
E-mail: maikel_dooren@live.nl

Graduation Committee:

Prof. dr. ir. D. A. Hordijk	Delft University of Technology
Dr. ir. drs. C.R. Braam,	Delft University of Technology
Dr. ir. B. Savija	Delft University of Technology
Ir. C.A.J. Sterken	BAM Advies & Engineering



What's nice about concrete is that it looks unfinished.
Zaha hadid

Abstract

In this study the cracking and debonding behaviour of cementitious screeds bonded to concrete bearing floors is analysed. In order to obtain insight in this behaviour research is performed to the surface tensile strength of concrete, the bond strength of screeds on concrete bearing floors, the behaviour of screeds during shrinkage and the methods to determine the bond strength. This research is carried out by a theoretical study in which the screed shrinkage behaviour as well as the screed / concrete behaviour during testing of the bond strength is analysed by means of analytical and FEM studies. Besides this practical experiments are performed to obtain insight in the influence of different parameters on the surface tensile strength of concrete / the bond strength of screeds on concrete bearing floors. Furthermore practical experiments are executed to study the influence of different parameters on the outcome of a preferred bond strength testing method.

Cracking of screeds occurs when stresses in the screed have reached the tensile strength of the material. Stresses in screeds are in most cases induced by imposed deformations (due to shrinkage, temperature deformations or moisture changes) which arise as a result of restraint in movement of the screeds. The stresses are influenced by the amount of strain difference between the screed and bearing floor. The most relevant stresses that arise in the screed are horizontal tensile stresses (σ_{xx}). These stresses are zero at the edge of a floor and increase to its maximum at increasing distance from the edge. When the amount of shrinkage becomes that high that the tensile strength of the screed is reached cracks will occur in the screed. In the case of a crack a new 'edge' situation is formed, where the horizontal stress increases from zero to its maximum value at increasing difference from the crack.

Debonding of screeds occurs when the stresses at the bonding interface have reached the bond strength. Stresses at the interface are caused by strain differences between the screed and bearing floor and exist of vertical (σ_{yy}) and shear (τ_{xy}) interface stresses. The vertical and shear interface stresses that arise due to strain differences are maximal at the edge of a floor field, decreasing to zero at increasing distance from the edge. In the case a crack is formed the stresses are again maximal at the location of the crack and decrease to zero at increasing distance from the edge.

The main influencer of strain differences is screed shrinkage. In the case that for the hydration shrinkage of cementitious screeds a value can be assumed equally to concrete, the shrinkage is $\epsilon_{s,max} = 0.3\%$. According to the FEM study this shrinkage results in a cracked screed (with properties equal to C20/25 concrete, thickness 50 mm), with maximal values for the interface stresses of $\sigma_{yy} = \pm 1.8 \text{ N/mm}^2$ and $\tau_{xy} = \pm 1.3 \text{ N/mm}^2$ were obtained. The stresses increase if a higher screed height is applied or if the screed concrete class is increased.

The bond between screed and bearing floor is based on a combination of Van der Waals forces and mechanical interlocking. Van der Waals forces are electromagnetic forces that work between two molecules and can be positively influenced by decreasing the distance between molecules. In practice this means that liquid mixtures for screeds will obtain stronger Van der Waals forces than earth dry mixtures. Mechanical interlocking contains a mechanical anchorage that is created by mortar that covers the roughness of the substrate. The contact surface is essential in creating a good bond. The bigger the contact area, the bigger the potential of creating a good bond. Interlocking can be improved by improving the surface roughness and improving the absorption capacity of the substrate, however caution is required with improving the absorption of the substrate. Too large absorption can extract moisture from the adhesive interface, resulting in a lower screed quality at the interface.

Factors that influence the adhesion of screeds to concrete bearing floors concerning the concrete surface are surface cleanliness, laitance, surface moisture, surface roughness and substrate porosity. Factors concerning the overlay include the application of a bonding agent, overlay compaction and overlay curing.

In practical experiments the influence of roughening treatments on the substrate surface tensile strength and the bond strength is studied. From these experiments it is concluded that the order of mean surface tensile strength of the concrete substrate per surface treatment is: 'no treatment (0.68 N/mm^2)' - 'milling (0.98 N/mm^2)' - 'sanding (1.30 N/mm^2)' - 'grit blasting (1.57 N/mm^2)'. In the standards for screeds the requirement is drafted that the substrate surface tensile strength must be at least 1.5 N/mm^2 to provide a good bond between screed and substrate. Grit blasting is the only method with which a mean value of at least 1.5 N/mm^2 is achieved. Yet some of the results were still below 1.5 N/mm^2 so this method does not ensure the surface tensile strength to be minimal 1.5 N/mm^2 at every location.

Provided with a liquid cementitious layer the order of mean bond strength per surface treatment is: 'no treatment (0.94 N/mm^2)' - 'sanding (1.14 N/mm^2)' - 'milling (1.29 N/mm^2)'. No valid results were found for the bond strength of the grit blasted situation. In no situation a mean bond strength was measured above 1.29 N/mm^2 . For a screed with properties equal to C20/25 concrete and thickness 50 mm it was given that a strain of 0.3% leads to a maximal interface stress of $\sigma_{yy} = \pm 1.8 \text{ N/mm}^2$. This indicates that none of the situations would be strong enough to prevent debonding.

The best applicable test to determine the bond strength of screeds bonded to concrete bearing floors till so far is the Pull-Off test, mostly due to its possibility to perform the test in situ. However this method is found to be very sensitive to give results that do not represent the actual surface tensile / bond strength. When applying this method it is of importance that a minimum depth for a drilled core of 15 mm is applied and the diameter of the dolly is minimal 50 mm. Furthermore the test should be carried out with good accuracy, as small eccentricities induced by diagonal drilling, partly gluing of the dollies or diagonal loading can directly influence the outcome of the tests to be lower than in the case of a perfectly performed test.

Preface

This report presents the results of the thesis project 'Bond strength of cementitious screeds on concrete bearing floors' which was carried out as part of the fulfillment for the Master of Science degree in Structural Engineering at Delft University of Technology. The study was conducted commissioned by and the majority of this report was written at BAM Advies & Engineering in Bunnik.

In the summer of 2016 I have been working part time as Structural Engineer at BAM. During work I heard one of the employees talking on the phone about problems concerning cracking and debonding of screeds at a project in Rotterdam. As this was a problem where no direct solution could be found for it aroused my interest, with the fact in my mind that I had to start writing a thesis within half a year. After several conversations with multiple BAM and TU employees I started the working on the thesis project in February 2017. Now, eight months later, I present the results of this study.

I would like to thank my supervisor at BAM, Rene Sterken and colleagues with in specific Jaap Cederhout and Jan de Goede, for helping me to think about practical problems about the thesis subject and providing me with information and helping me to get in contact with the right persons to obtain information from.

Furthermore I would like to thank my supervisors from TU Delft, Professor Dick Hordijk, Dr. René Braam and Dr. Branko Savija for supporting me throughout the process and providing me with space in the TU Delft Stevinlab to perform the experiments for this thesis.

Also, I would like to thank Jan and Herbert Nieuwenhuis from Nieuwenhuis Stofvrij Stralen B.V. for assisting me with preparing the specimen for the experiments, executing the surface treatments and providing space to perform all this. And finally I would like to thank Ivo Verheijen from NEWA for lending me the Pull-Off testing device.

I have experienced the last period as very educational and because of the combination of a theoretical combined with a practical approach to the problem of this study it was very interesting to be busy with the project until the last day. I hope that I can provide you with interesting information through this report. If questions have arisen during reading of the report it is always possible to contact me by mail.

Bunnik, October 16, 2017
Maikel van Dooren

Table of Contents

1.	Introduction.....	7
1.1	Background.....	7
1.2	Aim.....	8
1.3	Outline of contents	8
2.	Characteristics of screeds	9
2.1	Introduction.....	9
2.2	Classification	9
2.3	Cracking in cementitious screeds	10
2.4	Loading on screeds.....	12
2.5	Debonding of screeds	12
2.6	Curling.....	15
2.7	Requirements in the standards.....	15
2.8	Review.....	16
3.	Concrete to concrete bond.....	17
3.1	Introduction.....	17
3.2	Van der Waals forces	17
3.3	Mechanical interlocking	17
3.4	Factors influencing bond	18
3.5	Requirements on the bond strength.....	20
3.6	Review.....	20
4.	Bond strength testing methods	21
4.1	Introduction.....	21
4.2	General classification.....	21
4.3	Tensile bond tests	21
4.4	Shear bond tests	22
4.5	Compressive-shear bond tests	23
4.6	Review.....	24
5.	Modelling of the pull-off test method.....	25
5.1	Introduction.....	25
5.2	Analytical approach	25
5.3	FEM approach.....	31
5.4	Review.....	39
6.	Modelling of shrinkage effects in screeds	41
6.1	Introduction.....	41
6.2	Analytical approach	41
6.3	FEM approach.....	45
6.4	Review.....	53
7.	Practical experiments	55
7.1	Introduction.....	55
7.2	Pull-Off testing method experiments	55
7.3	Bond experiments.....	61
7.4	Review.....	65
8.	Conclusions and recommendations.....	67
8.1	Conclusions	67
8.2	Discussion.....	69
8.3	Recommendations	69
	Lists of figures and tables	71
	References	73
	Appendix.....	75
A.1	Background information.....	75
A.2	Tables	77
A.3	Calculations.....	79

1. Introduction

1.1 Background

During the construction of the Erasmus MC in Rotterdam in 2014-2015 Bouwcombinatie Erasmus MC¹ has fabricated terrazzo screeds on structural concrete floors. After curing and finishing the terrazzo appeared to be fractured at various locations. By knocking on the floor it could furthermore be observed that the top layer of the terrazzo was debonded from the layer below for big parts of the surface².

As cracks were visible at the floor surface this indicated that stresses had been arisen in the floor in the period between casting and finishing that were higher than the strength of the terrazzo material at that specific moment. Furthermore the debonded floor parts indicate that stresses at the bonding interface had reached the bond strength that was developed at that specific moment.

In the construction specifications of this project it was prescribed that the bond strength between the top and lower layer terrazzo had to reach a minimum value of $1,5 \text{ N/mm}^2$. To achieve bond strength with this value it was of importance that the surface tensile strength was at least as high as the required bond strength. After observing the loose floor parts Bouwcombinatie Erasmus MC instructed Technoconsult to perform tests on unfinished construction floors in the Erasmus MC to determine the surface tensile strength [1]. In total 19 pull-off tests were executed with an automatic motorized Pull-Off bond strength tester (Figure 1- Figure 3), where values were found varying between $0,26 - 1,05 \text{ N/mm}^2$. The mean value of the test appeared to be $0,52 \text{ N/mm}^2$, less than 35% of the requirement prescribed in the construction specifications.



Figure 1: the automatic motorized Pull-Off bond strength tester [2]



Figure 2: fracture surface after executing the Pull-Off test [2]



Figure 3: fracture surface on the substrate [2]

Because of the negative results of the research described above several Pull-Off tests were executed on behalf of BAM on in-situ casted concrete floors at projects in Utrecht, Amsterdam and The Hague [2]. From these tests it was concluded that the surface tensile strength of concrete floors in Utrecht and Amsterdam with strength class C28/35 had values of $0,16 - 0,47 \text{ N/mm}^2$. At a concrete floor with strength class C30/37 in The Hague a value of $1,11 \text{ N/mm}^2$ was measured.

In none of the above mentioned situations the requirement of $1,5 \text{ N/mm}^2$ for the surface tensile strength was achieved. From this point the question arose on what basis this requirement was drafted and how this requirement could have been fulfilled.

The tests that were performed to determine the surface tensile strength were Pull-Off tests that were performed by gluing a steel dolly to the surface which was then pulled off the surface with an automatic motorized Pull-Off tester. In the regulations for Pull-Off testing [3] [4] one of the requirements is drafted that a hollow core has to be drilled in the concrete around the dolly, before the Pull-Off test is performed. This indicates that the performed tests did not meet the requirements of the regulations.

In [5] Hordijk described among others a research to the validity of tests where the purely tensional strength of concrete specimen was measured. From this research it was concluded that eccentricities during testing (due to eccentric applying of the forces/ irregularities in the materials) can seriously influence the results of the tensional tests. The Pull-Off test is a method that belongs to these tests.

In conclusion, the tests that were performed to measure the surface tensile strength of the substrates did not meet the requirements drafted in the regulations and in general the validity of tensional tests is questioned. Hence, the results of the previously performed tests are doubted.

¹ Bouwcombinatie Erasmus MC is a partnership between BAM Utiliteitsbouw and Ballast Nedam Bouw Speciale Projecten

² A more detailed explanation of the debonding and cracking at the Erasmus MC is given in Appendix A.1.1

1.2 Aim

The main objective of this study was to improve the knowledge about the causes and mechanism of cracking (Figure 4) and debonding (Figure 5) and the formation of the bond of cementitious screeds casted on structural concrete floors. For that reason the aim was to indicate the causes of the development of stresses in the screed and at the interface. Furthermore the behaviour of screeds in different stress situations had to be studied. As this behaviour is influenced by the strength properties of the bond between screed and bearing floor insight had to be obtained in the formation and the influencing factors of the bond strength.

Since the results of the test method that was named in the background of this research (section 1.1) were distrusted a substantial part of this research was related to the method to determine the concrete surface tensile strength (Figure 6) / concrete to concrete bond strength (Figure 7). The objective was to prescribe a method with which the appropriate results could be obtained. In this way the formation and influencing factors of the bond strength could be analysed in the correct way.

Concluding, the aim of the study was to:

Obtain insight in the cracking and debonding behaviour of screed and provide a guideline which describes in what way the properties of bonded screeds can be controlled and which requirements must be met to control debonding/cracking of screeds.

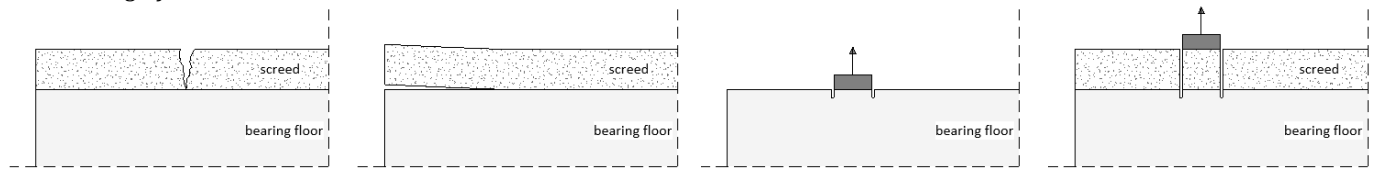


Figure 4: screed cracking

Figure 5: screed debonding

Figure 6: surface tensile strength testing

Figure 7: tensile bond strength testing

1.3 Outline of contents

The design of the research consisted of three parts. The first part of the research included a literature study (chapter 2 - 4), the second part existed of an analytical study (chapter 5 - 6) and the third part contained a practical experiment (chapter 7). An outline of contents covered in this report is given below.

In chapter 2 basic characteristics of screeds are discussed, containing information about the different classifications of screeds, the onset of cracking in cementitious screeds and debonding. Furthermore the consequences of debonding of screeds are clarified in this chapter and the requirements given in the standards are considered.

Chapter 3 contains information about the bonding of two layers of concrete, where besides the mechanisms causing adhesion also factor influencing the bond strength are explicated.

The methods to measure the bond strength of two layers of concrete are enlightened in chapter 4. Different methods are compared in this chapter, whereafter a statement is made which method is the best applicable to determine the bond strength of screeds on concrete floors.

In chapter 5 a parametric study is discussed where the influence of eccentricities on the results of Pull-Off tests is investigated. The outline of this study consisted of an analytical as well as an FEM approach.

The behaviour of bonded screeds during shrinkage is studied by means of an analytical and a FEM approach. A prescription of the study together with the results is discussed in chapter 6.

In addition to the theoretical researches that are discussed in chapter 5 - 6 practical experiments were performed. The first experiments that were carried out compose a research to the influence of different practical parameters to the results of Pull-Off tests. The second experiments were executed to obtain insight in the influence of substrate roughening treatments on the substrate surface tensile strength and the bond strength of screeds on concrete floors. An analysis of the results of both experiments is included in chapter 7.

The conclusions, discussion and recommendations of this study are presented in chapter 8.

2.Characteristics of screeds

2.1 Introduction

In housing as well as commercial or industrial buildings screeds are cast on top of structural bearing floors. Screeds are casted to fulfil multiple purposes, containing smoothening and levelling of a floor surface, serving as a bearing layer for a later to apply finishing layer, it can be used to apply underfloor heating or it can serve as a finishing layer by itself. In this chapter the characteristics of screeds are discussed in detail.

In section 2.2 a classification is given in which screeds are classified. Subsequently the subject cracking of screeds is discussed in section 2.3, including the causes and consequences of cracking. Different types of loading on screeds are considered in section 2.4 and the causes and consequences of debonding of screeds from the structural floors are clarified in section 2.5. In section 2.6 a typical screed damage is exposed, the requirements in the standards are discussed in section 2.7 and finally a review of this chapter is incorporated in section 2.8.

2.2 Classification

In the introduction different purposes of screeds are illustrated. From this can be concluded that screeds do not serve as structural elements. In [6] screeds are classified on the basis of different factors:

- the bonder type: cement, calcium sulphate, resin, bitumen/ asphalt or magnesite;
- the detailing:
 - o bonded to the bearing floor, with or without floor heating (Figure 8);
 - o unbonded on a separation layer, with or without floor heating (Figure 9);
 - o floating on a compressive insulation layer, with or without floor heating (Figure 10 & Figure 11);
- the execution method: liquid self-levelling screeds or earth dry hand-levelled screeds;
- the layer structure: single layered (Figure 8 - Figure 11) or multiple layered (Figure 12 & Figure 13).

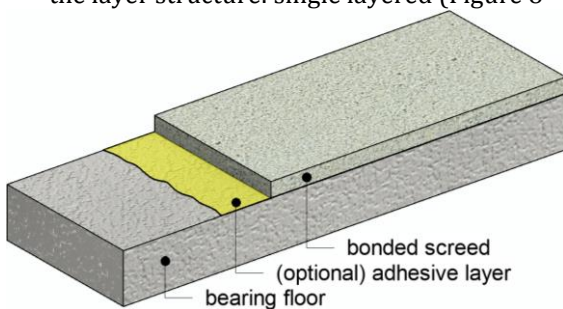


Figure 8: bonded screed

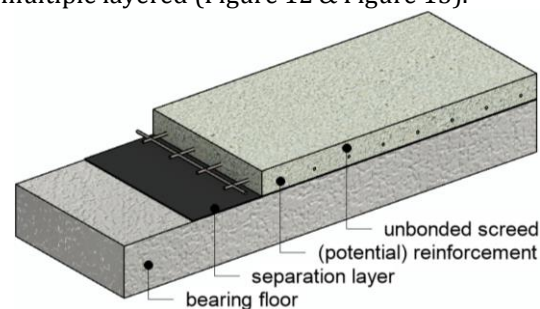


Figure 9: unbonded screed on a separation layer

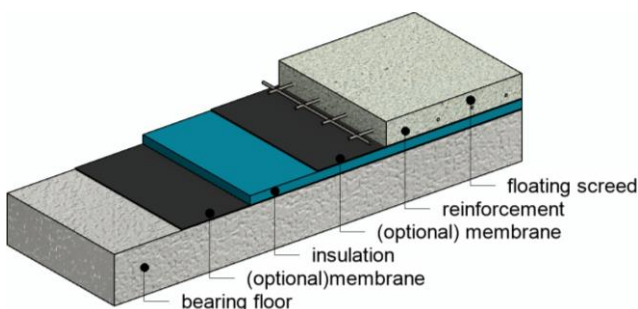


Figure 10: floating screed on an insulation layer

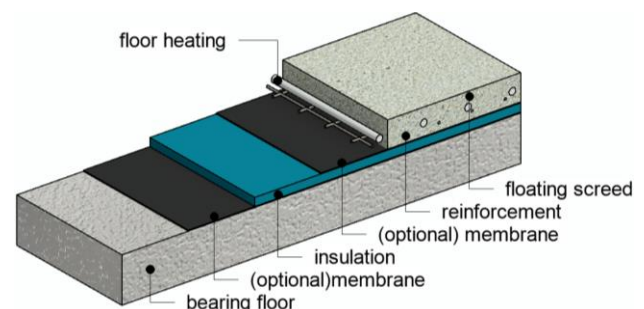


Figure 11: floating screed with floor heating

The types of screeds investigated in this research are cementitious screeds. Screeds manufactured from other binding materials were not regarded. Cementitious screeds are built up of mixtures existing of cement, water, aggregates (e.g. sand, fine gravel, cork or other light aggregates) and fillers and additives that influence the properties of the (hardened) mortar. Depending on the ratio between the previously mentioned materials a liquid mortar can be fabricated which can be used to pour a self-levelling screed or an earth dry mortar can be fabricated that has to be levelled on the site by hand.

Bonding of screeds to concrete bearing floors was a central subject in the research. The focus of the discussions in this report is therefore on bonded screeds with and without the application of an adhesive layer.

In this report distinction is made between single layered and multiple layered screeds (terrazzo). The main difference between the two types - besides the amount of layers - is that the multiple layered screeds function as finishing layer, whereas the single layered screeds mostly will be finished with a finishing layer such as carpet, laminate etc.. Both types are discussed in this report.

Terrazzo floors

Terrazzo floors are multiple layered screeds existing of two layers. The first layer is called the intermediate layer and is applied on the bearing floor with (Figure 12) or without bonding (Figure 13). The mortar that is used for this intermediate layer is equal to the mortar that is used for single layered screeds. The intermediate layer can be provided with shrinkage reinforcement and/ or floor heating. On this layer a top layer is casted bonded to the intermediate layer which serves as finishing layer. The mortar that is used for the top layer is a cementitious mortar that can be provided with aggregates and by finishing the surface by making use of sanding/ sweetening/ polishing/ impregnating/ crystallizing the functional/ esthetical requirements are achieved.

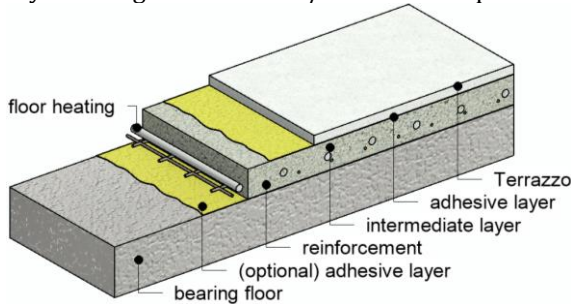


Figure 12: bonded Terrazzo

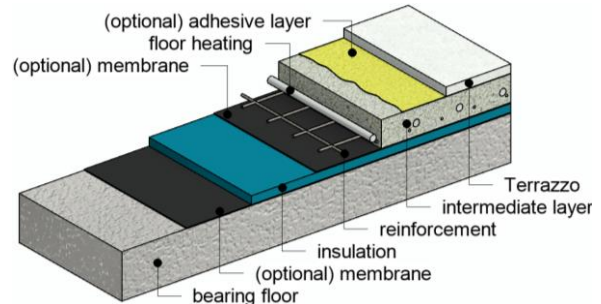


Figure 13: floating Terrazzo on an insulation layer

2.3 Cracking in cementitious screeds

2.3.1 Concrete tensile strength

Screeds manufactured from a cementitious material (concrete) have a tensile strength which is relatively low compared to the compressive strength (Figure 14). When stresses in concrete reach the tensile strength cracks will appear in the structure. This also applies to cementitious screeds. In this section the different mechanisms causing stresses in screeds are discussed, starting with stresses caused by restrained imposed deformations and ending with stresses induced by loading on screeds.

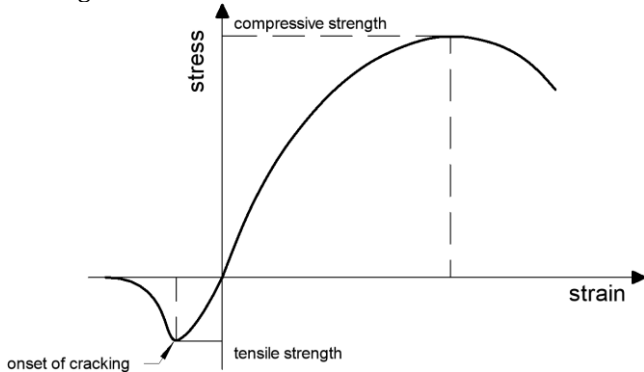


Figure 14: stress-strain diagram concrete

2.3.2 Restrained imposed deformations

The main cause of stresses in screeds is stress caused by imposed deformations. When a cementitious screed is caused to shorten or extend - as a result of for example temperature changes - but the screed is restrained to deform stresses will appear in the screed. This phenomenon is called imposed deformation.

Restriction in deformation of screeds

An example for restriction of screeds is when the screed is applied bonded to the bearing floor. This is explained by means of Figure 15. In the left figure the screed is casted on the bearing floor after applying a foil on the bearing floor. This foil causes the screed not to bond with the bearing floor. When the screed is caused to shorten no restrictions are present, so the screed is free to deform. In the figure on the right the screed is casted directly on the bearing floor, where a bond is created between the screed and the bearing floor. The bond between the bearing floor and the screed makes a restriction for the screed to move. When the screed is now caused to shorten this is not possible and so tensile stresses will appear in the screed. The more the screed is caused to shorten the bigger the tensile stresses will become. When the tensile strength of the cementitious screed is reached cracks will appear.

Another phenomenon that can cause stresses in concrete is the so called 'eigentemperature'. When the top of a screed is heated a distribution of temperatures will arise in the floor. This temperature distribution is usually not linear, causing a distribution of temperatures existing of a mean temperature, linear temperature distribution and an eigentemperature distribution in the structure (Figure 16). The temperature changes are converted to stresses by multiplying the temperature change with the CTE value of the material (see section 2.5.2). Typical to this kind of

stresses is that the eigenstresses are always balanced in a section. When reaching the tensile strength the eigenstresses can cause cracking in screeds.

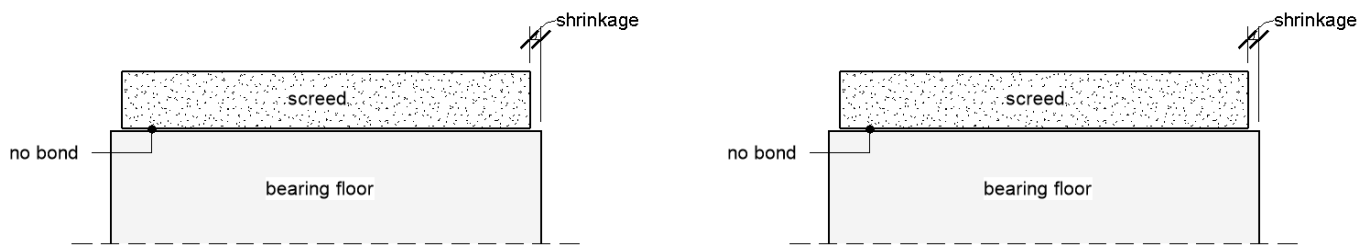


Figure 15: cementitious screed casted on a concrete bearing floor

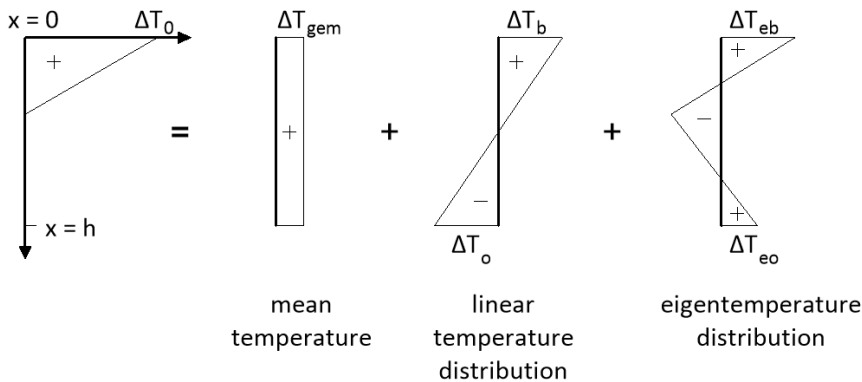


Figure 16: local heating can cause eigenstresses in sections

Actions causing imposed deformations

Temperature load

Concrete has the property to shrink when the temperature drops and expand when the temperature increases. Temperature changes may arise as a result of development of hydration heat in hardening concrete, climate influences, processes (e.g. industrial processes of storage of warm/ hot cargo) or calamities like fire. The change of strain in the concrete due to a temperature change is dependent on the linear expansion coefficient. The relation is given in formula (1). The linear expansion coefficients of rock-like materials are given in Appendix Table 29.

$$\Delta\varepsilon = \Delta T * \alpha_c \tag{1}$$

Where:

- $\Delta\varepsilon$ is the change in concrete strain;
- ΔT is the change in temperature (K);
- α_c is the linear expansion coefficient (K⁻¹)

Concrete shrinkage and swelling

Shrinkage in concrete occurs in the hardening stage of the mixture as well as in the hardened stage. In Table 1 four types of concrete shrinkage are described. Swelling of hardened concrete can occur when a relatively dry concrete is saturated with water completely. However, swelling of hardened concrete is hardly taken into account in design calculations, while the deformations caused by swelling are significantly smaller than shrinkage deformations. In [7] it is given that swelling deformations are about 6 – 8 times smaller the deformations caused by shrinkage.

Table 1: four types of concrete shrinkage

Type	Description	Mixture stage
Plastic shrinkage	Evaporation of water from the surface of the concrete	Hardening stage
Chemical shrinkage	The volume of the reaction product of water and cement is smaller than the individual volume of the materials, causing the mixture to shrink while reacting.	Hardening stage
Autogenous shrinkage	At low w/c ratios the water in the mixture is rapidly drawn into the hydration process, causing surface tension within the capillary pores which leads to shrinkage.	Hardening stage
Drying shrinkage	An exchange of moisture with the environment causes a reduction of the relative humidity and an increase of capillary forces in the pore water. This causes the concrete to contract.	Hardened stage

2.4 Loading on screeds

Besides imposed deformations applying loads on screeds will cause stresses as well. When applied on a screed bonded to a bearing floor the stresses will mostly be compressive stresses which will not cause cracks in the concrete. When applied without bond on a bearing floor bending stresses can occur in the screed, which can get rather high when the screed is supported by a soft layer like insulation (Figure 17). For this reason the minimal thickness of floating screeds given in the standards (see section 2.6) is bigger than screeds casted directly on bearing floors.

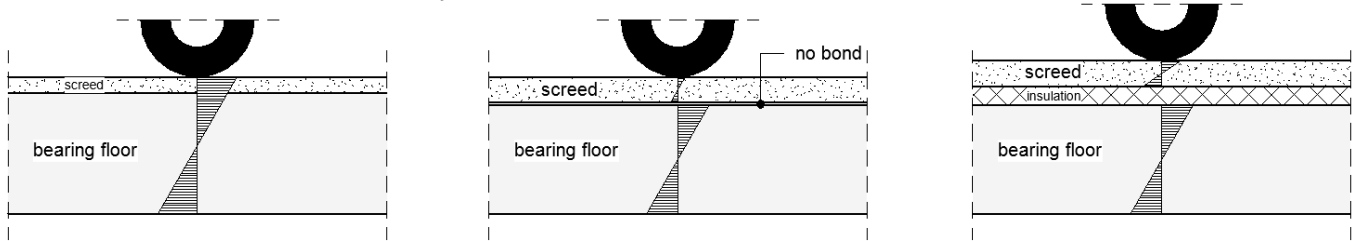


Figure 17: difference in stress distribution in screed applied with bond, without bond and on an insulation layer

2.5 Debonding of screeds

2.5.1 Bond strength

When stresses in the adhesive surface between two concrete layers the bond strength debonding will occur. Debonding can appear at several locations in the structure. In appendix A.1.2 a summary is given of the different places where debonding could occur in a multiple layered concrete floor and the corresponding tensile strength.

Several sources can cause stresses in the adhesive surface. In the next subsection these causes are further defined. Subsequently the stress distribution in the adhesive layer is discussed in subsection 2.4.3. The development of the bond strength is evaluated in the next chapter.

2.5.2 Stresses in the adhesive surface

Stresses in the adhesive surface are results of strain differences between the substrate and screed. These strain differences can arise due to shrinkage differences, temperature expansion/ moisture changes, differences in stiffness and deflection.

Shrinkage differences

Shrinkage differences are a result of drying of a new material that is cast on an already developed subsurface. This drying shrinkage correlates with the hydration of the product. In [6] it is stated that the drying of cementitious screeds has a higher speed than concrete because of its open structure. The magnitude of shrinkage is dependent on the thickness of the floor, the density of the material and the drying conditions such as heat and relative humidity. An indication for the hydration shrinkage (ϵ_s) of different building materials is given in Table 2. In the case that for the hydration shrinkage of cementitious screeds a value can be assumed equally to concrete, the shrinkage is $\epsilon_{s,max} = 0.3\%$.

Strain differences due to temperature expansion/ moisture changes

Because of temperature and moisture changes porous materials will expand/ shorten. Temperature changes play a dominant role in the expansion/ shortening of concrete. The amount of deformation of the material is determined by the Coefficient of Thermal Expansion (CTE) and the temperature change relative to the mean temperature. At screeds thermal changes play an important role in case of the application of underfloor heating. The CTE values of different building materials as well as an indication for the strain caused by moisture absorption (ϵ_h) are included in Table 2.

Stiffness differences

A material that has a high stiffness will attract at an equal deformation more stress than a material with a low stiffness. When materials with a different stiffness are applied and the surface is connected this can lead to high stresses in the adhesive surface.

Deflection

At the deflection of a floor consisting of multiple layers that span a room the lower part of the floor will be on tension, while the upper part will be on compression. This leads to shear stresses at the interface of the different layers (Figure 18). The permissible deflections according to the Dutch building codes are quite large ($0,004 * \text{span}$), what makes that the shear stresses can become rather high.

Product	CTE ($10^{-6}/^{\circ}\text{C}$)	ε_s (‰)	ε_h (‰)
Concrete ($\rho \pm 2300 \text{ kg/m}^3$)	12	0.3	0.2-1.0
Light concrete	6-12	(*)	(*)
Anhydrite	10	0 - 0.02	(*)
Bonding agents	30-80	4 - 20	(*)
Steel	12	-	-
Aluminium	24	-	-
Copper	20	-	-
	(*) no data available		

Table 2: hydrothermal deformations of building materials [8]

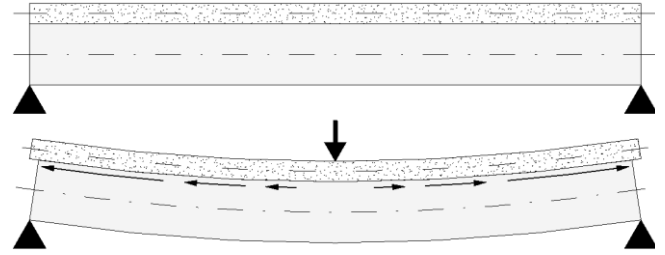


Figure 18: interface shear stresses as a result of deflection of a multiple layered floor

2.5.3 Stress distribution

As explained in previous subsection strain differences lead to stresses in concrete floors. When stresses in the adhesive layer between the substrate and the floor screed reach the bond strength or if the tensile strength of one of the materials is reached debonding will occur. The stress distribution in a floor consisting of several layers is first explained in case of deflection. Subsequently the stress distribution because of strain differences introduced by (imposed) deformations is discussed.

Deflection

The shear stress in longitudinal direction in a section that is subjected to deflection is calculated by formula (2).

$$\tau = -\frac{V_z * E_i * S_z}{b * EI_{zz}} \quad (2)$$

Where:

- τ is the shear stress in longitudinal direction (N/mm^2);
- V_z is the shear force in vertical direction (N/mm^2);
- E_i is the young's modulus of the concrete (N/mm^2);
- S_z is the first moment of area (mm^3);
- b is the width over which the longitudinal shear force is distributed (mm);
- EI_{zz} is the flexural rigidity of the composite structure (Nmm^2)

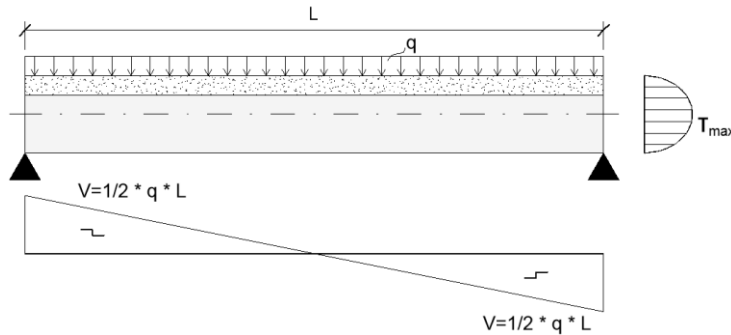


Figure 19: shear distribution and shear stress in a single span floor

The vertical shear force at a single span floor is maximal at the edges of the floor (Figure 19). This causes the shear stress in longitudinal direction of a floor with a constant section over the length to be maximal at the edges.

Strain differences

To calculate the stresses in the adhesive surface and in the screed different formulas are available. In [9] formulas to calculate stresses in screeds which are casted with bond to the bearing floor are discussed. The shear stress in a screed is maximal at the boundaries of the bonded surface and can be approached with formula (3).

$$\tau_{\text{edge}} = \varepsilon \sqrt{k * E * h} * \tanh\left(\frac{L}{2} * \sqrt{\frac{k}{E * h}}\right) \quad (3)$$

Where:

- τ_{edge} is the shear stress at the boundary of the bonded surface (N/mm^2);
- ε is the shrinkage/ deformation difference between the floor screed and substrate (mm/mm);
- k is the resistance of the substrate against horizontal shifting of the floor screed (N/mm^3);
- E is the young's modulus of the floor screed (N/mm^2);
- h is the thickness of the floor screed (mm);
- L is the length of the floor or the length between two cracks (mm).

Characteristics of screeds

From this formula it can be concluded that:

- the occurring shear stress in the adhesive surface of a screed is highly dependent on the magnitude of shrinkage of the screed;
- the occurring shear stress is in a lower rate dependent on the stiffness and thickness of the screed;
- at an increasing length of the floor (L) the tanh-function will approach the limit value of 1. This causes the maximal shear stress never to be bigger than:

$$\tau_{\max} = \lim_{L \rightarrow \infty} (\tau_{\text{edge}}) = \lim_{L \rightarrow \infty} \left(\varepsilon \sqrt{k * E * h} * \tanh \left(\frac{L}{2} * \sqrt{\frac{k}{E * h}} \right) \right) = \varepsilon \sqrt{k * E * h} * 1$$

$$\tau_{\max} = \varepsilon \sqrt{k * E * h} \quad (4)$$

The adhesion between screed and bearing floor will cause restraining of the screed. When the screed shrinks this means that imposed deformations will be present, inducing tensile stresses in the screed. The stresses caused by restrained shrinkage in a screed are maximal at the middle between the boundaries of the adhesive surface. These boundaries can be the edges of a floor or dilatations or at the location of cracks in the screed. According to [9] tensile stresses in the middle of a screed can be approached with formula (4).

$$\sigma_{\text{mid}} = \varepsilon * E * \left(1 - \frac{1}{\cosh \left(\frac{L}{2} * \sqrt{\frac{k}{E * h}} \right)} \right) \quad (5)$$

From this formula it can be concluded that:

- the occurring tension stress in a screed is highly dependent on the rate of shrinkage and the stiffness of the screed;
- the thickness of the screed is of minor importance;
- at an increasing length of the floor (L) the cosh-function will approach infinity. This causes the maximal shear stress never to be bigger than:

$$\sigma_{\max} = \lim_{L \rightarrow \infty} (\sigma_{\text{mid}}) = \lim_{L \rightarrow \infty} \left(\varepsilon * E * \left(1 - \frac{1}{\cosh \left(\frac{L}{2} * \sqrt{\frac{k}{E * h}} \right)} \right) \right) = \varepsilon * E * (1 - 0)$$

$$\sigma_{\max} = \varepsilon * E \quad (6)$$

Formula (3) and (5) show that the shear stress in the adhesive surface as well as the tension stress in the screed is dependent on the length of the floor. The stresses will be fully developed when the tanh-function of formula (3) and/ or the cosh-function in formula (5) reaches its maximum. This maximum is reached when a floor has a certain length (L_{\min}). The minimal floor length can be calculated knowing that the tanh-function tends to reach its maximal value for $x=3$:

$$\tanh(3) = \tanh \left(\frac{L_{\min}}{2} * \sqrt{\frac{k}{E * h}} \right) \approx 1 \quad \rightarrow \quad \frac{L_{\min}}{2} * \sqrt{\frac{k}{E * h}} = 3$$

$$L_{\min} = \frac{6}{\sqrt{\frac{k}{E * h}}} = 6 * \sqrt{\frac{E * h}{k}} \quad (7)$$

To give insight in the development of shear and tensile stresses the stress distribution in a bonded screed is pictured in Figure 20. In this figure it is clear to see that the shear stresses in the adhesive surface are maximal at the locations where the tensile stresses in the screed are minimal. These locations are at the boundary of the restraining of the screed. In this figure the boundaries are the edges of the floor and the location where a crack in the screed occurred.

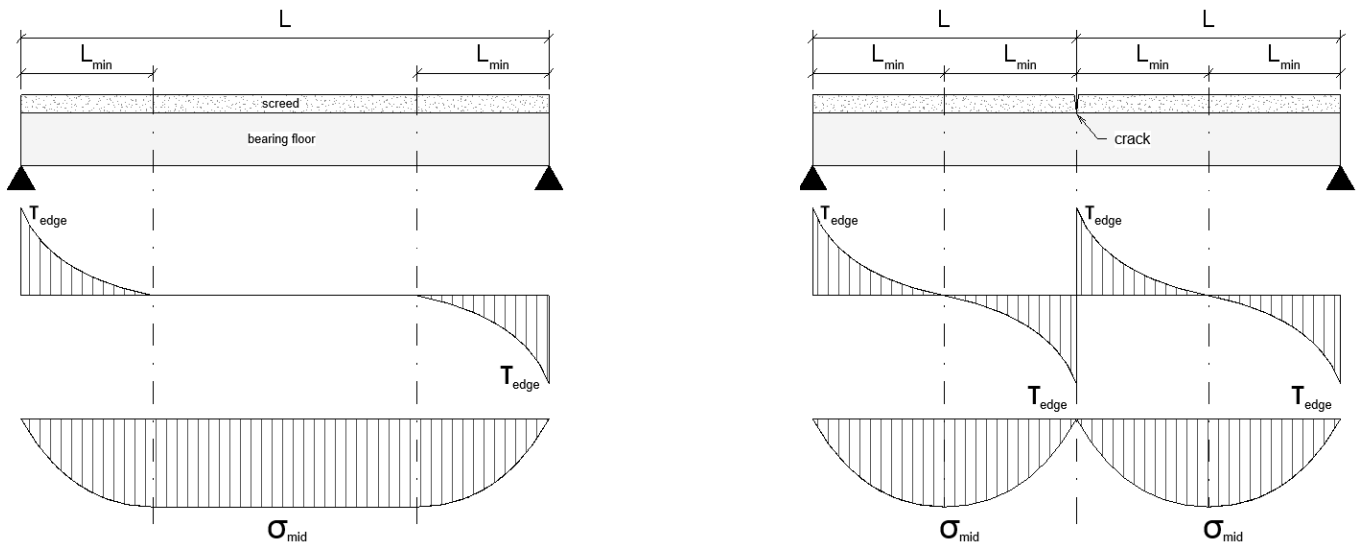


Figure 20: development of shear and tensile stresses in a screed [6]

2.6 Curling

A typical problem that can arise due to debonding of floor screeds is curling. In the case of a debonded floor screed the screed can curl at the edges of the floor fields. This curling is caused by an unequal drying of the floor. When the upper side of the floor dries more rapidly than the lower side, the upper side shrinks faster than the lower side which causes the floor to bend upwards (Figure 21). If the floor screed is loaded on the floating edge cracks can arise because the screed floor does not have enough capacity to distribute the load without cracking.

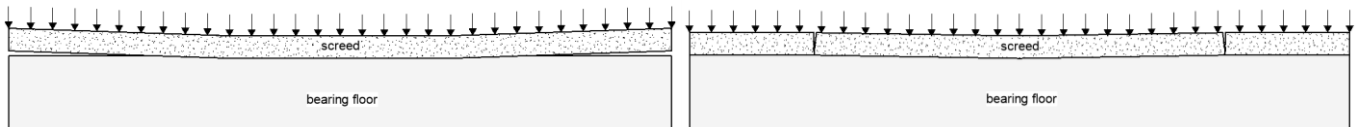


Figure 21: schematic representation of curling leading to cracking

2.7 Requirements in the standards

2.7.1 Dutch standards

In the Netherlands several standards are drafted in which the functional requirements for screeds are formulated. In Table 3 an overview is included of the standards that apply in the Netherlands.

Table 3: Dutch standards concerning screeds

Code	Description	Year
NEN 1042	Quality and execution of cementitious terrazzo	2001
NEN 2741	Quality and execution of cementitious screed	2001
NEN 2741/A1	Quality and execution of cementitious screed	2008
NEN 2742	Floating screed – terms, construction and quality	2007
NEN-EN 13813	Screed material – properties and requirements	2002
CUR 92	Floor heating in terrazzo flooring	2002
CUR 110	Cementitious self-levelling screeds	2012

The Dutch standards for screeds are mainly focussed on compressive and bending strength. In this subsection the subjects that are included in the Dutch standards concerning bond strength and the onset of cracking in screeds are discussed.

Requirements concerning bonding of screeds

An overview of the requirements given in the Dutch standards concerning bond strength is included in Appendix Table 30. For the several types of cementitious screeds the text given in the standards is all quite the same. In the standards the most attention is paid to the way of execution. Here comments are made on cleaning and roughening the substrate before casting the screed. No quantitative requirements are given in the norms on these subjects. On the other hand, on the bonding capacity of the substrate as well as the screed surface tensile strength quantitative requirements are made. The most important requirement that is given is the value 1.5 N/mm^2 that is demanded for the bonding capacity of the substrate in the NEN 2741/A1. This requirement is drafted to ensure that the substrate will not be a weak link in the adhesion between the layers.

Requirements concerning cracking

In Appendix Table 31 the requirements given in the Dutch standards concerning cracking of screeds are given. In the standards also on this subject the most attention is paid to the way of execution, about applying reinforcement and providing foil on the screed after casting to prevent evaporation. No quantitative requirements are given in the norms on this subject.

2.7.2 Other standards

The standards concerning screeds that apply to Germany and the UK are given in Table 4. Concerning bonding/cracking of screeds no requirements are given in the German standards. The requirements given in the British standards are equal to the Dutch requirements, informing about the way of execution that is advised to be applied to create good bonding and controlling the formation of cracks.

Table 4: German and British standards concerning screeds

Code	Description	Year
DIN 18353	Allgemeine Technische Vertragsbedingungen für Bauleistungen - Estricharbeiten	2016
DIN 18560	Estriche im Bauwesen	2015
BS 8204-1	Screeds, bases and in situ floorings. Code of practice	2009
BS 8204-2	Screeds, bases and in situ floorings. Concrete wearing surfaces. Code of practice	2011
BS 8204-4	Screeds, bases and in situ floorings. Cementitious terrazzo wearing surfaces. Code of practice	2011

2.8 Review

In this chapter the characteristics of screeds casted on concrete bearing floors were discussed. Screeds are classified on the basis of different factors, concerning the bond type, detailing, execution method and layer structure. The types of screeds investigated in this research are cementitious screeds. A property of these screeds is that the tensile strength is relatively low, causing the onset of cracking at relatively low stresses.

Cracking of screeds is in the most cases induced by imposed deformations which arise as a result of restraint in movement of the screeds for example a bond between screed and bearing floor, when the screed is caused to shorten / extend. Besides stresses in the screed, stresses will also appear in the adhesive surface between the screed and bearing floor in the case of imposed deformations. Stresses in the adhesive surface are results of strain differences between the substrate and screed. These strain differences can arise due to shrinkage differences, temperature expansion/ moisture changes, differences in stiffness and deflection. The main influencer of strain differences is screed shrinkage. In the case that for the hydration shrinkage of cementitious screeds a value can be assumed equally to concrete, the shrinkage is $\epsilon_{s,max} = 0.3\%$.

In this chapter different formulas are derived for the stresses in the screed and adhesive surface as a result of strain differences. Furthermore an indication is given for the distribution of the stresses along the adhesive surface in these situations. From this it is concluded that the shear stresses at the interface are the biggest at the edges of a floor or at the location of a crack. The tensile stresses in the screed are the biggest in the middle of a floor.

A typical screed damage that is induced by debonding of screeds is curling. In the case of curling the screed curls at the edges of the screed as a result of strain differences in the screed. When the screed is then loaded at the location of a curl failure occurs quickly at the curled part of the screed.

In the Dutch as well as other international standards the most attention is paid to the way of executing the screeds. Here comments are made on cleaning and roughening the substrate before casting the screed, but no quantitative requirements are drafted.

For the bonding capacity of the substrate quantitative requirements are made. The most important requirement that is given is the value 1.5 N/mm^2 that is demanded for the bonding capacity of the substrate in the NEN 2741/A1. This requirement is drafted to ensure that the substrate will not be a weak link in the adhesion between the layers. In chapter 3 adhesion of two layers of concrete is discussed in further detail.

3. Concrete to concrete bond

3.1 Introduction

The bond strength describes the adhesion between two layers of concrete, in this case cementitious screed (overlay) and concrete bearing floors (substrate). Usually the bond strength is defined as the tensile strength perpendicular to the interface plane, but bond strength in shear may also be considered. In chapter 4 the way of testing the bond strength is further defined. The bond between two concrete layers is generally not based on a chemical bond between substrate and the applied layer, but on a combination of different physical forces [10]. These physical forces are in particular the so called Van der Waals forces and mechanical interlocking. Besides these forces in some extend also hydrogen bond and for young concrete capillary forces could play a role [11].

In the following two sections the different mechanisms causing adhesion are further explicated. Subsequently different factors influencing the bond strength are discussed in section 3.4, where a differentiation is made between factors concerning the substrate surface and overlay properties. Finally requirements for the bond strength of concrete repairs are discussed in section 3.5 in comparison with the requirements for bonded screeds.

3.2 Van der Waals forces

Van der Waals forces are electromagnetic forces that work between two molecules at a distance smaller than 30 – 100 nanometers. The forces (F) decrease by an increasing distance (r) conform formula (8), making the forces at bigger distances than previously mentioned negligible.

$$F_{\text{Van der Waals}} = \frac{\text{constant}}{r^7} \quad (8)$$

To provide a bond in the form of Van der Waals forces it is of importance that the distance between the substrate and the applied layer is small. The consistency of the mortar is of big influence on this distance. When an earth dry, relatively coarse mortar is applied there will hardly be any Van der Waals forces. Applying a liquid adhesive layer before casting the mortar can reduce this distance.

3.3 Mechanical interlocking

Mechanical interlocking contains a mechanical anchorage that is created by mortar that covers the surface roughness of the substrate (Figure 22). In some cases the mortar even enters the pores of the substrate, creating a strong anchorage. Interlocking can be improved when the substrate has a large absorption capacity. The liquid parts of the mortar can then be sucked into the substrate by underpressure, bringing the solid parts of the mortar closer to the substrate. This improves the attractive forces and enlarges the contact surface.

The contact surface is essential in creating a good bond. To bind there must be contact between the substrate and the applied mortar. This is an important reason why the mortar needs to have certain liquidity. When applying a solid material the points of contact are scarce, making a good bond difficult to create (Figure 23). Applying a liquid adhesive layer before casting the mortar can improve the contact surface.

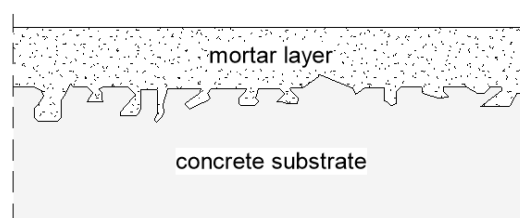


Figure 22: mechanical interlocking

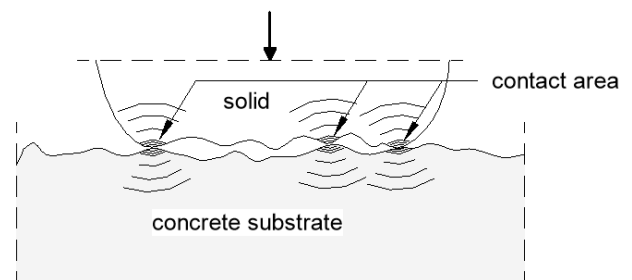


Figure 23: contact area of solid materials applied on a concrete substrate

In cementitious mortar the liquids will wet the concrete of the substrate, but the binding agent will finally be formed by the reaction of cement with water. The reaction products of cement with water have a relatively rough structure causing the contact surface to be relatively small. The bond can be improved with filling the hollow spaces by adding fine fillers like silica fume or polymers to the mortar (Figure 24).

Concrete to concrete bond

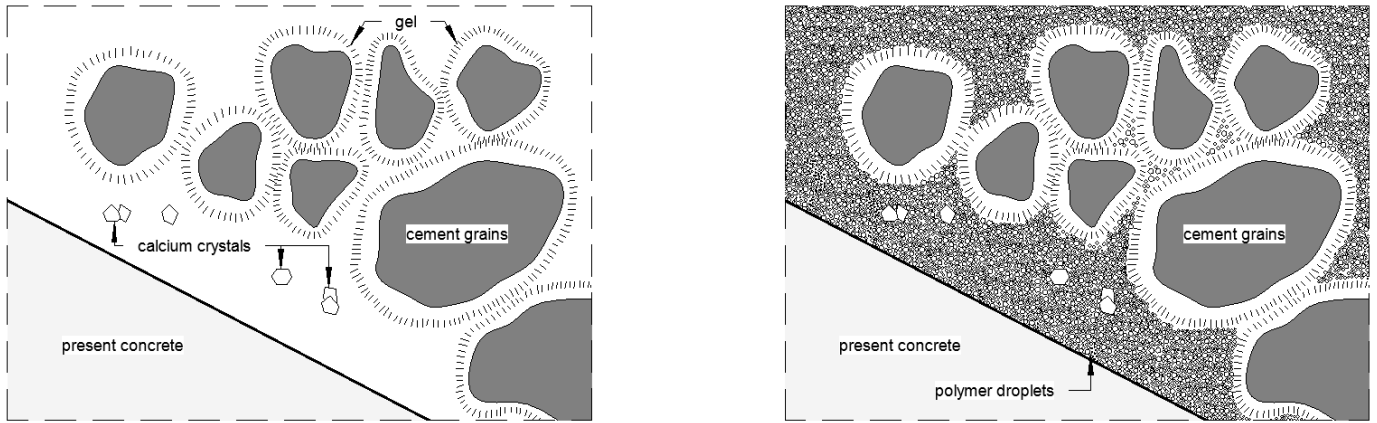


Figure 24: rough hydrated cement grains with small contact points (left) versus polymer modified mortar (right) [11]

3.4 Factors influencing bond

3.4.1 Substrate surface

Surface cleanliness

In the occasion that dust, oil, grease or other contaminants are present on a surface that will function as bonding substrate it will have influence on the bond strength if remaining when casting the overlay. The bond strength will decrease in comparison to a clean surface while wetting of the surface is prevented. Furthermore the friction is decreased and a preventive layer for interlocking between the substrate and overlay is created. In [12] it is given that the best methods to clean the surface are hosing down with high pressure water and vacuum cleaning.

Laitance

After casting the concrete substrate bleeding brings water, cement and fines from aggregates to the top layer of the concrete. When hardened a weak layer is created on top of the concrete which is called laitance. Laitance will considerably lower the bond strength between substrate and overlay, making it important to remove this layer before casting the overlay.

Microcracking

When microcracking is present in the surface of the substrate the top layer will be a zone of weakness. Microcracking can be present when mechanical methods (e.g. pneumatic hammering) are applied to roughen the surface. Laboratory tests [13] have shown that these microcracks lead to low bond strengths.

Surface moisture

The surface moisture content of the substrate is of great influence on the bond strength. When a surface is too-dry it will absorb water from the mortar casted on the substrate. This prevents the cement particles at the surface to hydrate and creates a porous zone close to the interface. A too-wet surface will cause a local high water-cement ratio (w/c) close to the interface, leading to a reduction in strength. In [14] it is given that the optimal moisture condition can be found at a saturated, dry surface.

Surface roughness

Surface roughness is of importance to provide friction between the layers and to improve mechanical interlocking (Figure 22). Furthermore the specific area of a rough surface is bigger than a smooth surface, creating more area for the development of Van der Waals forces. Several methods to roughen the surface are given in Table 5.

Table 5: methods to roughen the substrate surface, ranked in increasing roughness

Method	Description	Characteristics
Wire-brushing	Removing the laitance by brushing with steel bristles	No microcracking, clean surface
Grit-blasting	Blasting with steel grit to expose the aggregates of the concrete	No microcracking, sand on surface
Scabbling	Removing a thin layer of the concrete by hammering on the surface with compressed air powered machines	Microcracking, low production rate
Water-jetting	High pressure water blasting to expose the aggregates	No microcracking, clean surface
Milling	Cutting longitudinal tracks from the substrate by rotating metal lamellas	Microcracking is likely, fast production

An easy way to determine the surface roughness is the sand patch method (Figure 25). With this method a predetermined volume of fine sand is rubbed into the floor in a circle form. The rubbing proceeds until the level of the sand is equal with the highest level of the surface. The diameter of the circle is then decisive for the average texture depth, which is calculated by formula (9).

$$ATD = \frac{4 * V}{\pi * d^2} \quad (9)$$

Where:

ATD is the Average Texture Depth (mm);

V is the volume of fine sand (mm^3)

d is the mean diameter of the sand circle, measured at 4 places (mm).

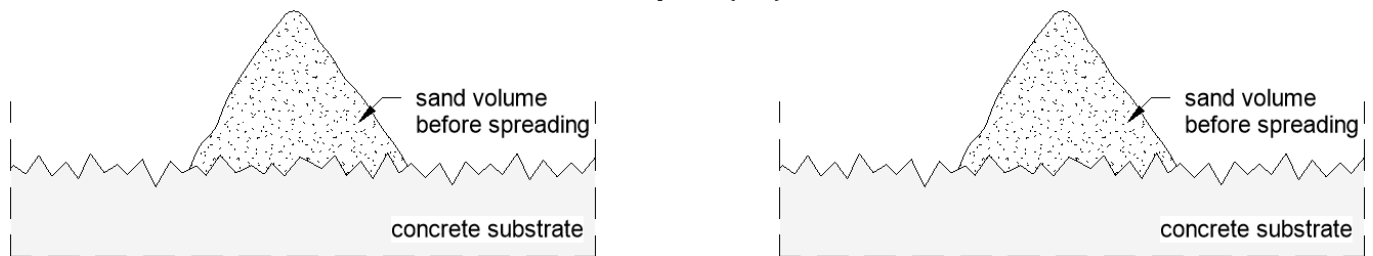


Figure 25: the sand patch method is used to determine the Average Texture Depth (ATD)

Substrate porosity

A porous surface improves the specific area, what ensures a better bond and increases the amount of cracking energy required when debonding. Pores as a result of air inclusions will lead to a bigger specific area. However, capillary pores with a size of several nanometers to micrometers will probably not lead to an improved bonding area. This is due to the fact that the mean size of a cement particle (± 30 micrometer) is then not able to enter these pores [11]. Furthermore a porous surface provides a more permeable concrete which means that the absorption capacity increases, creating a stronger mechanical interlocking.

3.4.2 Overlay

Bonding agent

Before applying the overlay a bonding agent can be applied on the substrate. This bonding agent has several functions: it wets the surface, it fills small pockets in the substrate that cement particles would bridge and it increases adhesion. As bonding agent a special acrylic modified coat can be applied or a bonding slurry of cement can be used. In [14] the remark is made that if the bonding agent is allowed to dry before applying the overlay this can lead to a decrease in bond strength, so it is of importance that the top layer is casted on a moisture bonding agent.

Overlay compaction

To prevent development of air pockets in the valleys of the rough surface of the substrate sufficient compaction is important. At this way it is made sure that the contact area as depicted in Figure 24 is as optimal as possible to create a good bond.

Overlay curing

Curing of the overlay is of importance to reduce the risk of cracking and debonding as a result of shrinkage. A high amount of shrinkage can be prevented by wetting the surface and applying a vapor barrier foil, as well as by regulating the temperature.

3.4.3 Degree of influence

As discussed in the previous subsections the bond between substrate and the overlay is dependent on a large number of factors. Besides the explained factors there are more factors influencing the bond strength, e.g. substrate properties, time and early traffic. The degree of influence of the different factors is researched by Silfwerbrand [15] and the results are shown in Figure 26.

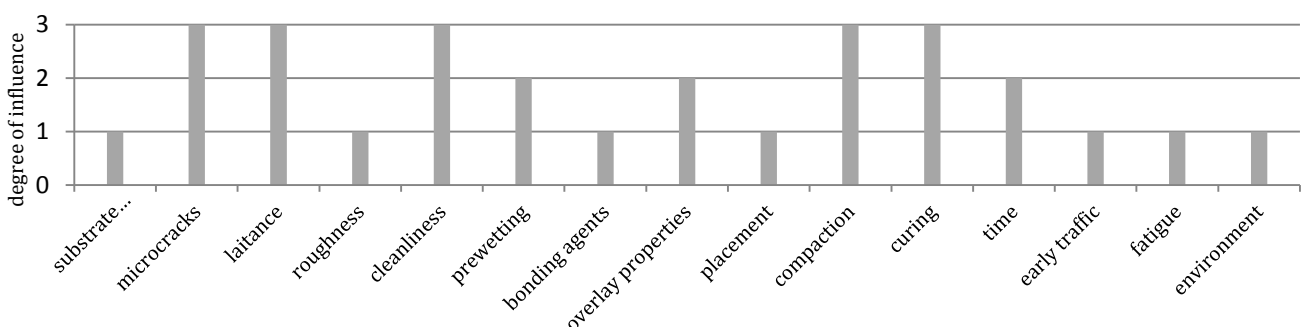


Figure 26: degree of influence of different factors influencing bond strength

In Table 5 different methods to prepare the surface before applying the overlay are given. In the past several investigations are done to the influence of the different methods on the bond strength between substrate and overlay [16] [17] [18] [19] [20]. The results of these tests have divergent results, but generally can be said that the methods can be ordered from low influence to high as follows:

1. Milling
2. Scabbling
3. Wire brushing
4. Grit-blasting
5. Hydrojetting

From this can be concluded that the surface roughness does have influence on the bond strength, but if heavier methods are applied to roughen the surface like milling or scabbling this has negative influence on the bond strength. Milling and scabbling causes microcracking in the surface, which has a negative influence on the bond strength. In [19] is given that when the more aggressive methods are applied to roughen the surface, the application of a bond coat before casting the overlay can reduce the negative effects of microcracking.

3.5 Requirements on the bond strength

Concerning the bond strength of screeds to concrete bearing floors little literature is available. Literature concerning concrete repairs includes more information about the bond of concrete to concrete. To gain more insight in the requirements that can be demanded for the bond strength of concrete to concrete layers, the requirements in the Dutch standards for screeds are compared with the requirements in the Eurocode for concrete repairs.

In the NEN-EN 1504-3 [21] requirements are given to the quality of constructive and non-constructive concrete repairs. In this standard a classification is made, where concrete structures are divided in structural and non-structural classes. For repairs in non-structural classes the minimum adhesive bond strength has to fulfil the minimum requirement of $0,8 \text{ N/mm}^2$, tested using the Pull-Off test in accordance with the NEN-EN 1542 [3]. For structural repairs this is a minimum of $1,5 \text{ N/mm}^2$ to $2,0 \text{ N/mm}^2$.

The requirements for the bond strength of concrete repairs drafted in American standards are quite similar to the previously mentioned values, with values ranging from 100 psi ($0,7 \text{ N/mm}^2$) to 250 psi ($1,7 \text{ N/mm}^2$) [22].

As screeds are mostly applied as non-structural element it was expected for the minimum bond strength of screeds - when following the requirements according to the NEN-EN 1504-3 - to be $0,8 \text{ N/mm}^2$. Yet the requirements drafted in the NEN 2741/A1 demand a minimum value of $1,5 \text{ N/mm}^2$ for the substrate surface tensile strength.

3.6 Review

In this chapter the adhesion between overlay and substrate was discussed in further detail. The bond between two concrete layers is based on a combination of two physical forces, consisting of Van der Waals forces and mechanical interlocking. Van der Waals forces are electromagnetic forces that work between two molecules. To obtain strong Van der Waals forces it is of importance to make the distance between the molecules as small as possible. In practice this means that liquid mixtures will obtain stronger Van der Waals forces than earth-dry mixtures.

Mechanical interlocking contains a mechanical anchorage that is created by mortar that covers the roughness of the substrate. The contact surface is essential in creating a good bond. The bigger the contact area, the bigger the potential of creating a good bond. Interlocking can be improved by improving the surface roughness and improving the absorption capacity of the substrate.

The adhesion between two layers of concrete is influenced by different factors. Factors concerning the substrate surface include surface cleanliness, laitance, surface moisture, surface roughness and substrate porosity. The factors concerning the overlay include the application of a bonding agent, overlay compaction and overlay curing.

To prepare the surface before applying the overlay different methods are available. Researches in the past have shown that ordered from low influence to high the methods that can be applied consist of milling, scabbling, wire brushing, grit blasting and hydrojetting.

Requirements given in the standards for concrete repairs are compared to the requirements for screeds. As screeds are mostly applied as non-structural element the minimum bond strength of screeds according to the NEN-EN 1504-3 (concerning concrete repairs) is $0,8 \text{ N/mm}^2$. Yet the requirements drafted in the NEN 2741/A1 (concerning screeds) demand a minimum value of $1,5 \text{ N/mm}^2$ for the substrate surface tensile strength.

4. Bond strength testing methods

4.1 Introduction

To determine the bond strength between two layers of concrete different testing methods are available. In this chapter the currently available methods are discussed. Bond strength testing methods can be classified in different classes, depending on the stress combination that is applied to measure the bond strength. In order to evaluate the different bond tests some requirements are drafted in different literature [14] [23] [24] [25]. A summation of these requirements is given below:

- Ability to simulate site conditions;
- Ability to expose only the bond to environmental conditions;
- Ability to reflect stress state of fairly typical service conditions;
- High sensitivity to variation of bond strength;
- Ability to evaluate in-situ bond strength;
- Reproducibility of test results.

In section 4.2 first an explanation is included concerning the classification. Subsequently the available tests are discussed per category. The tests are compared in the review in section 4.5, where an evaluation is made about the method that is the best applicable for testing the bond strength of screeds on concrete bearing floors. In the evaluation the aforementioned requirements are included in the discussion.

4.2 General classification

The available methods to determine the bond strength can be divided into three categories [23] [24]. With the test methods of the first category the bond under tension stress is measured. The second category measures the bond under shear stress and with methods from the third category the bond strength under a combination of shear and compressive stress is measured (Figure 27). The stress states which occur at the different bond strength measuring categories are depicted by making use of Mohr's circles in Figure 28.

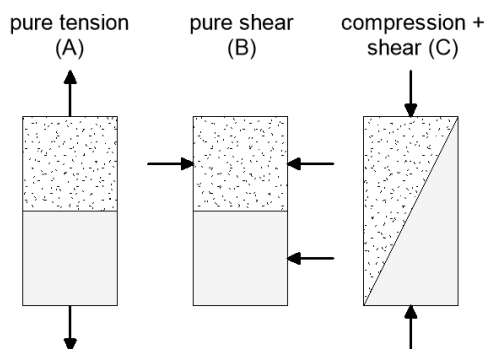


Figure 27: three bond strength measuring categories

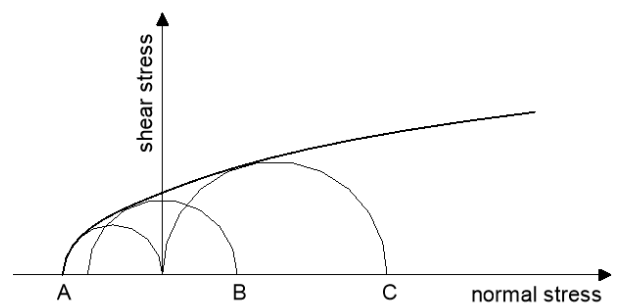


Figure 28: failure envelope of the different measuring categories presented in Mohr's circles

4.3 Tensile bond tests

Test methods where the tensile strength is measured to determine the bond strength have gained the most popularity throughout the years [14] [24]. The tensile strength can be measured by making use of direct or indirect techniques. Indirect tensile tests include the cylinder splitting test and flexural tests [26]. Direct tensile tests include among others direct tension and pull-off tests (Figure 26).

Flexural tests seem to be of low efficiency, because the area of the bonded surface that is subjected to loading is small compared to the specimen volume. In this way only a small part of the bonded plane is subjected to the maximum stress [25]. According to [24] splitting tests give more efficient results. The splitting test is regarded to give an indication of the tensile stress of the concrete. The tests are performed by making use of cylindrical specimen with different concrete layers on the left and right half of the cylinder in a standard compression test machine (Figure 29).

More exact insight in the tensile bond strength between two layers of concrete is given by direct tensile tests in which tension forces are applied on a specimen. Examples of direct tensile tests are the pipe nipple grip uniaxial tensile bond test, friction grip tensile bond test and the dog-bone test [27]. A disadvantage of all the previously mentioned tests are executed in laboratory by preparing specimen on beforehand, whilst the bond strength mostly has to be determined in situations on site. For this reason the Pull-Off test is developed.

Bond strength testing methods

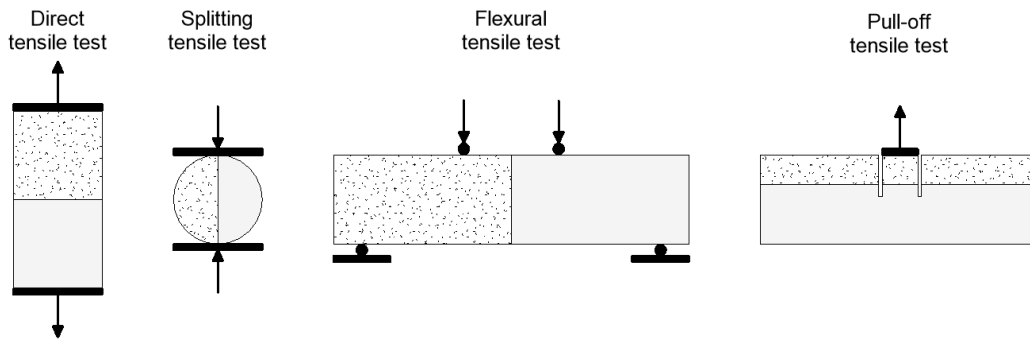


Figure 29: different methods to determine the tensional bond strength of two concrete layers

Pull-Off test

As a result of the simplicity and the possibility to execute the test both in the field and in the lab the Pull-Off test is the most popular bond testing method [14]. This method is executed by drilling a core through the two layers of concrete. When carrying out the test in laboratory the core is carefully broken at the bottom, the top and bottom surfaces are made even and after gluing steel plates to the core the tensile strength is measured in a test machine. On site the test is carried out by gluing a steel dolly at the top surface of the core. After this a loading tripod is placed above and connected to the dolly and the tensile bond strength is measured by applying a tensile load on the dolly.

Pull-off tests are included in several Dutch and foreign standards. A small summation of the standards is given in Table 6. The description of the pull-off tests is roughly the same for all the standards. The difference between the standards is made in the application and the depth of the core drilling depth. Where the CUR-20 does not prescribe any drilling, the other standards variate in values of 5 – 25 mm drilling depth in the substrate.

Table 6: overview of the available standardisation of pull-off tests

Code	Description	Year
NEN-EN 1542	Measurement of bond strength by pull-off of repaired concrete structures	1999
NEN-EN 13892-8	Determination of bond strength of screed materials	1990
CUR 20	Determination of the bond strength of mortars on concrete	1990
ASTM C1583	American standard for testing tensile strength of concrete surfaces and the bond strength of concrete repair and overlay materials by direct tension	2004
BS 1881: part 207	Testing concrete. Recommendations for the assessment of concrete strength by near-to-surface tests	1992

Apart from the fact that the Pull-Off test is a popular test and included in several Dutch and foreign standards, the method has a flaw that has influence the results of the tests. When the loading tripod is not placed precisely centrally above the dolly, or the drilling of the core is not executed in a precise angle of 90° with the surface, the specimen will be loaded eccentrically (Figure 30). When loaded eccentrically the specimen will not be subjected to pure tension, but to bending as well. This means that the resulting force will not be representative for the tension bond strength of the specimen.

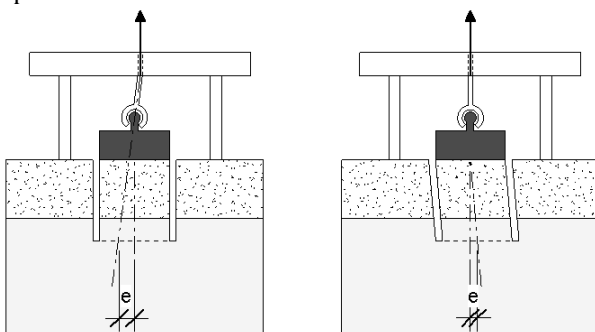


Figure 30: eccentric loading as a result of not-centric placing of the tripod or drilling the core under an angle

4.4 Shear bond tests

In order to determine the shear strength at the interface of two layers of concrete several tests have been developed. In these tests a shear force parallel to the interface is subjected to the interface. Most common methods to determine the shear bond strength are the mono-surface and the L-shaped mono-surface shear test (Figure 31). A drawback of these methods is that the bond surface in these tests is not only subjected to direct shear stress, but to small bending stresses as well [24]. This causes difficulty in determining the exact shear stress working on the interface when failure occurs.

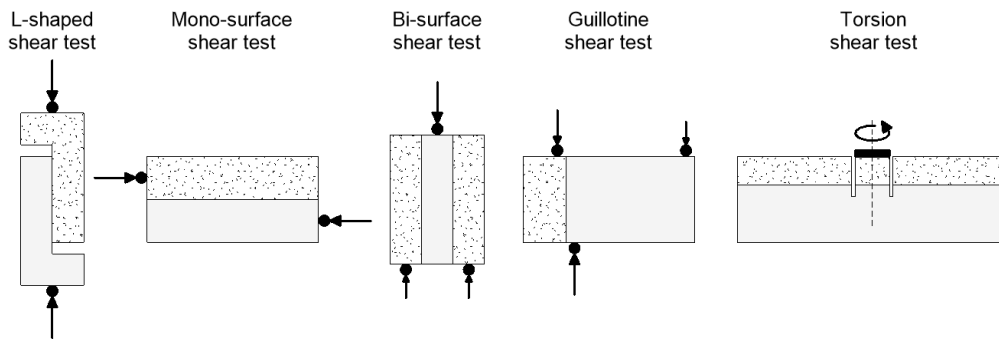


Figure 31: shear bond test methods

To eliminate the bending stresses other tests are developed. In these tests is made use of more contact points to transmit the forces to the specimen or an extra layer is added to the specimen. Examples of these tests are the Bi-surface shear test and the Guillotine test [28]. The results of these give a better insight in the shear bond strength. A disadvantage of the shear methods described above is that the test specimens have to be prepared in laboratory, what makes testing on site not possible. In order to test bond strength of concrete structures on site the torsion test is developed.

Torsion test

The procedure for the torsion test is similar to the pull-off test procedure, but differs in the way of applying the load. In the situation of the torsion test a torsional force is applied instead of a tensile force. To apply this torsional load a special device is used that is bolted to the surface. The force that is measured by this device is the torsional moment at failure of the specimen. From here the shear strength is calculated by formula (10) or (11).

$$\tau = \frac{T}{\varnothing^3} * \frac{16}{\pi} \quad (\text{Linear elastic behaviour}) \quad (10)$$

$$\tau = \frac{T}{\varnothing^3} * \frac{12}{\pi} \quad (\text{Purely plastic behaviour}) \quad (11)$$

Where:

- τ is the shear stress at failure (N/mm²);
- T is the torsional moment at failure (Nmm);
- \varnothing is the core diameter (mm).

Concrete is a brittle material which is not fully elastic or purely plastic. In reality the relationship could be something between the two values of formula (10) and (11). In [29] is given that the elastic relationship may be handled.

The device that is used to apply the torsional moment is equipped with special bearings that are designed to minimize the influence of normal forces. Nevertheless it is still inevitable that normal forces will be transmitted to the specimen. This causes the maximal torsional force that is measured to be not fully representative for the shear strength of the interface. Nevertheless a lower bound of the shear bond strength is indicated by this method. In order to use this method for standardised tests further development and studies are required [29] [30].

4.5 Compressive-shear bond tests

The previously mentioned bond tests aim at determining the bond strength in 'pure' tension and 'pure' shear (see Mohr's circle A and B in Figure 28). Besides these methods, other methods are developed where the specimen is subjected to a combination of shear and compressive stresses. This causes the Mohr's circle to shift more to the direction of the compressive side (circle C of Figure 25).

Two common methods to test the bond between two concrete layers under compression and shear stresses are the modified shear bond test [31] and the slant shear test [32] (Figure 32). Both tests were developed to load a larger area of the specimen with shear stresses than with the regular shear bond tests.

The slant shear test is the most common compressive-shear test and is included in different standards, viz. the British Standard BS6319: part 4 [33] and the ASTM C882-99 [34]. The test method is relatively simple to execute since it has a similar procedure as a regular compressive test. However, research has shown that the method has its shortcomings [32].

Failure of the interface is highly dependent on the angle of the interface. According to the standards this angle has to be 30°. When applying an interface surface with a higher roughness the critical angle decreases. For the tests done by the authors of [32] the critical bond angles for smooth, medium rough and rough surfaces were 27°, 23° and 19° respectively. The angle applied in the standards corresponds to a fully smooth surface. This causes the results of the shear bond strength at the slant shear test in the case of rough surfaces to be higher than the actual shear bond strength.

Bond strength testing methods

Another problem that arises while applying the slant shear test method concerns modulus mismatches. When the elastic modulus of one of the overlay is significantly lower than that of the substrate, an increase of stresses at the ends of the interface will arise causing the specimen to be loaded eccentrically, inducing a lower failure load.

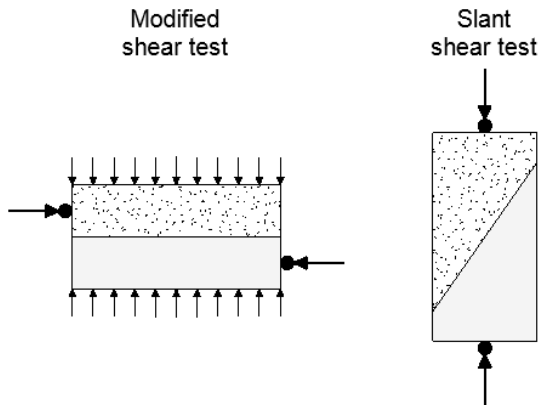


Figure 32: compressive-shear bond test methods

4.6 Review

In this chapter different methods were discussed to determine the bond strength of concrete to concrete. The test methods were divided in three categories: tensile bond tests, shear bond tests and compressive shear bond tests. Relating the results of these tests is difficult since the bond mechanisms have significantly different characteristics. Nevertheless a correlation has been found between shear and tension tests in different studies, where a mean ratio is found of 2.04 (shear bond divided by tension bond) [29] [35].

The introduction of this chapter included a summation of requirements that are drafted in different literature for methods to determine the bond strength of concrete to concrete. According to the author, a very important requirement for bond testing is the possibility to determine the in situ bond strength. From the methods discussed in previous sections two methods are applicable in situ: the pull-off test and the torsion shear test.

Both tests still contain flaws and especially the torsion shear test is a test that requires more research and development. The method of the Pull-Off test is prescribed in different standards (for screeds and concrete repairs) and is the most common method. However, eccentricity appears to be of big influence on the results of the tests.

5. Modelling of the pull-off test method

5.1 Introduction

The Pull-Off tests appears to be the best applicable test to determine the bond strength between two layers of concrete. Yet in section 4.3 is notified that eccentricities can influence the results of the test. In this chapter the influence of eccentricities on the results of the Pull-Off tests is studied by means of an analytical approach (section 5.2) and a FEM study (section 5.3).

5.2 Analytical approach

5.2.1 Calculation method

In the analytical approach of the Pull-Off test the influence of eccentric pulling is investigated. A schematic representation of the situation is included in Figure 33. The method that is applied to calculate the maximal outer force that can be applied to a dolly glued on a concrete specimen is discussed in this section. For the determination of the mechanism of concrete reacting to eccentric pulling there is made use of a model that is deviated from the simple analytical model for structural concrete behaviour in an uniaxial test as described in [5].

In the calculation a square dolly is assumed to simplify the problem. In practice a cylindrical dolly is applied. The consequences of this schematisation are discussed in sub-section 5.2.2. As the subject of the research consists of eccentric loading no axial-symmetric modelling is applied.

Step 1: determination of the specimen properties

The first step of the calculation involves the determination of the stress-deformation relation of the concrete specimen. By making use of the relations given in formula (12) - (14) the graph of Figure 35 is composed.

$$\delta_1 = \frac{f_t}{E_c} * h \quad (12)$$

$$w_c = 5.14 \frac{G_f}{f_t} \quad (13)$$

$$G_f = \int_0^{w_c} f_t * e^{-w*a} * dw \quad (14)$$

Where:

- δ_1 is the deformation of the concrete specimen at which the tensile strength is reached (mm);
- f_t is the tensile strength of the concrete (N/mm²);
- E_c is the Young's modulus of the concrete (N/mm²);
- h is the specimen height (mm);
- w_c is the crack width from which no tensile forces can be transferred by the concrete anymore (mm);
- G_f is the concrete fracture energy (N/mm);
- a is a factor in the exponential formula representing the stress-deformation relation of the concrete after cracking.

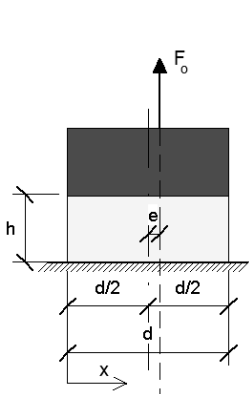


Figure 33: setup Pull-Off test with eccentric tensile force

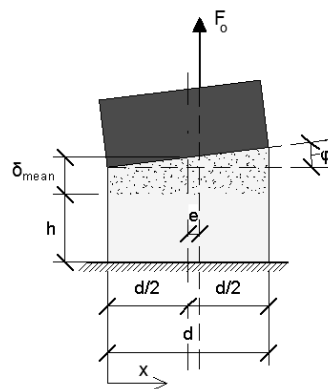


Figure 34: deformation after applying eccentric tensile force

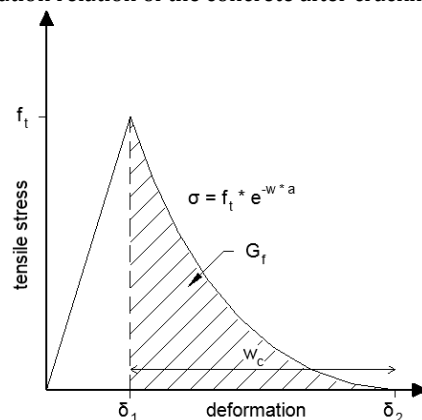


Figure 35: stress- deformation relation concrete specimen

Step 2: determination of the inner force – mean deformation relation

The goal of the calculation is to find the maximal tensile force (F_o) that can be applied to the specimen at different eccentricities. In order to obtain this maximal tensile force the inner force (F_i) – mean deformation (δ_{mean}) relation of the specimen is determined at different deformation angles (ϕ).

In Figure 34 a deformed specimen is shown schematically. The deformation of the specimen over the width is represented by formula (15). By making use of the stress-deformation relation of Figure 35 the stress distribution over the width of the specimen is determined (Figure 36 and formula (16)). The total inner force of the specimen is then calculated by formula (17). By calculating the inner force at different mean deformations (δ_{mean}) the force-deformation relation at a certain deformation angle is obtained.

$$\delta(x, \varphi, \delta_{\text{mean}}) = \varphi * x + \left(\delta_{\text{mean}} - \varphi * \frac{d}{2} \right) \quad (15)$$

$$\sigma(\delta) = \begin{cases} \frac{f_t}{\delta_1} * \delta & \text{for } \delta \leq \delta_1 \\ f_t * e^{-a * (\delta - \delta_1)} & \text{for } \delta > \delta_1 \end{cases} \quad (16)$$

$$F_i = b * \int_0^d \sigma(\delta(x, \varphi, u_{\text{mean}})) * dx \quad (17)$$

Where:

F_i is the inner force in the specimen (N);

φ is the internal angle of rotation;

d is the width of the dolly (mm);

b is the width of the dolly in the direction perpendicular to d (mm). In this calculation the geometry of the dolly is assumed to be square. In practice the dolly is a cylinder.

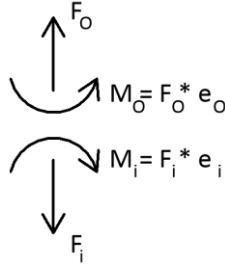
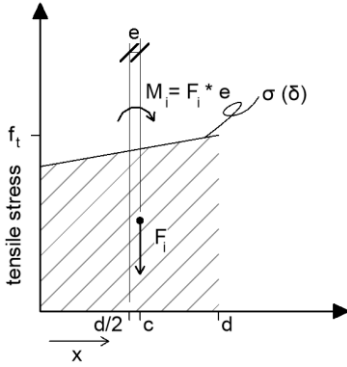


Figure 36: distribution of tensile stresses along the width of the dolly
Figure 37: to obtain stability the outer forces have to equal the inner forces

Step 3: determination of the eccentricity - deformation relation

Due to the fact that the stress distribution in the specimen is not equal over the width the inner force has an eccentricity relative to the centroid of the specimen. This eccentricity varies when increasing the mean deformation and is calculated by formula (18) - (19). Calculating the eccentricity at different mean deformations gives the eccentricity - deformation relation.

$$c(\varphi, \delta_{\text{mean}}) = \frac{\int_0^d x * \sigma(\delta(x, \varphi, u_{\text{mean}})) * dx}{\int_0^d \sigma(\delta(x, \varphi, u_{\text{mean}})) * dx} \quad (18)$$

$$e_i(c) = \frac{d}{2} - c \quad (19)$$

Where:

c is the centroid of the inner force (mm);

e_i is the eccentricity of the inner force (mm);

Step 4: determination of the maximal force per eccentricity

When executing the pull of test the outer forces applied to the specimen have to be in balance with the inner forces in the specimen to ensure stability. This relation is translated by means of formula (20) - (21).

$$M_i = F_i * e_i(c(\varphi, \delta_{\text{mean}})) \quad M_o = F_o * e_o$$

$$M_i = M_o \rightarrow e_i * e_o \quad (20)$$

$$F_i = F_o \quad (21)$$

M_i is the inner moment in the specimen (Nmm);

M_o is the outer moment applied to the specimen (Nmm);

e_o is the eccentricity of the outer force (mm).

By making use of the relations drafted in step 2 and 3 the set of inner forces per eccentricity can be found for the entered deformation angles. As a result of the relations drafted above the maximal outer force per eccentricity is equal to the highest value of the set of inner forces.

Input variables

The variables that are used for the input of the calculation exist of material, geometrical and step size parameters. For the material parameters the values prescribed in the MC 2010 are used (Table 7). The applied step size is $100 \cdot 10^{-6}$ rad. The geometry parameters are given in Table 8.

Table 7: material parameters according to MC 2010

	f_{ck} (N/mm ²)	Δf (N/mm ²)	f_{cm} (N/mm ²)	f_{ctm} (N/mm ²)	G_f (N/m)	E_{c0} (N/mm ²)	E_c (N/mm ²)	ν
C12/15	12	8	20	1.57	125	21,500	27,088	0.2
C20/25	20	8	28	2.21	133	21,500	30,303	0.2
C30/37	30	8	38	2.90	141	21,500	33,551	0.2
C40/50	40	8	48	3.51	147	21,500	36,268	0.2
C50/60	50	8	58	4.07	152	21,500	38,629	0.2

Table 8: geometry parameters

Parameter	Value
Specimen height h	30 mm
Dolly diameter d	50 mm
Dolly width b	50 mm

5.2.2 Results and discussion

The influence of eccentric pulling on the maximal tensile force that can be applied to the specimen is analysed in a parameter study. The results of this research are discussed in this paragraph. The research is divided in several sub-researches, where the influence of the concrete class, fracture energy and dolly size is investigated. An example of the maple file that is used for the calculations is enclosed in appendix A.3.1. First of all the regular behaviour of concrete subjected to a perfectly centric and an eccentric tensile force is explained. Subsequently the results of the different sub-researches are discussed.

General behaviour concrete during Pull-Off test

The general behaviour of a concrete specimen during a perfectly centric executed Pull-Off test is explained by means of Figure 38. In this explanation the Pull-Off test is assumed to be displacement driven, in order to show the behaviour of the concrete after cracking. In the first step the starting situation is shown. Here the deformations as well as the stresses are zero. In the second step the dolly is subjected to an upward vertical displacement. Because the dolly is glued to the concrete this induces tensile forces to the concrete, resulting in tensile stresses.

When increasing the deformation at a certain deformation ($u = \delta_1$) the tensile strength (f_t) of the concrete is reached. At this point the force that is applied to the concrete has reached its maximum and cracks will appear in the concrete. When increasing the deformation further to step 4 these cracks will grow and depending on the fracture energy the concrete will still be able to distribute stresses. However, the force that can be distributed decreases rapidly. After reaching the ultimate deformation the concrete is fully broken and disconnected from the lower layer (step 5).

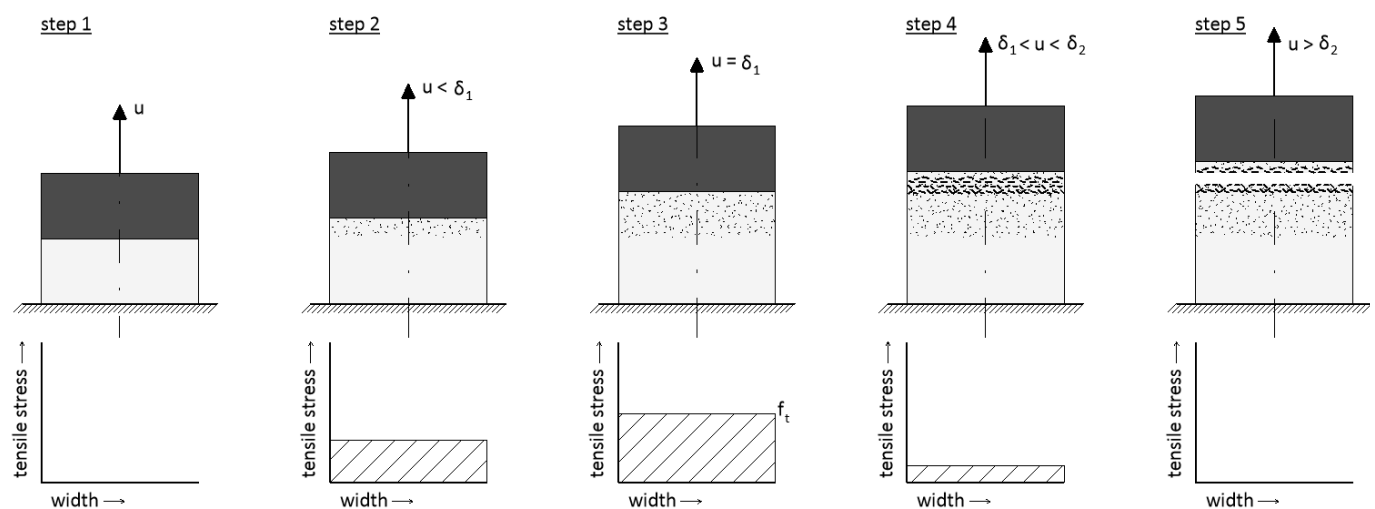


Figure 38: schematisation Pull-Off test executed perfectly centric

Modelling of the Pull-Off test method

In the case that a force is subjected to the dolly with an eccentricity the behaviour is different. In Figure 39 a schematisation of the behaviour is included. In step 1 the starting situation is given, where the deformations as well as the stresses are zero. In this step is indicated that the location where the force grasps to the dolly is at a distance e from the point of gravity of the dolly. In step 2 the deformation (u) is increased and due to the eccentricity the dolly is lifted with an angle to the surface. This causes tensile stresses in the concrete, which increase along the width of the dolly. When increasing the deformation the concrete tensile strength will be reached at the location in the concrete where the deformation are the biggest. In step 3 this location is at the right side direct below the dolly. Because the tensile strength is reached at this location cracks will appear in the concrete. However, the concrete on the left side of this location has not yet reached the tensile strength. Increasing the deformations will cause the concrete to crack at an increasing distance from the right side (step 4). At the locations of the cracks the concrete can distribute a rapidly decreasing amount of stresses, depending on the concretes fracture energy. The total force that can be distributed by the concrete decreases from this point at an increasing deformation. In the end, when the ultimate deformation is reached at all the locations of the concrete, the concrete is fully broken and disconnected from the lower layer (step 5).

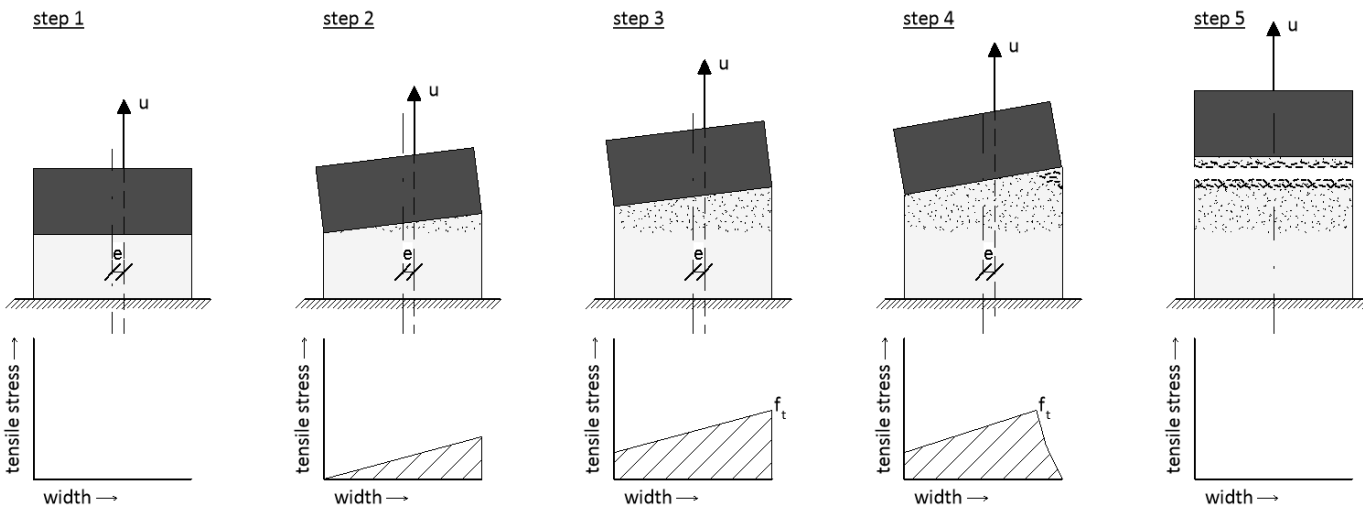


Figure 39: schematisation Pull-Off test executed with eccentricities

As described above the behaviour of concrete subjected to a centric / eccentric grasping tensile force is different. In Figure 40 a force – displacement diagram is included. In this diagram the locations of the steps that are described in of Figure 38 and Figure 39 are indicated with numbers. In this diagram it is clear to see that the maximal tensile force that can be applied to a specimen is reduced when the tensile force grasps eccentrically to the specimen.

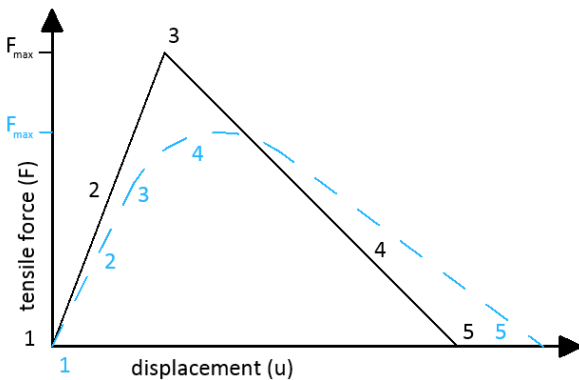
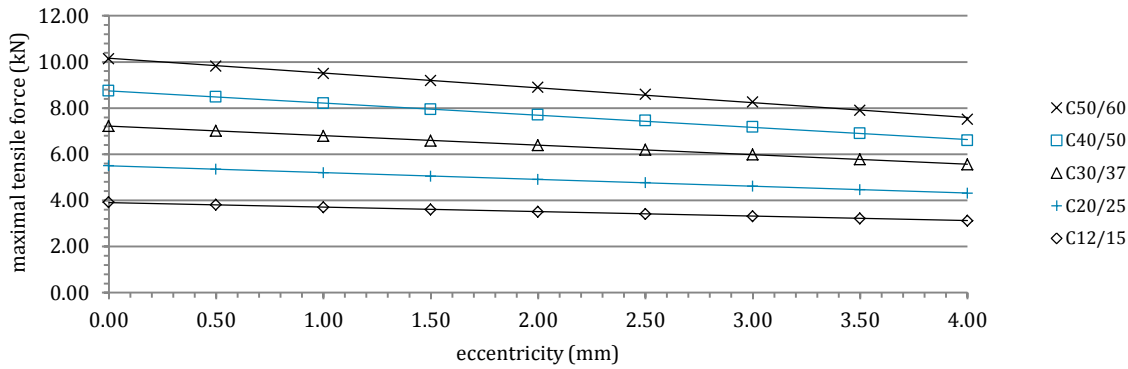


Figure 40: force – displacement diagram for centric (black line) and eccentric (blue hidden line) performed Pull-Off tests

Sub-research 1: concrete class

In the first sub-research the influence of the concrete class on the decrease of maximal tensile force at increasing eccentricity is studied. In Graph 1 the maximal tensile force that can be applied to the dolly at increasing eccentricity is displayed for various concrete classes. From this graph can be concluded that the maximal tensile force decreases when the eccentricity increases. This decrease has a linear relation to the increase of the eccentricity. Table 9 represents the deviation in maximal tensile force when applying an eccentricity of 1 mm. Here it can be found that the maximal tensile force is bigger for higher concrete classes, but the decrease of maximal tensile force per millimetre is bigger as well. This means that the influence of eccentric loading gets more prevailing at higher concrete classes. Overall it can be stated that the decrease of maximal tensile force is 6% per millimetre.



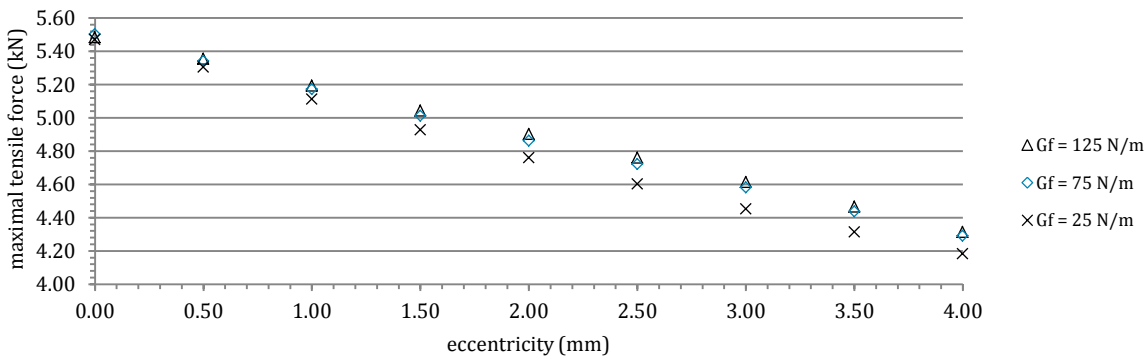
Graph 1: maximal tensile force - eccentricity relation of various concrete classes

Table 9: deviation of maximal tensile force at 1 mm eccentricity of various concrete classes

	C12/15	C20/25	C30/37	C40/50	C50/60
$F_{\max(e=0)}$ (kN)	3.92	5.51	7.23	8.75	10.14
$F_{\max(e=1)}$ (kN)	3.71	5.20	6.80	8.21	9.50
deviation	5.4%	5.7%	6.0%	6.1%	6.3%

Sub-research 2: fracture energy

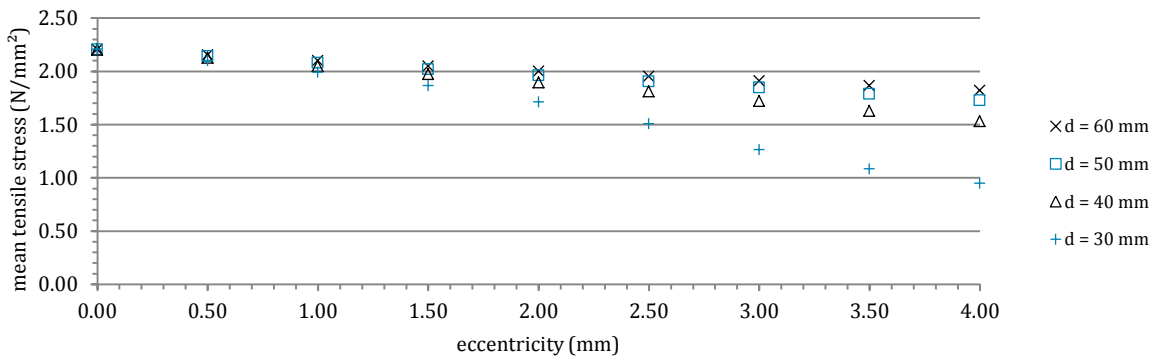
The influence of the concrete fracture energy on the maximal tensile force at eccentric loading is presented in Graph 2. The fracture energy has influence on the decrease of the maximal tensile force. The lower the fracture energy, the bigger the decrease of the maximal tensile force.



Graph 2: maximal tensile force - eccentricity relation of C20/25 concrete with varying fracture energy

Sub-research 3: dolly size

The influence of the dolly size is examined with help of Graph 3. In order to compare the results of the different dolly sizes the maximal tensile force is divided by the area of the dolly surface. The outcome of this represents the maximal mean tensile stress in the specimen. From the graph it is concluded that the size of the dolly has big influence on the maximal mean tensile stress when applying a tensile force eccentric to the dolly. The smaller the dolly, the faster the maximal mean tensile stress decreases when increasing the eccentricity.



Graph 3: maximal mean tensile stress - eccentricity relation of C20/25 concrete with various dolly sizes

Modelling of the Pull-Off test method

Note on the shape of the dolly

In order to simplify the calculations the dolly is assumed with a square shape. In practice the dolly has a cylindrical shape. The difference between the two shapes is that centre of gravity of the cylindrical dolly is more concentrated to the centre. This means that when a dolly is for example not glued to the surface for 5 mm from the edge of the dolly, the centre of gravity will shift less compared to the case of a square dolly (Figure 41). As a result of this it is expected that the influence of eccentricities on the result of the Pull-Off test will be slightly less in the case of a cylindrical dolly.

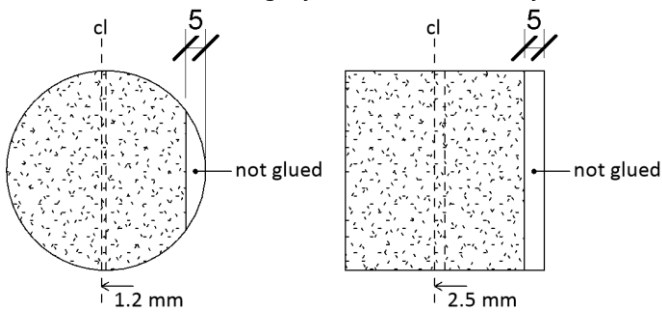


Figure 41: shift of centreline as a result of a not glued surface at 5 mm from the edge for a cylindrical and a square dolly

5.3 FEM approach

5.3.1 Calculation method

In the FEM approach the influence of several parameters on the maximal tensile force is investigated. The calculations of the FEM approach are executed using the FEM software ATENA. The schematisation used for these calculations is given in Figure 42. Specific characteristics of the calculations are summed up below.

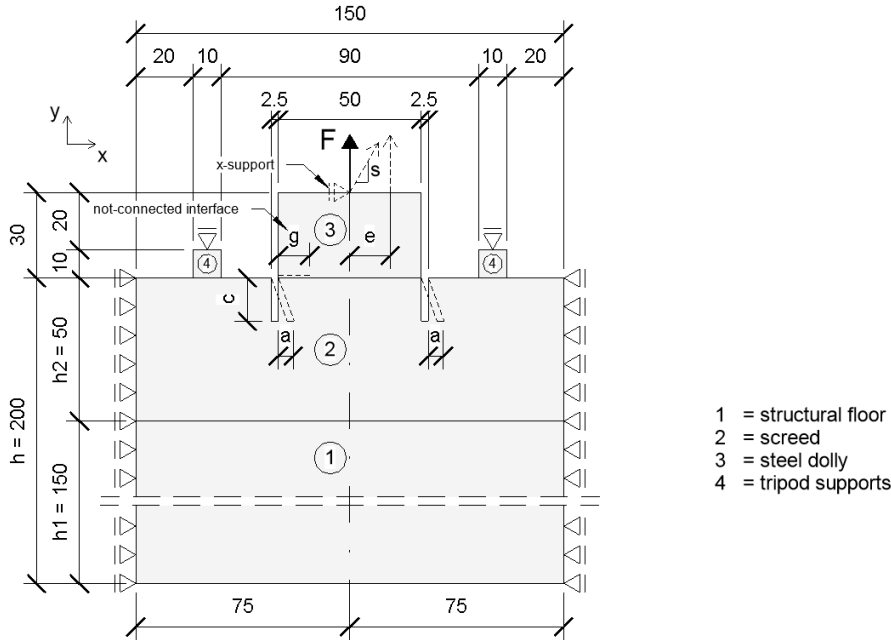


Figure 42: schematisation Pull-Off test used for the FEM approach

- The structure is schematised with 2D elements in a 2D environment. For the thickness of the elements a size of 50 mm is applied;
- In the schematisation the dolly is schematised as a 2D element with a thickness of 50 mm. Hence the shape of the schematised dolly is square. In reality the dolly is a cylinder. The consequences of this schematisation are discussed in sub-section 5.2.2;
- The steel parts (dolly (3) and tripod supports (4)) are modelled as plane stress elastic isotropic elements with Elastic modulus $E = 210,000 \text{ N/mm}^2$ and Poisson's ratio $\nu = 0.3$;
- The concrete parts (structural floor (1) and screed (2)) are modelled as SBeta Material elements, with exponential tension stiffening behaviour. The properties of the concrete parts are given in Table 10;
- The mesh is generated by ATENA as quadrilateral elements with an element size of 2.5 mm. For the structural floor a mesh size of 5 mm is applied.
- The elements are modelled as geometrical nonlinear materials, with element type CCIsoQuad. This element has two translational degrees of freedom: U_x and U_y ;
- As the calculation will be used to research the influence of eccentricities and therefore the reaction of the structure will not be symmetric, it is not possible to make use of axial-symmetric modelling;
- The interfaces are modelled as rigid connections. In one of the sub-researches the influence of a partly glued dolly is investigated. Here the not-glued interface is modelled as a not-connected interface;
- The left and right side of the structure are restrained for deformation in U_x direction;
- The tripod supports are restrained on the top for deformation in U_y direction;
- The load that is applied on the structure exists of a prescribed deformation on top of the steel dolly. In the calculation this prescribed deformation is increased in 40 steps of $1 \cdot 10^{-3} \text{ mm}$;
- The self-weight of the elements is disregarded in the calculation;
- The solutions are calculated by making use of the Newton-Raphson solution method.

Table 10: material properties concrete elements

		f_t (N/mm^2)	f_c (N/mm^2)	E (N/mm^2)	$G_{f;high}$ (N/m)	$G_{f;low}$ (N/m)	ν
Structural floor	C40/50	3.51	40	36,268	147	56	0.2
Screed	C20/25	2.21	20	30,303	133	35	0.2

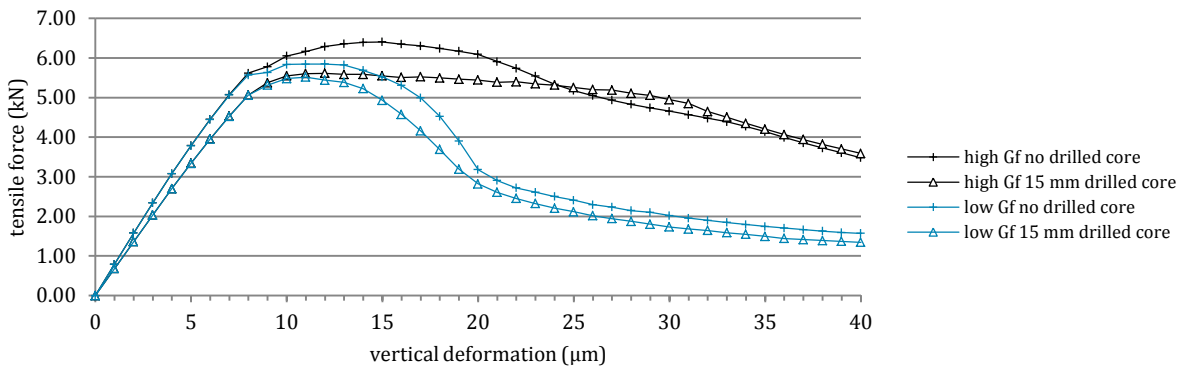
5.3.2 Results and discussion

The influence of several parameters on the maximum tensile force that can be applied to a dolly until the specimen fails is investigated. The results of this research are discussed in this paragraph. The research is divided in several sub-researches, where the influence of the core drilling depth, eccentric applying of the load, diagonal loading, eccentric gluing and diagonal drilling is investigated. In Figure 42 the parameters of the sub-researches are plotted by the dotted lines.

Sub-research 1: variable core drilling depths

In the standards available for the Pull-Off tests the value of the depth of the drilled core varies from 0 to 25 mm (chapter 4.3). In order to make a decision what core drilling depth has to be applied to achieve the best results at the Pull-Off test the influence of the core drilling depth on the maximal tensile force is investigated with help of ATENA. In Graph 4 the tensile force – deformation diagram is included of situations with no / 15 mm drilled cores with low and high fracture energy. In this graph it can be seen that the fracture has no significant influence on the situation with a drilled core. Yet the situation in case of a plane surface is influenced by the fracture energy. In the case of high fracture energy the maximal tensile force that can be applied to the specimen is increased with 10% compared to the situation with low fracture energy.

Table 11 shows the maximal tensile force at core drilling depths of 0 to 30. The theoretical tensile force is included in this table as well to observe the deviation of the test with the theoretical tensile force. This value is achieved by multiplying the tensile strength of the specimen ($f_t = 2.21 \text{ N/mm}^2$) with the area of the square dolly (50x50mm).



Graph 4: tensile force – deformation diagram at no / 15 mm drilled cores, variable fracture energy

Table 11: maximal tensile force at various core drilling depths and their deviation from the theoretical force

	$F_{\text{theoretical}}$ (kN)	$F_{\text{max}(d=0)}$ (kN)	$F_{\text{max}(d=5)}$ (kN)	$F_{\text{max}(d=10)}$ (kN)	$F_{\text{max}(d=15)}$ (kN)	$F_{\text{max}(d=20)}$ (kN)	$F_{\text{max}(d=30)}$ (kN)
low FE	5.53	5.85	5.46	5.46	5.52	5.51	5.52
deviation		5.8%	1.2%	1.2%	0.1%	0.3%	0.1%
high FE	5.53	6.41	5.81	5.65	5.61	5.61	5.60
deviation		16.0%	5.2%	2.3%	1.6%	1.6%	1.4%

From the results it is concluded that applying a tensile force to a dolly glued to a plane surface without a drilled core gives a big deviation from the theoretical value. For a specimen with low fracture energy this deviation is 5,8%, for specimen with high fracture energy this is 16%. The deviation is caused by the fact that the tensile force from the glued dolly is distributed to a bigger surface than when a drilled core is applied. This enables the dolly to be loaded with a bigger tensile force before the specimen fails (Figure 43 and Figure 44).

Furthermore it can be seen that the fracture energy influences the deviation. When the specimen has larger fracture energy the deviation increases. This is due to the fact that the concrete has more capacity left after cracking what makes that the forces are distributed to a bigger area of the concrete, increasing the maximal tensile force before failing (Figure 45 and Figure 46).

The maximum tensile force almost reaches the theoretical tensile force at a minimum core drilling depth of 15 mm. Applying a bigger depth does not significantly decrease the deviation for both the specimen with high and low fracture energy. From this it can be concluded that the minimal core drilling depth has to be 15 mm to obtain the best results, given that concrete is an uniform material. In practice concrete is a composite material what makes that the properties are hardly ever uniform. Differences in for example stiffness, strength and sizes of the composed materials like aggregates can cause the results of the research above to be different in practice.

Step 10, Pull off test no drilled core low Gf
 Scalars isolines + cuts:, Basic material, in nodes, Principal Total Strain, Max., <-1.797E-05;1.343E-03>[None]
 Cracks: in elements, Opening: <4.609E-09;5.047E-06>[m], SigmaN: <1.443E+00;2.088E+00>[MPa], SigmaT: <-1.195E+00;1.195E+00>[MPa]

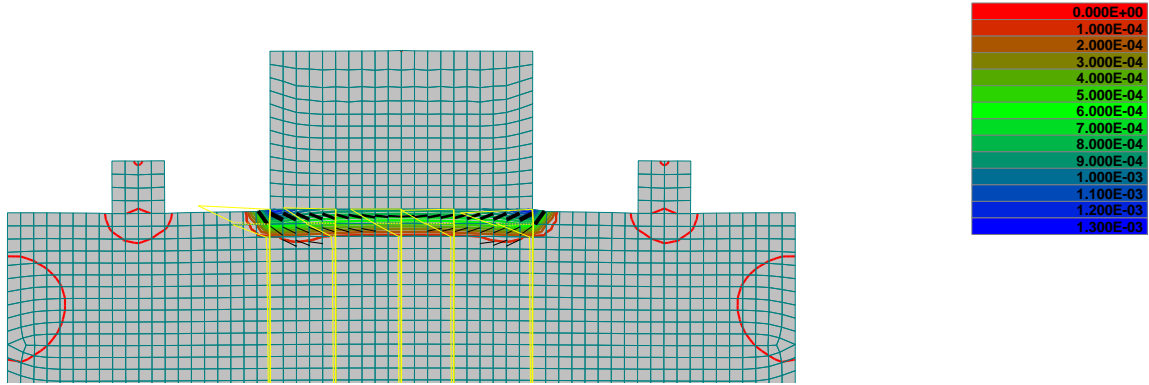


Figure 43: principal total strain and crack formation for specimen with low G_f at maximal tensile force ($u_y = 10 \mu\text{m}$), plane surface

Step 10, Pull off test 15 mm drilled core low Gf
 Scalars isolines + cuts:, Basic material, in nodes, Principal Total Strain, Max., <-1.844E-05;7.692E-04>[None]
 Cracks: in elements, Opening: <2.893E-10;4.440E-06>[m], SigmaN: <1.060E+00;2.210E+00>[MPa], SigmaT: <-4.114E-01;3.899E-01>[MPa]

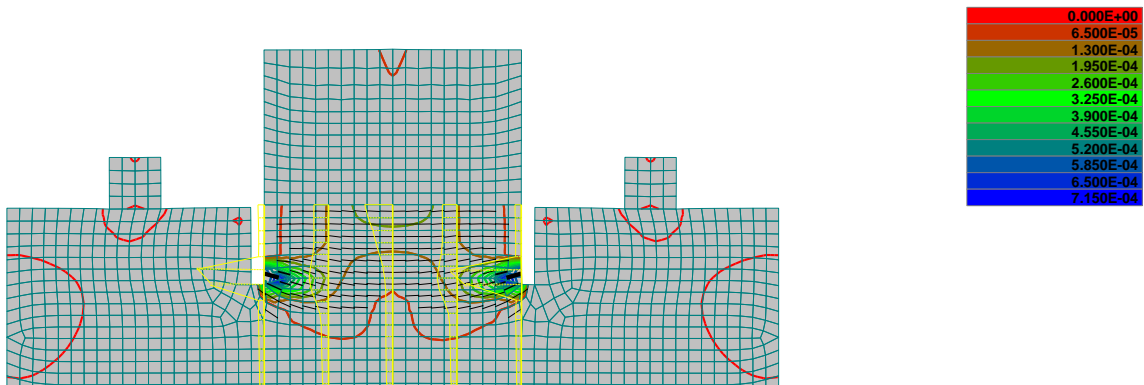


Figure 44: principal total strain and crack formation for specimen with low G_f at maximal tensile force ($u_y = 10 \mu\text{m}$), 15 mm drilled core

Step 14, Pull off test no drilled core high Gf
 Scalars isolines + cuts:, Basic material, in nodes, Principal Total Strain, Max., <-2.295E-05;2.147E-03>[None]
 Cracks: in elements, Opening: <2.341E-09;7.968E-06>[m], SigmaN: <1.848E+00;2.209E+00>[MPa], SigmaT: <-1.560E+00;1.560E+00>[MPa]

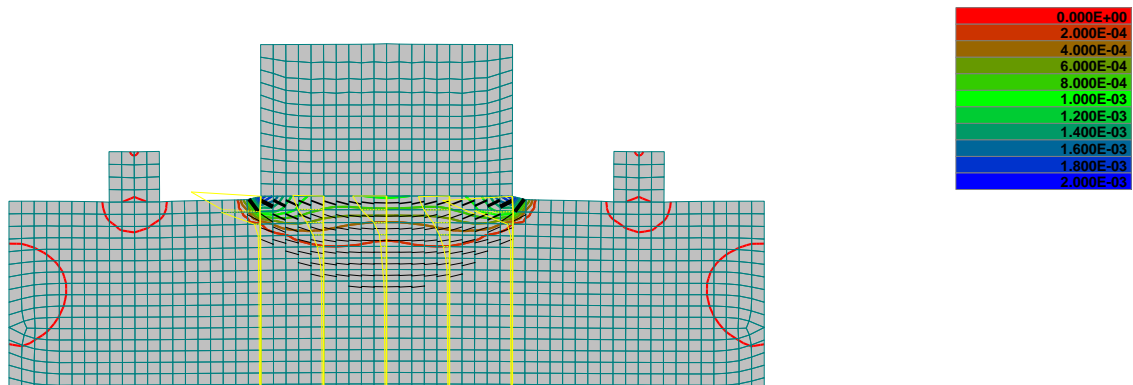


Figure 45: principal total strain and crack formation for specimen with high G_f at maximal tensile force ($u_y = 14 \mu\text{m}$), plane surface

Step 10, Pull off test 15 mm drilled core high Gf
 Scalars isolines + cuts:, Basic material, in nodes, Principal Total Strain, Max., <-1.917E-05;6.326E-04>[None]
 Cracks: in elements, Opening: <2.239E-10;3.641E-06>[m], SigmaN: <1.564E+00;2.210E+00>[MPa], SigmaT: <-3.297E-01;3.270E-01>[MPa]

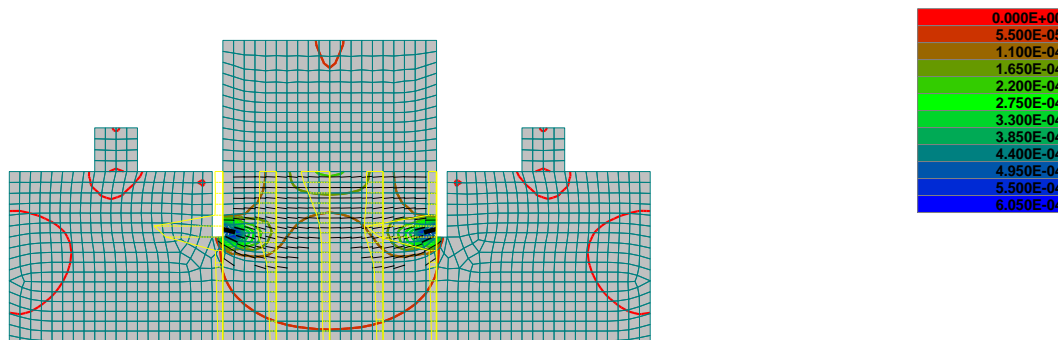
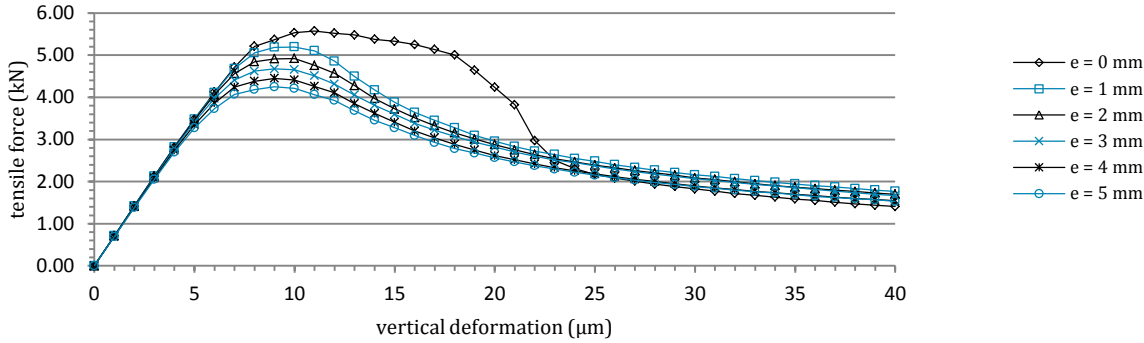


Figure 46: principal total strain and crack formation for specimen with high G_f at maximal tensile force ($u_y = 10 \mu\text{m}$), 15 mm drilled core

Sub-research 2: eccentric loading

In chapter 5.1 the influence of eccentric applying of the tensile force is investigated by an analytical approach with a parameter study. In order to validate the results of this research the influence of eccentricities is investigated by the FEM approach as well. The results of this research are presented in Graph 5. As the results of the analytical study have shown, the maximal tensile force decreases when applying a tensile force eccentric to the dolly.

The results of the FEM approach with a drilled core of 15 mm deep are compared to the results of the analytical approach in Table 12. As the maximum deviation between both results is <1.2% it is concluded that the calculations made in the analytical approach give proper results.



Graph 5: tensile force – eccentricity relation Pull-Off test

Table 12: comparison of results FEM and Analytical approach

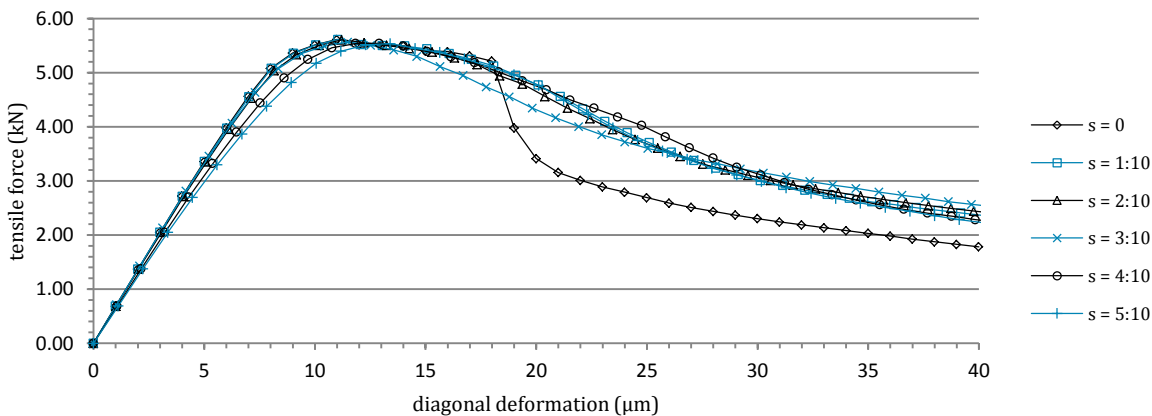
	$F_{max}(e=0mm)$ (kN)	$F_{max}(e=1mm)$ (kN)	$F_{max}(e=2mm)$ (kN)	$F_{max}(e=3mm)$ (kN)	$F_{max}(e=4mm)$ (kN)
FEM approach	5.58	5.20	4.92	4.67	4.45
Analytical approach	5.51	5.21	4.93	4.68	4.43
deviation	1.18%	0.32%	0.27%	0.12%	0.52%

Sub-research 3: diagonal loading

When executing the Pull-Off test especially on a rough surface it is possible that the tripod will not be placed in a place precisely above, or not perpendicular to the dolly (Figure 30 section 4.3). When applying the tensile force in this situation, the dolly will be loaded by a force at an angle not equal to 90° to the surface. The influence of diagonal applying of the tensile force is displayed in Graph 6 and Table 13.

. In the table the deviation of the maximal tensile force applied at a slope (s) compared to a precisely perpendicular applied tensile force is presented as well.

In the case that a diagonal load is applied to the specimen, stresses will concentrate on the tip of the drilled core in an early stadium (Figure 47). Because the tensile force does not only have a component in u_y direction but also in u_x direction, stresses will increase in u_x direction as well. The stress concentration will cause the specimen to start failing at a lower tensile force (Figure 48). Yet the decrease in maximal tensile force however is not big due to the fact that the failing mechanism transforms from purely tension to shear-tension. The maximal force at a slope of 5:10 has a deviation of 1.4% from the perpendicular situation.



Graph 6: maximal tensile force per diagonal loading slope

Table 13: maximal tensile force per diagonal loading slope

	$F_{\max(s=0)}$ (kN)	$F_{\max(s=1:10)}$ (kN)	$F_{\max(s=2:10)}$ (kN)	$F_{\max(s=3:10)}$ (kN)	$F_{\max(s=4:10)}$ (kN)	$F_{\max(s=5:10)}$ (kN)
max. tensile force	5.61	5.61	5.61	5.57	5.54	5.53
deviation		0.0%	0.1%	0.8%	1.3%	1.4%

Step 6, Pull off test 15 mm drilled core
 Scalars isolines + cuts: Basic material, in nodes, Principal Total Strain, Max., <-1.348E-05;2.320E-04>[None]
 Cracks: in elements, Opening: <-3.932E-10;1.256E-06>[m], SigmaN: <-1.960E+00;2.210E+00>[MPa], SigmaT: <-5.660E-02;1.092E-01>[MPa]

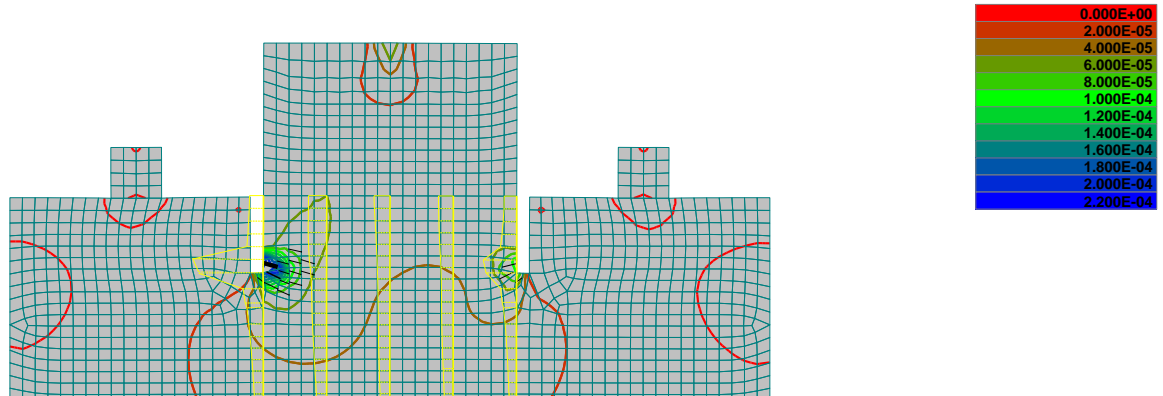


Figure 47: principal total strain and crack formation for a diagonal loaded specimen ($s = 2:10$) at $u_y = 6 \mu\text{m}$

Step 12, Pull off test 15 mm drilled core
 Scalars isolines + cuts: Basic material, in nodes, Principal Total Strain, Max., <-1.938E-05;1.374E-03>[None]
 Cracks: in elements, Opening: <-3.219E-09;8.037E-06>[m], SigmaN: <-8.870E-01;2.208E+00>[MPa], SigmaT: <-4.519E-01;5.394E-01>[MPa]

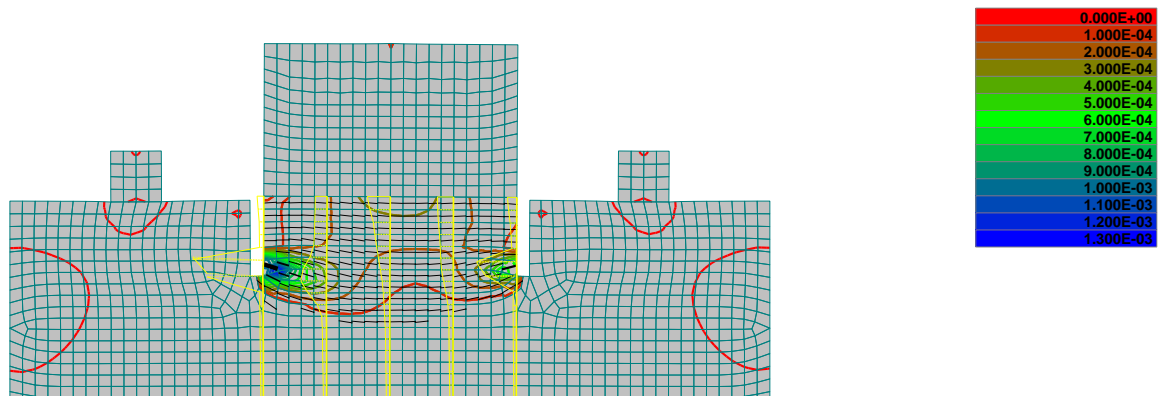


Figure 48: principal total strain and crack formation for a diagonal loaded specimen ($s = 2:10$) at maximal pulling force ($u_y = 12 \mu\text{m}$)

Sub-research 4: eccentric gluing

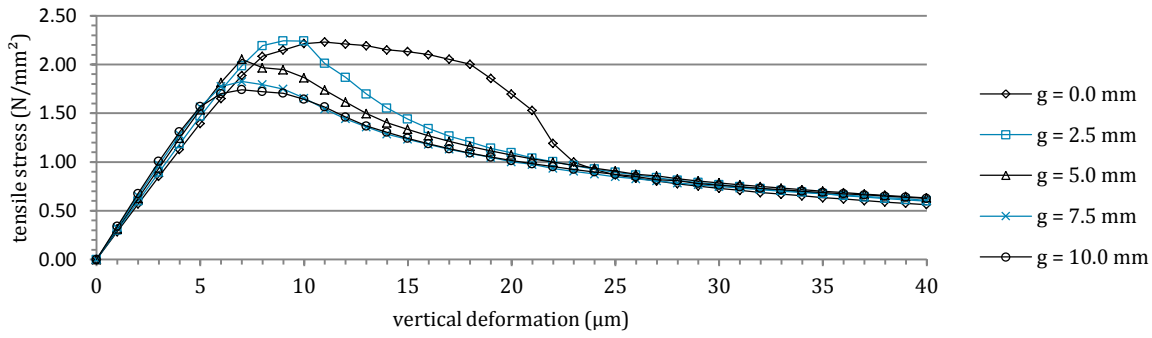
When executing the Pull-Off test there is a risk that the dolly will not be equally glued over the full surface area. Causes for this problem can be that dust was present at the concrete surface, the dolly was partly glued to weak spots of the concrete or the glue did not touch the surface (especially at rough surfaces this risk is present). A partly glued dolly will cause the tensile force to be distributed to the specimen with eccentricity. The influence of this eccentricity is investigated in this sub-research.

No support in x-direction

The research involves two schematisations. In the first schematisation the tensile force is applied to the eccentric glued dolly without supporting the dolly in x-direction. In order to compare the results of the partly glued dollies equally, the maximal tensile force is divided by the glued area, representing the mean maximal tensile stress of the specimen. The results of the ATENA calculations are shown in Graph 7 and Table 14. The graph shows that partly gluing the dolly will decrease the mean maximal tensile stress. This tensile stress decreases further as the not-connected interface increases.

When the dolly is not-connected to the surface for 5 mm from the edge of the dolly (a decrease of 10% of the glued surface) the mean maximal tensile stress decreases with 8%. In the first deformation steps the specimen cracks at the location of the tip of the drilled core, equal to the regular situation (Figure 49). After the formation of the first cracks the stresses are redistributing and a stress concentration arises at the interface between the dolly and the concrete specimen. Finally the specimen fails around this interface (Figure 50).

Modelling of the Pull-Off test method



Graph 7: maximal mean tensile stress for eccentric glued dollies

Table 14: maximal mean tensile stress with partly glued dollies

	$\sigma_m(g=0mm)$ (N/mm ²)	$\sigma_m(g=2.5mm)$ (N/mm ²)	$\sigma_m(g=5mm)$ (N/mm ²)	$\sigma_m(g=7.5mm)$ (N/mm ²)	$\sigma_m(g=10mm)$ (N/mm ²)
max. tensile stress	2.23	2.24	2.05	1.82	1.74
deviation		0.5%	8.0%	18.2%	22.0%

Step 6, Pull off test 15 mm drilled core
 Scalars isolines + cuts: Basic material, in nodes, Principal Total Strain, Max., <-1.325E-05;1.506E-04>[None]
 Cracks: in elements, Opening: <3.922E-09;6.164E-07>[m], SigmaN: <2.138E+00;2.208E+00>[MPa], SigmaT: <-8.492E-02;5.580E-02>[MPa]

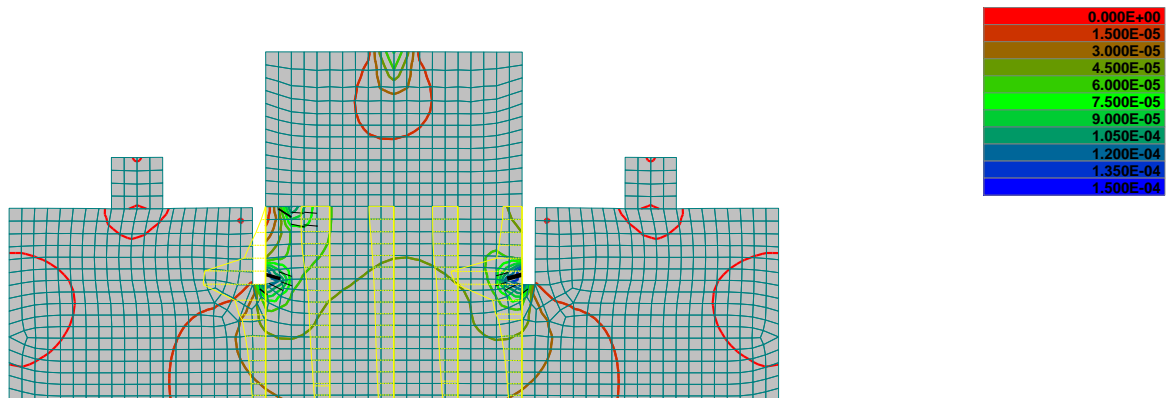


Figure 49: principal total strain and crack formation for a partly glued specimen ($g = 5 \text{ mm}$) at $u_y = 6 \text{ }\mu\text{m}$

Step 12, Pull off test 15 mm drilled core
 Scalars isolines + cuts: Basic material, in nodes, Principal Total Strain, Max., <-1.215E-05;4.891E-03>[None]
 Cracks: in elements, Opening: <2.998E-10;1.516E-05>[m], SigmaN: <1.167E+00;2.183E+00>[MPa], SigmaT: <-4.158E-01;3.606E-01>[MPa]

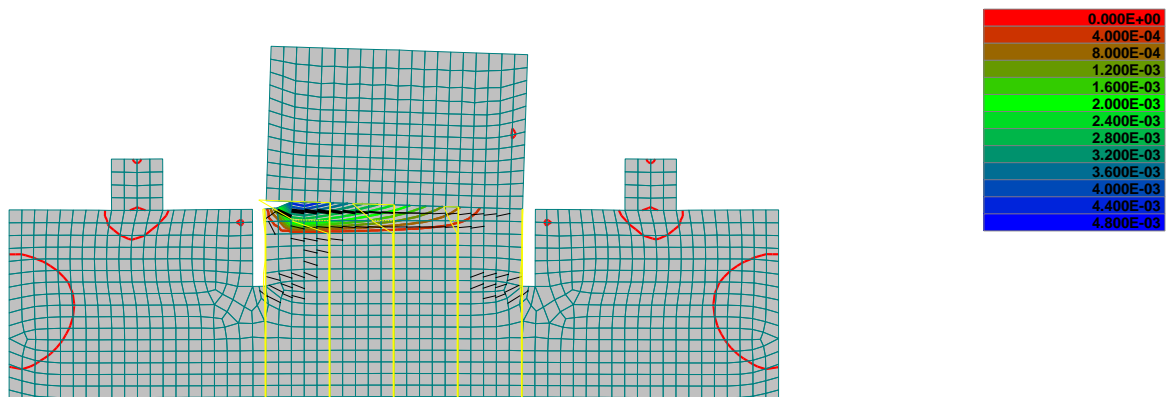


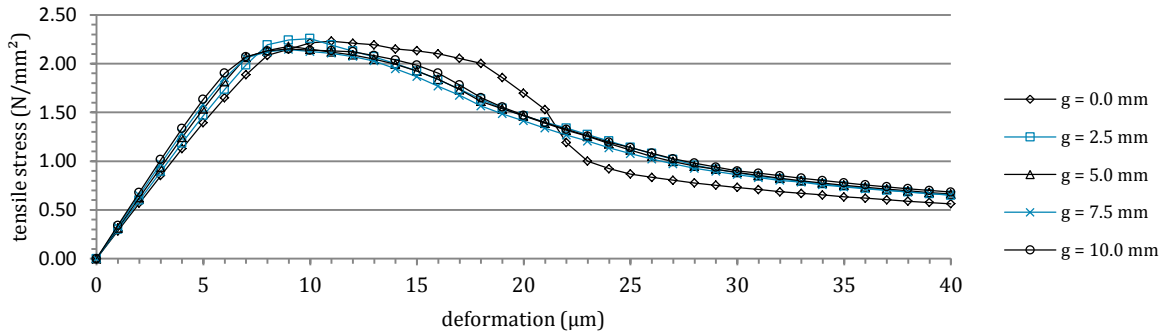
Figure 50: principal total strain and crack formation for a partly glued specimen ($g = 5 \text{ mm}$) at $u_y = 12 \text{ }\mu\text{m}$

Supported in x-direction

The second schematisation involves the situation where the dolly is restrained from moving in x-direction at the location where the tensile force attaches to the dolly. The results of the ATENA calculations are shown in Graph 8 and Table 15. Also in this situation the mean maximal tensile stress decreases when the not-connected interface increases. However the decrease is significantly smaller compared to the situation of no support in x-direction.

When the dolly is not-connected to the surface for 5 mm from the edge of the dolly (a decrease of 10% of the glue surface) the mean maximal tensile stress decreases with 2.4%. The decrease in case of a support in x-direction is

smaller because the dolly will rotate less than in case of no support in x-direction. Because of this the tensile force will be more equally distributed in u_y direction, causing a more gradual distribution of the tensile stresses. In Figure 52 it can be seen that the forces are distributed over a bigger area, as there are more cracked elements visible compared to the not-supported situation in Figure 50.



Graph 8: maximal mean tensile stress for eccentric glued dollies, supported in x-direction

Table 15: maximal mean tensile stress with partly glued dollies, supported in x-direction

	$\sigma_m(g=0 \text{ mm})$ (N/mm ²)	$\sigma_m(g=2.5 \text{ mm})$ (N/mm ²)	$\sigma_m(g=5 \text{ mm})$ (N/mm ²)	$\sigma_m(g=7.5 \text{ mm})$ (N/mm ²)	$\sigma_m(g=10 \text{ mm})$ (N/mm ²)
max. tensile stress	2.23	2.26	2.18	2.14	2.15
deviation		1.1%	2.4%	3.9%	3.6%

Step 6, Pull off test 15 mm drilled
 Scalars isolines + cuts: Basic material, in nodes, Principal Total Strain, Max., <-1.328E-05;1.582E-04>[None]
 Cracks: in elements, Opening: <-1.830E-09;6.774E-07>[m], SigmaN: <-2.132E+00;2.209E+00>[MPa], SigmaT: <-8.787E-02;5.507E-02>[MPa]

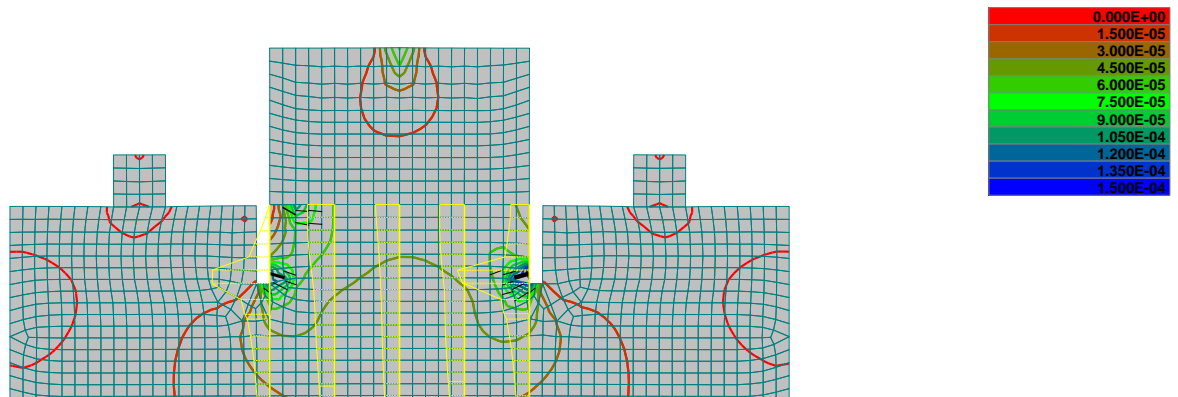


Figure 51: principal total strain and crack formation for a partly glued specimen ($g = 5 \text{ mm}$) at $u_y = 6 \text{ µm}$, x-supported

Step 20, Pull off test 15 mm drilled
 Scalars isolines + cuts: Basic material, in nodes, Principal Total Strain, Max., <-1.244E-05;7.568E-03>[None]
 Cracks: in elements, Opening: <-4.680E-08;2.133E-05>[m], SigmaN: <-4.968E-01;2.204E+00>[MPa], SigmaT: <-6.202E-01;7.130E-01>[MPa]

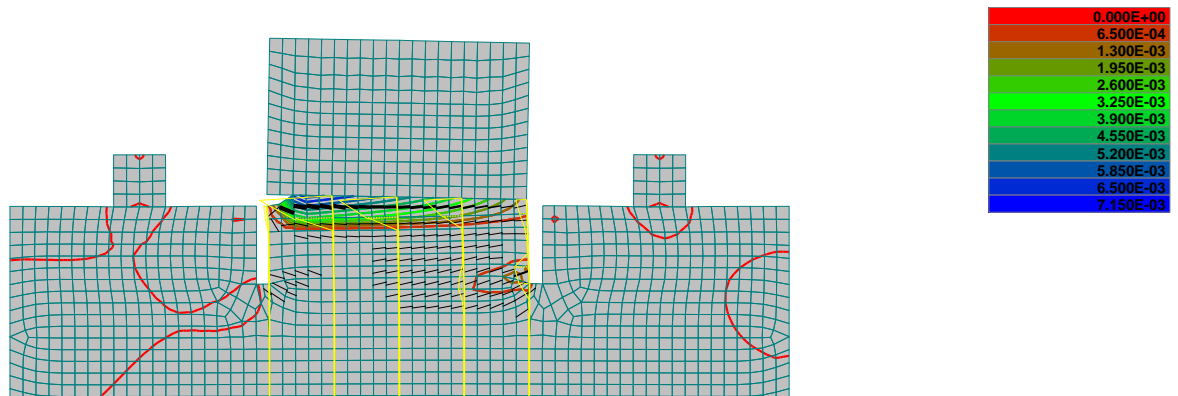


Figure 52: principal total strain and crack formation for a partly glued specimen ($g = 5 \text{ mm}$) at $u_y = 20 \text{ µm}$, x-supported

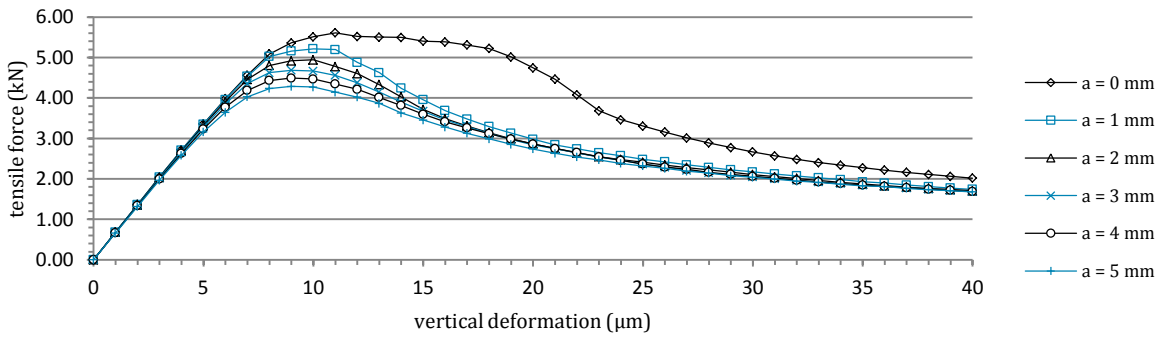
In sub-research 4 the influence of partly glued dollies is investigated. This research is split up in two situations, with and without restraining the dolly in x-direction. From the research it is concluded that partly connecting of the dolly to the specimen has big influence on the mean maximal tensile stress that can be measured. In practice the dolly will not be fully supported in x-direction by the tripod, but a certain restraining for displacements in x-direction will be present. This implies that the decrease in mean maximal tensile stress will be somewhere in between the two situations.

Sub-research 5: diagonal drilling

When the core is not drilled precisely perpendicular to the surface the maximal tensile force will be influenced (Figure 30 chapter 4.3). This influence is investigated in sub-research 5. The results of the ATENA calculations are presented in Graph 9 and Table 16. The research is again executed by schematising the situation with and without supporting the dolly in x-direction.

The maximal tensile force decreases almost linearly to an increasing eccentricity (a) for both situations. In the case of a 2 mm diagonal drilled core, what corresponds to an angle of 7.6° , the deviation of maximal tensile force is between 2.9% and 11.9%. Because the centreline of the dolly deviates from the centreline of the specimen at the location of the drilled core, the tensile force is distributed with eccentricities to the specimen. This causes an increased stress concentration at the location of the tip of the drilled core (Figure 53), causing the specimen to split open from this location.

When restraining the dolly to move in u_x direction the rotation of the dolly will be smaller, equal to the situation of an eccentric glued dolly. This causes the tensile force to be distributed more equally over the drilled core so the stress concentration decreases compared to the not-supported situation (Figure 54), leading to a bigger maximal tensile force.



Graph 9: maximal tensile force Pull-Off test with diagonal drilled cores, no support in x-direction

Table 16: maximal tensile force Pull-Off test with diagonal drilled cores

	$F_{\max(a=0)}$ (kN)	$F_{\max(a=1)}$ (kN)	$F_{\max(a=2)}$ (kN)	$F_{\max(a=3)}$ (kN)	$F_{\max(a=4)}$ (kN)	$F_{\max(a=5)}$ (kN)
no support in x deviation	5.61	5.22 7.0%	4.94 11.9%	4.69 16.5%	4.49 19.9%	4.29 23.6%
supported in x deviation	5.61	5.51 1.8%	5.45 2.9%	5.28 6.0%	5.05 10.1%	5.00 11.0%

Step 10, Pull off test 15 mm drilled core
 Scalars isolines + cuts:, Basic material, in nodes, Principal Total Strain, Max., <-1.733E-05;1.657E-03>[None]
 Cracks: in elements, Opening: <8.072E-10;9.156E-06>[m], SigmaN: <8.737E-01;2.210E+00>[MPa], SigmaT: <-1.888E-01;4.224E-01>[MPa]

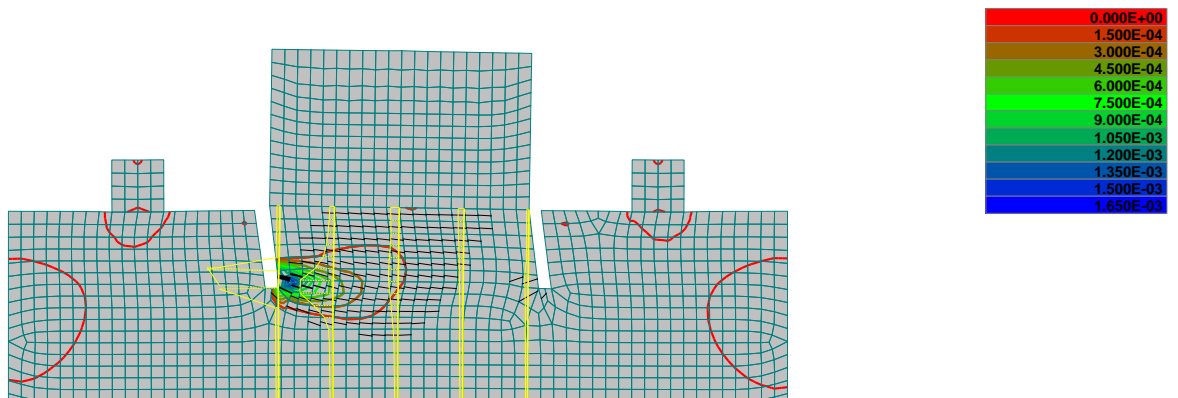


Figure 53: principal total strain and crack formation at maximal tensile force for a 2 mm diagonal, 15 mm drilled core, no support in x-direction

Step 10, Pull off test 15 mm drilled core
 Scalars isolines + cuts: Basic material, in nodes, Principal Total Strain, Max., <-1.873E-05;7.330E-04>[None]
 Cracks: in elements, Opening: <1.314E-09;3.973E-06>[m], SigmaN: <1.229E+00;2.209E+00>[MPa], SigmaT: <-4.476E-01;3.449E-01>[MPa]

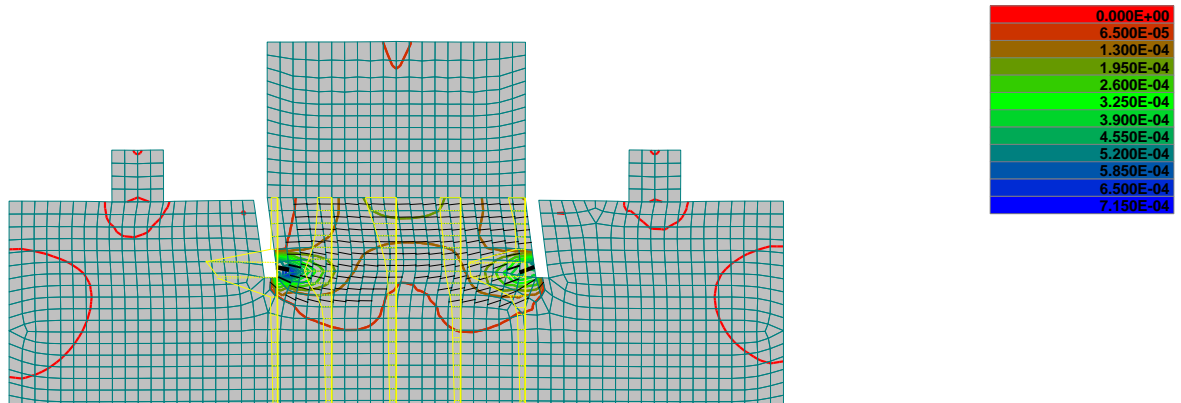


Figure 54: principal total strain and crack formation at maximal tensile force for a 2 mm diagonal, 15 mm drilled core, supported in x-direction

5.4 Review

In this chapter the influence of eccentricities on the results of the Pull-Off tests was studied by means of an analytical approach and a FEM study. The analytical approach consisted of a parametric study where the influence of applying eccentric tensile forces to a concrete specimen was analysed with varying concrete classes, concrete fracture energy and dolly size.

When applying an eccentric tensile force to a concrete specimen, the maximal load that can be distributed by the concrete is lower than in case of a perfectly orthogonal tensile force. The maximal tensile force decreases according to the analytical analysis linearly when increasing the eccentricity. The decrease of maximum force has a small increase when applying a higher concrete class but overall can be stated that the decrease is around 6% per millimetre eccentricity. This decrease is increased when the concrete contains smaller fracture energy.

Different dolly sizes were examined in the research. From this research it is concluded that a decrease of the dolly size has a big influence on the deviation of the results when applying eccentric tensile forces (especially at dolly sizes with diameter <40 mm). The difference in results of dollies with diameter >50 mm are relatively small (2% at an eccentricity of 2 mm). A dolly size with diameter $d = 50$ mm is maintained for the rest of the research.

In the FEM study Pull-Off tests are modelled in the FEM program ATENA. Here the influence of the depth of the drilled cores, diagonal loading, eccentric gluing and diagonal drilling is analysed. From the analysis it is concluded that applying no drilled core gives a big deviation on the maximal to be applied tensile force compared to the theoretical value. Depending on the fracture energy of the concrete this deviation is 5.8% - 16%. The theoretical value of the maximal to be applied tensile force is found in a better way when applying a drilled core of minimal 15 mm in the concrete. For drilled cores with a depth ≥ 15 mm deviations are found of 0.1% and 1.6% for concrete with low and high fracture energy. A drilled core of 15 mm is maintained for the rest of the research.

Diagonal loading does not directly lead to a decrease of the maximal pulling force, but it does lead to stress concentrations at the tip of the drilled cores in an early stadium. Because of this cracks will appear in an earlier stadium. However, because the pulling force has a horizontal component shear stresses will occur in the concrete as well, causing the result of the pulling test not to be representing the pure tensile strength.

Partly, eccentric gluing has a big influence on the results of the Pull-Off tests. Besides the fact that the pulling force is distributed to a smaller area of the concrete, the force is distributed with eccentricity to the specimen. This causes the plane of failure to be at the glued surface instead of the tip of the drilled core. The decrease in maximal pull off force gets up to 8% for a 5 mm not-glued dolly, increasing to maximal 22% for a 10 mm not glued dolly.

Diagonal drilling causes an increased stress concentration at the tip of the diagonal drilled core. This induces the concrete to split up from this location, resulting in lower pull off forces. The deviation can get up to 11.9% for a drilled core with a deviated angle of 7.6° . By increasing the angle the deviation increases almost linearly.

6. Modelling of shrinkage effects in screeds

6.1 Introduction

Shrinkage differences between bonded screeds and the bearing floor causes stresses at the interface and in the layers itself. In section 2.5 the causes of screed shrinking and the development of stresses in the adhesive surface are already explained. When the stresses in the screed and in the adhesive surface reach the strength of the bond / the screed debonding / cracking will occur. In this chapter the influence of different parameters on the distribution of stresses at the interface and in the screed is studied by means of an analytical approach (section 6.2) and a FEM study (section 6.3).

6.2 Analytical approach

6.2.1 Calculation method

In the analytical approach the effect of shrinkage differences between a screed and bearing floor on the stresses at the interface and in the screed is investigated. In paragraph 2.5.3 different formulas are derived for the shear stress at the interface and the mean tensile stress in the screed. The formulas that are used in the analytical approach are included in (22) and (23). A schematisation of the shrinkage model that is used for the analysis is included in Figure 55.

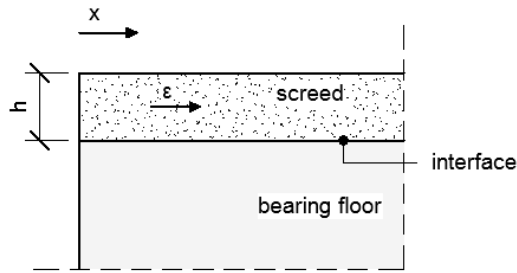


Figure 55: schematisation shrinkage model used for the analytical approach

$$\tau(x) = \varepsilon \sqrt{k * E * h} * \frac{\sinh\left(\sqrt{\frac{k}{E * h}} * \left(\frac{L}{2} - x\right)\right)}{\cosh\left(\sqrt{\frac{k}{E * h}} * \frac{L}{2}\right)} \quad (22)$$

$$\sigma(x) = \varepsilon * E * \left(1 - \frac{\cosh\left(\sqrt{\frac{k}{E * h}} * \left(\frac{L}{2} - x\right)\right)}{\cosh\left(\sqrt{\frac{k}{E * h}} * \frac{L}{2}\right)}\right) \quad (23)$$

Where:

- $\tau(x)$ is the shear stress at a distance x from the edge of the bonded surface (N/mm^2);
- $\sigma(x)$ is the mean tensile stress in the screed at a distance x from the edge of the bonded surface (N/mm^2);
- ε is the shrinkage/ deformation difference between the screed and substrate (mm/mm);
- k is the resistance of the substrate against horizontal shifting of the screed (N/mm^3);
- E is the young's modulus of the screed (N/mm^2);
- h is the thickness of the screed (mm);
- L is the length of the floor or the length between two cracks (mm).

Input variables

The variables that are used for the input of the calculation exist of material and geometrical parameters. The parameters applied in the calculations are included in Table 17.

Table 17: parameters applied in analytical approach

Parameter		Value	
Screed shrinkage	ε	0.1	‰
Screed height	h	50	mm
Specimen length	L	1000	mm
Interface shear stiffness	k	50	N/mm^3
Screed stiffness	E	30.000	N/mm^2

6.2.2 Results and discussion

The influence of screed shrinkage on the development of stresses in the screed and in the interface between bearing floor and screed is analysed in a parameter study. The research is divided in several sub-researches, where the influence of the screed thickness, screed stiffness and interface stiffness is investigated. In this paragraph the results of the sub-researches are discussed. Important is to note that there is no concrete tensile strength / bond strength taken into account in the calculations. The results that are shown are purely used to analyse the stress distribution due to shrinkage over the length of a screed.

Sub-research 1: variable screed thickness

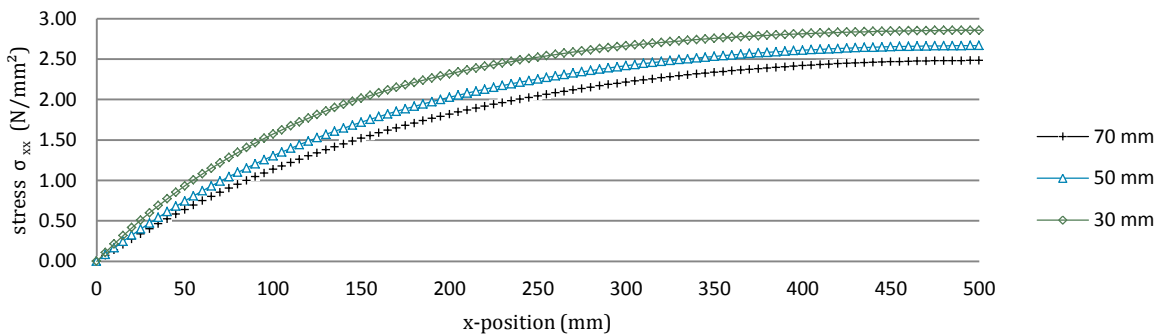
In Graph 10 the horizontal stress that arises due to a 0.1‰ shrinkage difference between the screed and bearing floor is shown for variable screed thicknesses. In this graph it can be seen that the horizontal stress develops from zero at the edge of the floor to a constant maximal value that reached around 450 mm from the edge. The maximal value of the stress differs for the different screed thicknesses. An increasing screed thickness gives a lower horizontal stress in the screed. This is due to the fact that the area of restraint is in percentage of the screed volume smaller at thicker screeds. Because of less restraint the screed is more free to deform at increasing height from the interface, causing a lower stress at the top of the screed. Because the stress that is shown in Graph 10 is a mean stress over the screed height this results in a lower mean stress.

Graph 11 shows the interface shear stresses at 0.1‰ screed shrinkage. The shear stress has a maximal value at the edge of the floor and decreases at increasing distance from the edge to zero. In this graph it can be seen that the screed thickness influences the maximum value of the shear stress. A thicker screed induces bigger interface shear stresses at the edge of the floor. Because the area that is enforced to shrink is bigger at thicker screeds the horizontal force that works on the interface has a higher value (formula (24)). This induces bigger shear stresses at the interface. An increase of 20 mm in screed thickness increases the maximum tensile stress with 0.15 N/mm².

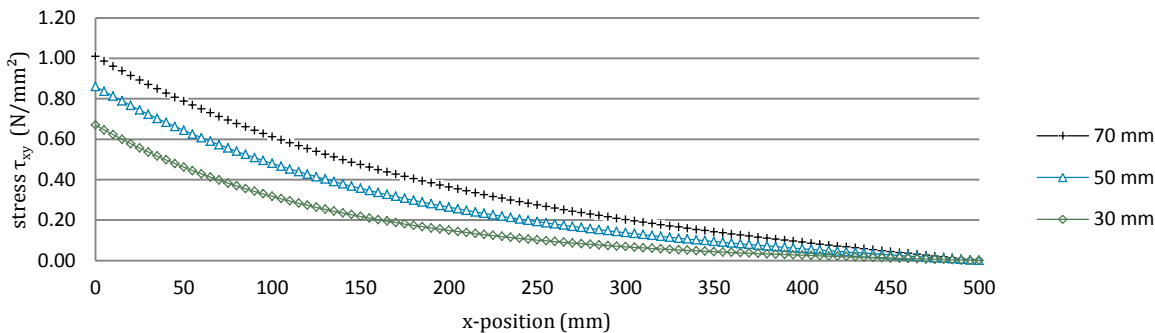
$$N_{int} = A_{sr} * \epsilon * E \tag{24}$$

Where:

- N_{int} is the shear force that works on the interface (N);
- A_{sr} is the screed area over the section that is restrained to deform (mm);
- ϵ is the amount of shrinkage (mm/mm);
- E is the Young's modulus of the screed (N/mm²);



Graph 10: horizontal screed stresses at 0.1‰ shrinkage difference, variable screed thickness



Graph 11: interface shear stresses at 0.1‰ shrinkage difference, variable screed thickness

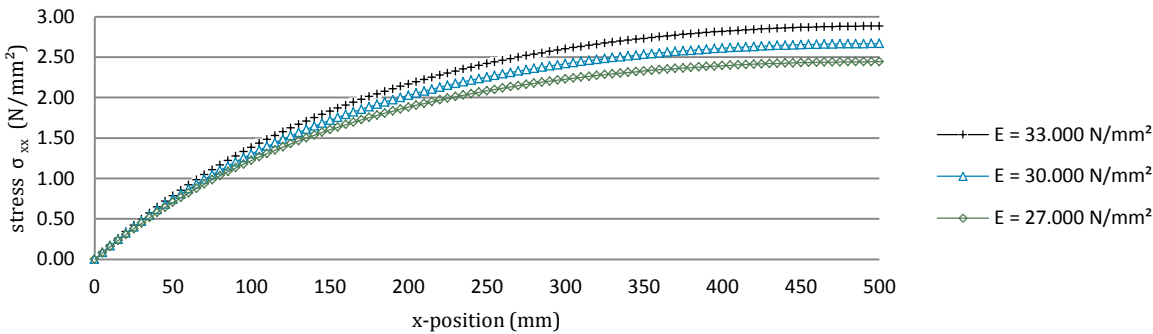
Sub-research 2 :variable screed stiffness

In Graph 12 the horizontal stress that arises due to 0.1‰ screed shrinkage is shown for variable screed stiffness. Graph 13 shows the interface shear stresses for these situations. In both graphs it can be seen that the stresses increase when increasing the screed stiffness. This increase can be explained by making use of Hooke’s law of elasticity. Shrinkage of a stiffer material induces bigger forces, resulting in bigger stresses in the screed and at the interface (formula (26)).

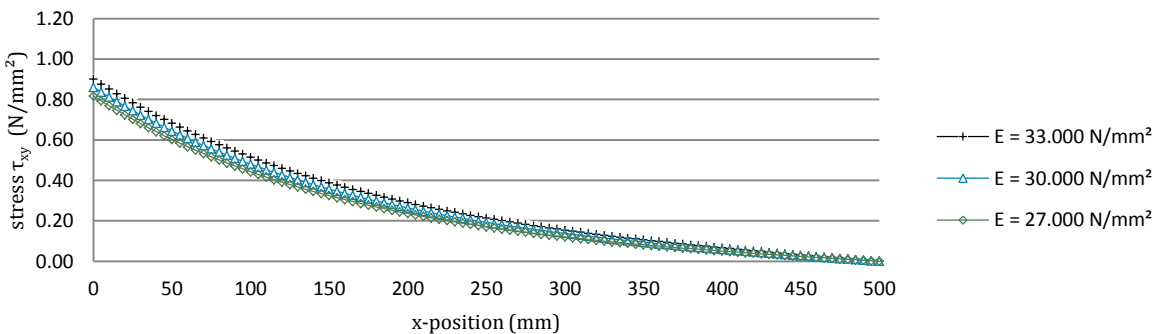
$$\sigma = \varepsilon * E \tag{25}$$

Where:

- σ is the stress in the material (N/mm²);
- ε is the amount of shrinkage (mm/mm);
- E is the Young’s modulus of the material (N/mm²).



Graph 12: horizontal screed stresses at 0.1‰ shrinkage difference, variable concrete class

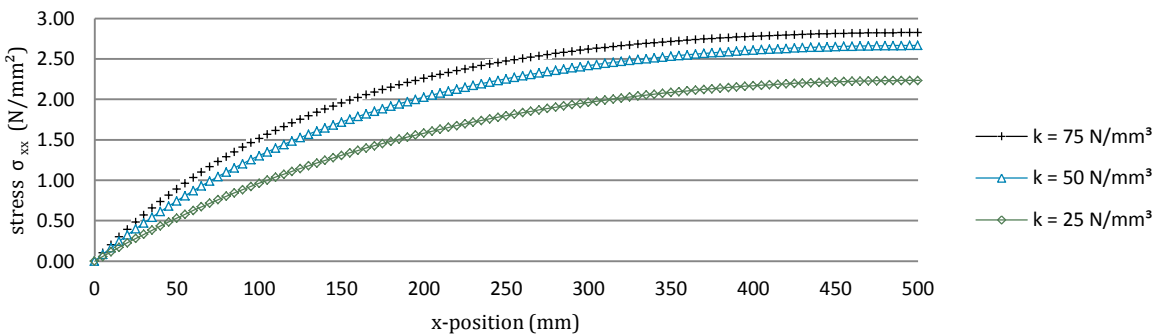


Graph 13: interface shear stresses at 0.1‰ shrinkage difference, variable concrete class

Sub-research 3 :variable interface stiffness

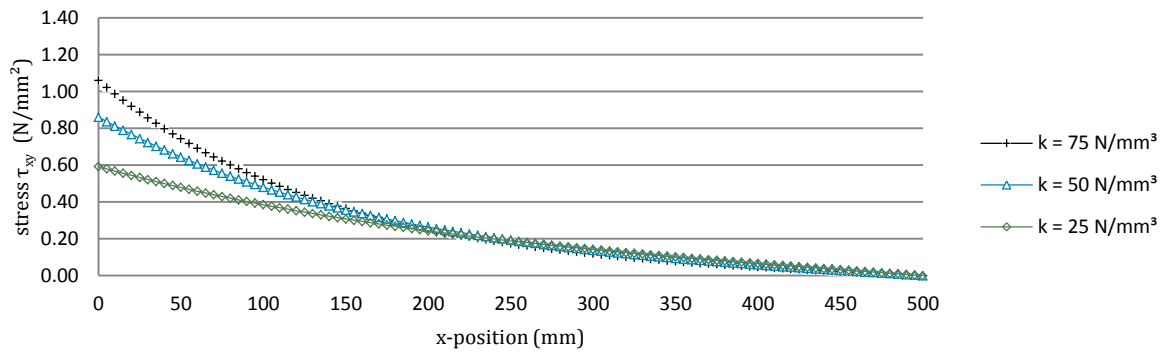
In formula (22) and (23) a parameter k is included that represents the stiffness of the interface connection against shifting horizontal of the screed. In literature no direct answer is given to the question what value belongs to this parameter [6] [9]. In the previous calculations a value of $k = 50 \text{ N/mm}^3$ is used. Graph 14 and Graph 15 show the influence of a higher and lower value for the interface stiffness on the stresses in the screed and interface. From these graphs it can be concluded that a higher stiffness results in higher stresses. This seems to be logical because higher interface stiffness induces a bigger restraintment on the screed to deform, resulting in bigger forces.

The increase of the interface has the biggest influence on the interface shear stress. An increase of 25 N/mm³ results in an increase of around 0.25 N/mm² on the interface shear stress. This represents an increase of ± 40% of the interface shear stress that is present when applying a value $k = 50 \text{ N/mm}^3$.



Graph 14: horizontal screed stresses at 0.1‰ shrinkage difference, variable interface stiffness

Modelling of shrinkage effects in screeds



Graph 15: interface shear stresses at 0.1‰ shrinkage difference, variable interface stiffness

6.3 FEM approach

6.3.1 Calculation method

In the FEM approach the influence of several parameters on the maximal tensile force is investigated. The calculations of the FEM approach are performed using the FEM software ATENA. The schematisation used for these calculations is given in Figure 56. Specific characteristics of the calculations are summed up below.

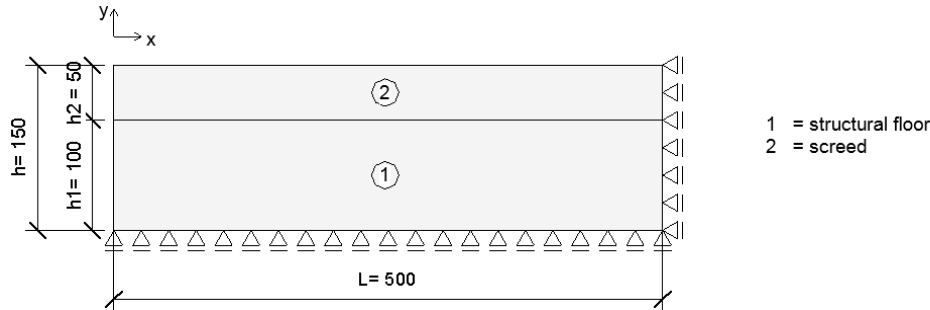


Figure 56: schematisation screed shrinkage model used for the FEM approach

- The structure is schematised with 2D elements in a 2D environment. For the thickness of the elements a size of 1000 mm is applied;
- The concrete parts (structural floor (1) and screed (2)) are modelled as SBeta Material elements with exponential tension stiffening behaviour. The properties of the concrete parts are given in Table 18;
- The mesh is generated by ATENA as quadrilateral elements with an element size of 5 mm;
- The elements are modelled as geometrical nonlinear materials with element type CCIsoQuad. This element has two translational degrees of freedom: U_x and U_y ;
- The interfaces are modelled as rigid connections for the first two sub-researches. In the other sub-researches the interface is modelled with 2D interface elements with thickness 1000mm. The properties of this interface are discussed in the third sub-research;
- Only a part of the floor at the edge with a length of 500mm is modelled. The right side of the structure is restrained for deformation in U_x direction. This is where the floor in reality continues;
- The lower edge of the bearing floor is restrained for deformation in U_y direction;
- The load that is applied on the structure exists of constant macro-element shrinkage at the screed elements. In the calculation this shrinkage is increased in 20 steps of 0.02‰;
- The self-weight of the elements is disregarded in the calculation;
- The solutions are calculated by making use of the Newton-Raphson solution method.

Table 18: material properties concrete elements

		f_t (N/mm ²)	f_c (N/mm ²)	E (N/mm ²)	G_f (N/m)	ν
Structural floor	C30/37	2.90	30	33,550	70	0.2
Screed	C30/37	2.90	30	33,550	70	0.2
	C20/25	2.21	20	30,303	59	0.2
	C12/15	1.57	12	27,088	49	0.2

6.3.2 Results and discussion

The influence of various parameters on cracking and debonding of screeds as a result of shrinkage difference between screed and structural floor is investigated. The research is divided in several sub-researches, where the influence of the screed thickness, concrete class and interface properties is investigated. In this paragraph first the general behaviour of a 50 mm screed (with properties equal to C20/25) on a concrete floor is discussed. Subsequently the influence of the different parameters is investigated.

General behaviour 50mm screed as a result of shrinkage differences

In Graph 16 the deformation of the screed in vertical direction as a result of screed shrinkage is shown for several shrinkage values. In the situations of 0.1 – 0.2‰ shrinkage it can be seen that the biggest vertical deformation is upwards at the edge of the specimen. At increasing distance of the edge the vertical deformation decreases within 80 mm to zero, whereafter a little downward deformation is encountered and 100 mm further the deformation becomes negligible ($< 0.5 \mu\text{m}$).

The stresses that arise with these deformations at the interface between screed and concrete floor are shown in Graph 17 for 0.1‰ and in Graph 18 for 0.2‰ shrinkage. In these graphs it can be seen that the interface shear stress (τ_{xy}) is the biggest at the edge of the specimen and decreases to zero at increasing distance from the edge.

Modelling of shrinkage effects in screeds

The area between the edge and the location where the shear stress is zero is the 'bonding' area, where the screed builds up its bond with the concrete floor and increases its capability to transfer forces to the concrete floor. Within this area the horizontal tensile stress (σ_{xx}) in the screed increases until the location where the shear stress is zero. This increase is due to the fact that the restraint to deformation of the screed at the interface increases as the bond increases. A stronger/ stiffer restraint gives bigger internal forces in the screed.

The vertical interface stress has a tensile peak at the edge of the specimen, whereafter the stress rapidly decreases to zero / a little compression after 50 mm. The arise of the vertical tensile stress is explained with help of Figure 57. In this figure it can be seen that the screed is restrained to deform at the interface between the screed and structural floor. When a shrinkage load is applied to the screed the upper layer of the screed shrinks, while the lower layer does not deform. Because the restraint is not fully developed at the edge of the screed, the screed is enforced to curve upwards, resulting in tensile stresses at the edge of the screed.

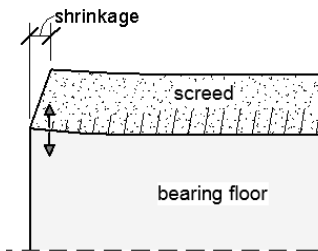
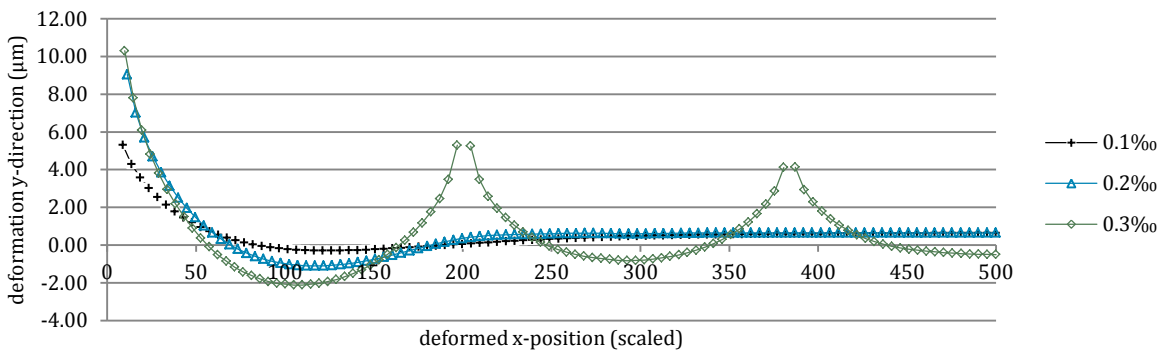
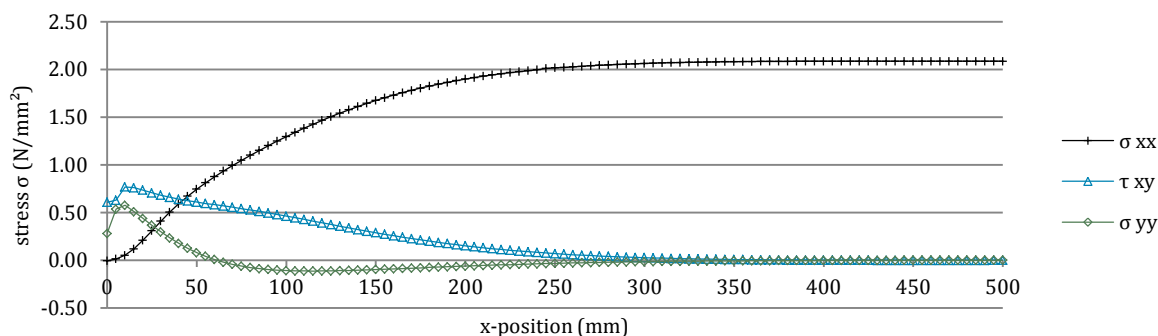


Figure 57: curling of the screed at the edge of the specimen causes vertical tensile stresses at the interface

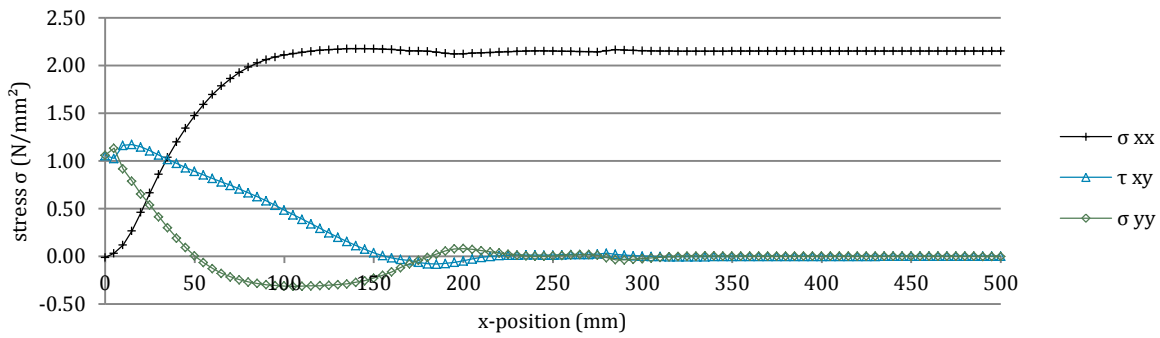
The distribution of the vertical deformation in the situation of 0.3‰ shrinkage that is shown in Graph 16 differs from the lower shrinkage values. Besides the peak at the edge of the specimen two other peaks are raised at a distance of ± 190 mm and 380 mm from the edge. These peaks are raised due to the fact that the horizontal stresses in the screed have reached the tensile strength of the screed, causing the screed to crack at these locations. At the location around a crack the distribution of the interface stresses are equal to the 'edge situation'. The shear (τ_{xy}) and vertical tensile stress (σ_{yy}) is high at the crack ($\sigma_{xx} = \pm 1.8 \text{ N/mm}^2$, $\tau_{xy} = \pm 1.3 \text{ N/mm}^2$), decreasing at increasing distance from the crack. The horizontal stress (σ_{xx}) is zero at the crack, increasing at increasing distance from the crack (Graph 19).



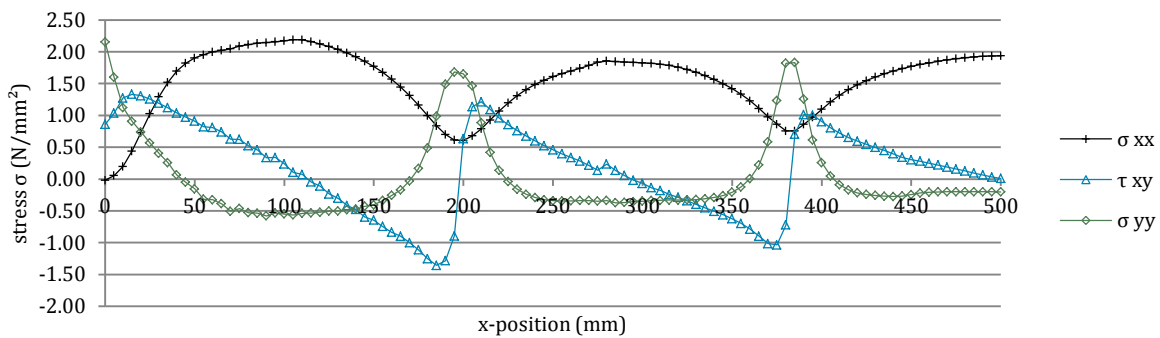
Graph 16: vertical screed deformation at shrinkage differences



Graph 17: screed and interface stresses at 0.1‰ shrinkage difference



Graph 18: screed and interface stresses at 0.2‰ shrinkage difference

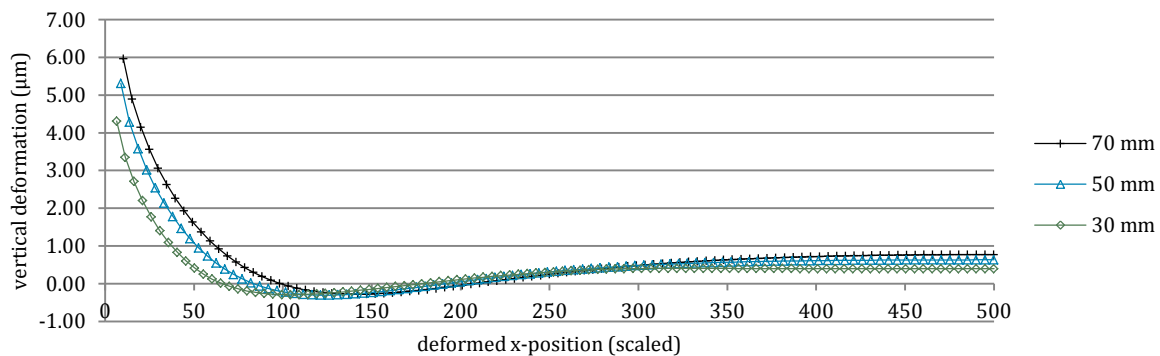


Graph 19: screed and interface stresses at 0.3‰ shrinkage difference

Sub-research 1: variable screed thickness

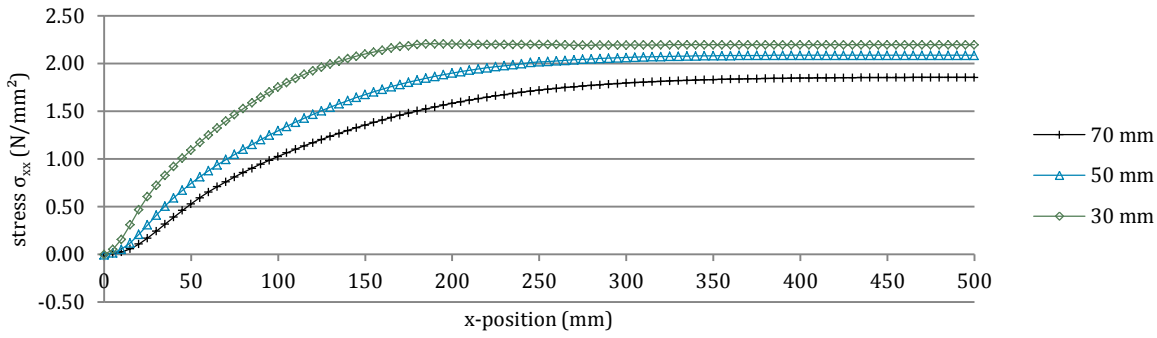
In the first sub-research the influence of the screed thickness on the deformation and stresses in the interface and screed caused by shrinkage is investigated. The vertical deformation of the screed at the interface is shown in Graph 20 for a screed thickness of 30, 50 and 70 mm at shrinkage of 0.1‰. In this graph it can be seen that the vertical deformation at the edge increases with an increasing screed thickness. The increase of vertical deformation is due to the fact that in case of shrinkage of a thicker screed the area that shrinks is bigger, inducing a bigger force on the interface. This can also be seen in Graph 22 and Graph 23. The interface shear and vertical tensile stresses at the edge are bigger at increasing screed thickness.

Graph 21 shows the horizontal stress in the screed. In this graph it can be seen that the stress in the screed at 0.1‰ shrinkage is smaller for thicker screeds. This is due to the fact that the area of restraint is in percentage of the screed volume smaller at thicker screeds. Because of less restraintment the screed is more free to deform, causing a more gradual distribution of stresses in the screed over the height.

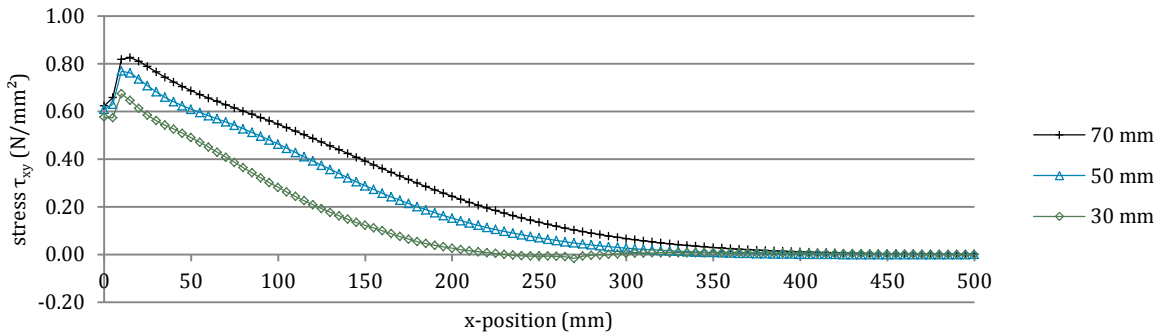


Graph 20: vertical screed deformation at 0.1‰ shrinkage difference, variable screed thickness

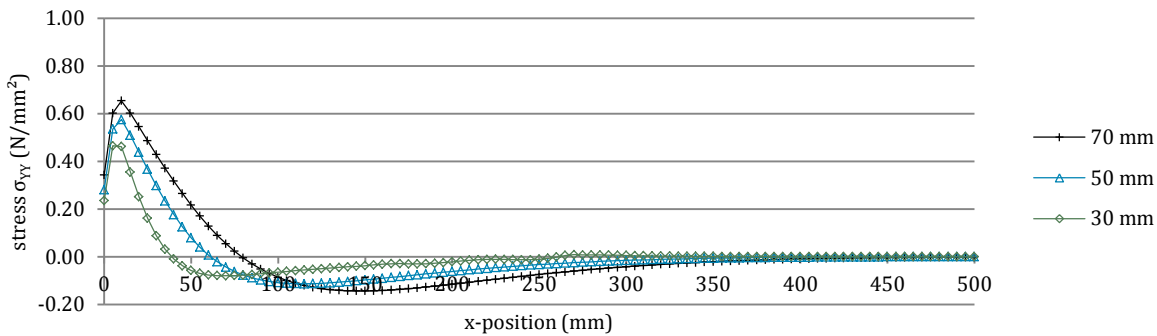
Modelling of shrinkage effects in screeds



Graph 21: horizontal screed stresses at 0.1‰ shrinkage difference, variable screed thickness



Graph 22: interface shear stresses at 0.1‰ shrinkage difference, variable screed thickness



Graph 23: vertical interface stresses at 0.1‰ shrinkage difference, variable screed thickness

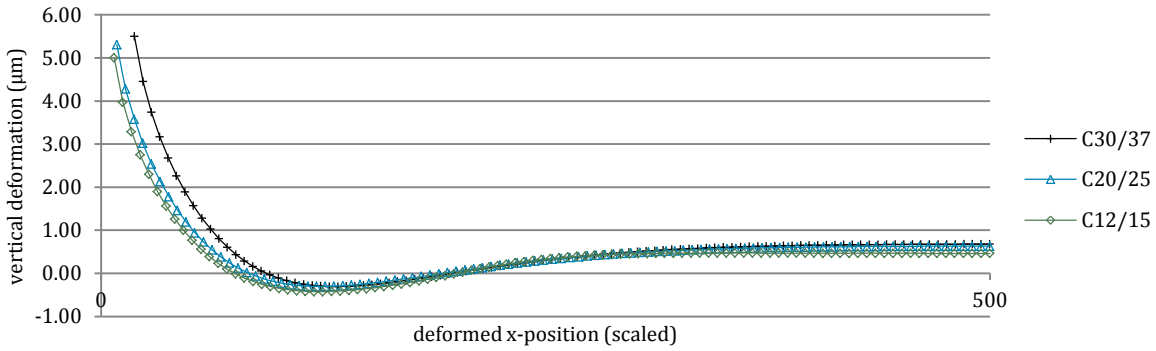
Sub-research 2: variable concrete class

The second sub-research is executed to investigate the influence of the screed concrete class on the deformation and stresses in the interface and screed caused by shrinkage. The deformations at the interface of the screed and bearing floor are shown in Graph 24. In this graph it can be seen that the deformations increase when increasing the concrete class. Graph 25 shows the horizontal screed stresses and Graph 26 and Graph 27 show the stresses at the interface. The stresses in the screed as well as the stresses at the interface increase at higher concrete classes. These increases can be explained by making use of Hooke’s law of elasticity. Because higher concrete classes represent stiffer concrete, the Young’s modulus of these materials is bigger. Shrinkage of a stiffer material induces bigger forces, resulting in bigger stresses in the screed and at the interface (formula (26)).

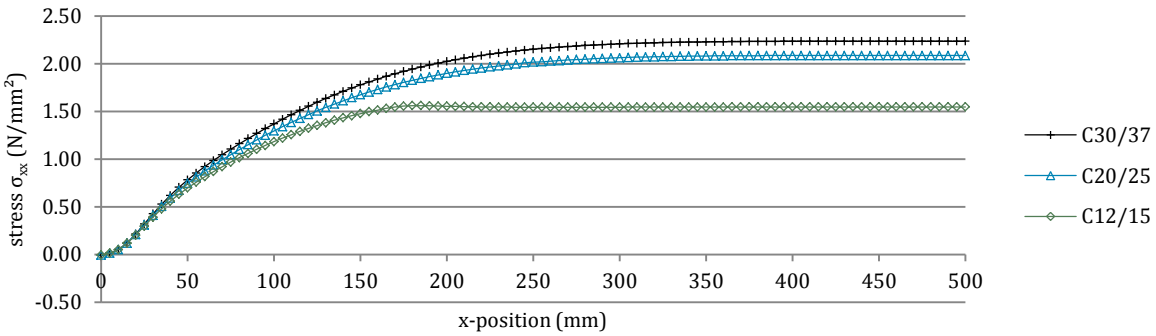
$$\sigma = \varepsilon * E \tag{26}$$

Where:

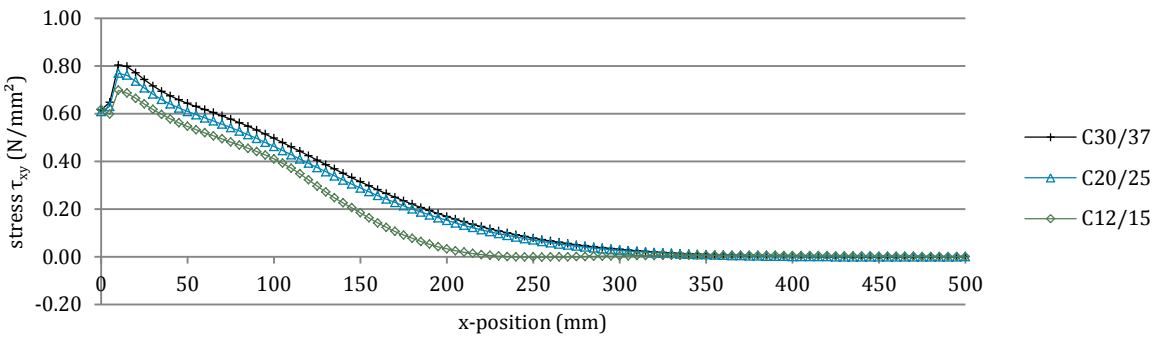
- σ is the stress in the material (N/mm²)
- ε is the amount of shrinkage (mm/mm);
- E is the Young’s modulus of the material (N/mm²);



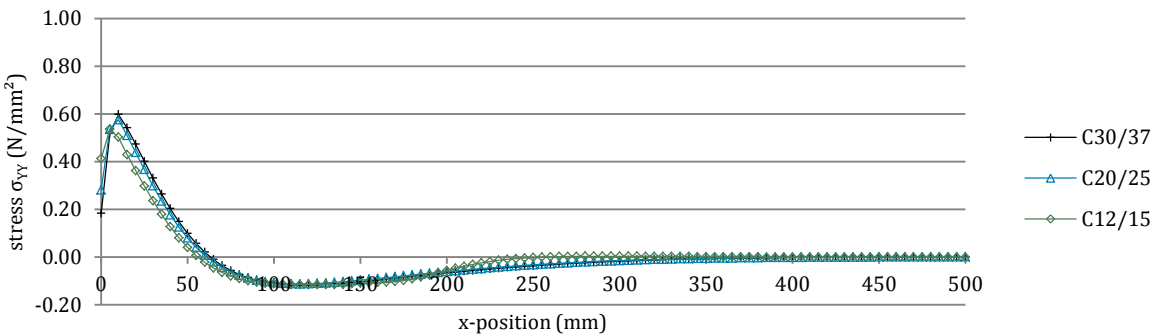
Graph 24: vertical screed deformation at 0.1‰ shrinkage difference, variable concrete class



Graph 25: horizontal screed stresses at 0.1‰ shrinkage difference, variable concrete class



Graph 26: interface shear stresses at 0.1‰ shrinkage difference, variable screed thickness



Graph 27: vertical interface stresses at 0.1‰ shrinkage difference, variable screed thickness

Sub-research 3: variable interface properties – tensile strength

Screed shrinkage at bonded screeds induces shear and tensile stresses in the interface between the screed and bearing floor. In the previous sub-researches the properties of the interface were modelled optimally. This implies that for the shear and tensile strength of the interface the properties of the weakest material are used (in this case the screed material). In practice it turns out that the interface properties are rarely equal to the weakest material (see chapter 2). In this sub-research the influence of the interface properties are investigated.

In the MC 2010 volume 1 [36] mean values are given for the interface shear strength provided by good bonding which is achieved by appropriate measures (clean surface, appropriate roughening, good concrete quality etc.). Besides the mean shear strength also a friction coefficient is given which gives extra frictional resistance to the interface in case of compression forces perpendicular to the interface. Both values are given in Table 19.

Table 19: Coefficients for the determination of interface shear strength according to the MC 2010 [36]

Surface characteristics of interface	v_{Rdi} (N/mm ²)	μ
Smooth	0 – 1.5	0.5 – 0.7
Rough (e.g. sand blasted)	1.5 – 2.5	0.7 – 1.0
Very rough (e.g. high pressure water jetted)	2.5 – 3.5	1.0 – 1.4

To gain insight in the screed shrinkage behaviour when the interface strength is reached analyses is executed at shrinkage differences from 0.1‰ – 0.3‰. In this analyses a tensile interface strength of $f_t = 0.5 \text{ N/mm}^2$ is introduced and the shear strength in this situation is modelled according to the MC 2010 assuming a rough interface surface ($v_{Rdi} = 2.0 \text{ N/mm}^2$, $\mu = 0.7$). For the shear-slip characteristics a very stiff value is assumed, which means that it is only effective at shear slips smaller than 0.05 mm. For the normal and tangential stiffness a value of $K_{nn} = K_{tt} = 3 \cdot 10^6 \text{ MN/m}^3$ is introduced in ATENA. In Figure 58 and Figure 59 the mentioned properties are represented in a stress – deformation curve.

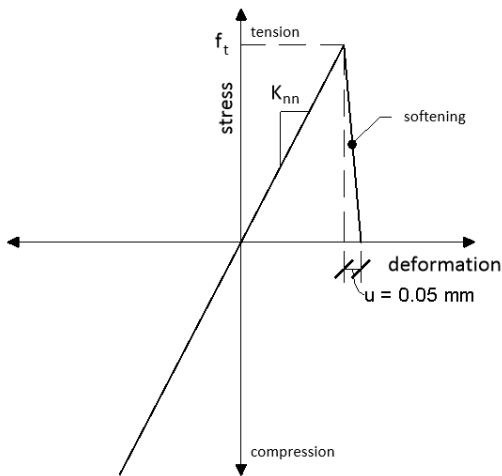


Figure 58: stress – deformation curve interface normal strength

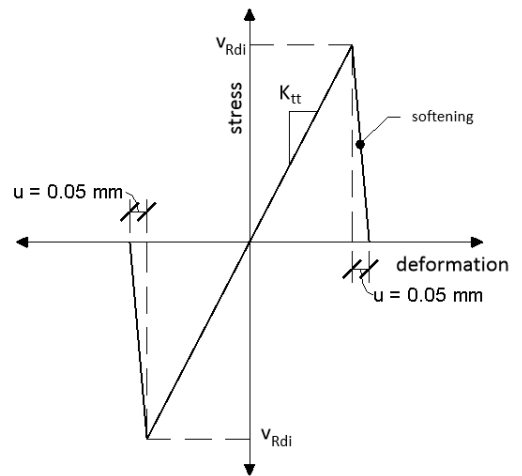


Figure 59: stress – deformation curve interface tangential strength

The vertical screed deformations are shown in Graph 28 for 0.1 – 0.3‰ screed shrinkage. The screed and interface stresses are shown per promille shrinkage in Graph 29 - Graph 31. By comparing these graphs with Graph 16 - Graph 19 (where the screed behaviour is shown with an optimal bond between screed substrate) the influence of the lower tensile interface strength is found.

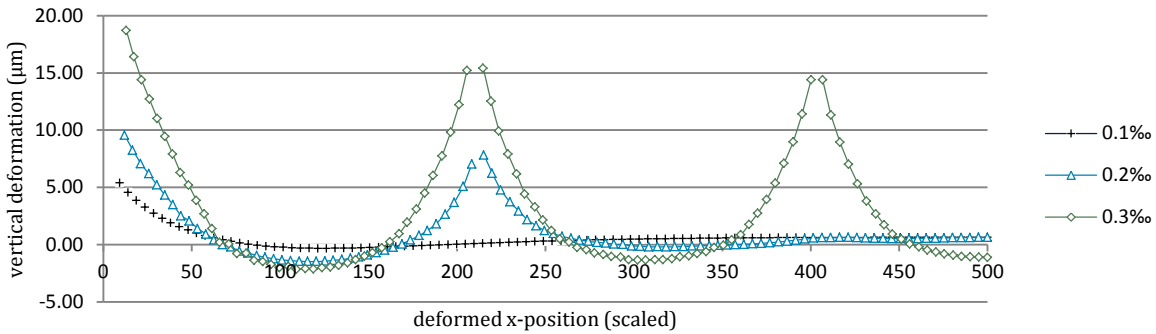
In Graph 29 it can be seen that the interface tensile strength of 0.5 N/mm^2 is reached at the first 25 mm from the edge of the specimen after 1‰ screed shrinkage. At this location the interface bond starts to decrease. Due to the softening behaviour that is modelled in ATENA there still is some tensile stress present at the interface in the first 25 mm, increasing to a maximum value of 0.5 N/mm^2 at 20 mm from the edge. By comparing this graph with Graph 17 it can be seen that the decrease of the bond in the first 25 mm causes the location of the maximal interface shear stress to shift from the edge. Because the amount of stress that can still be distributed in the first 25 mm (where the softening curve is reached for the interface stresses) there is no significant influence on the horizontal screed stresses.

When increasing the amount of shrinkage the influence of the lower interface tensile strength becomes more prevailing. In Graph 30 the screed and interface stresses are shown for 0.2‰ screed shrinkage. Here it can be seen that the location of the peak interface stress is moved to $\pm 50 \text{ mm}$ from the edge because of an increase of deformations of the screed. The shear stress at the location of the peak interface tensile stress reaches a value of 1.0 N/mm^2 , with softening behaviour in the part from the edge to this point.

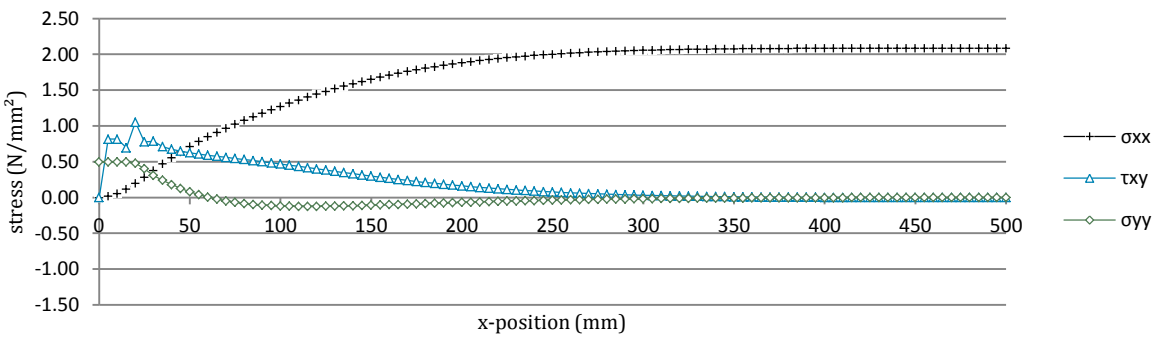
Due to the softening behaviour in the first part from the edge, shear forces can still be distributed at the interface. This causes a restraint for deformation of the screed, causing an increase in horizontal screed stresses. Because of this increase in stress the tensile screed strength is reached at $\pm 200 \text{ mm}$ from the edge of the specimen causing the screed

to crack. This crack can also be found in Graph 28, where the vertical deformations have a peak at 200 mm from the edge.

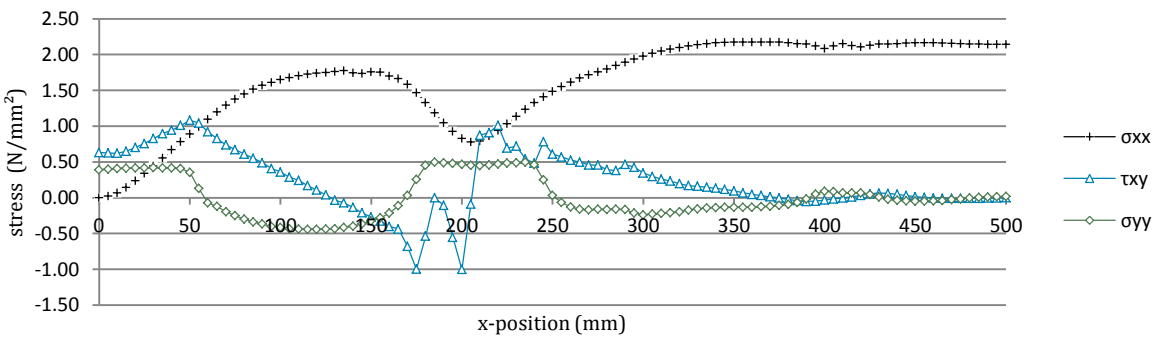
At the location of the crack a similar situation arises as at the edge of the specimen, with peak values for the interface stresses. Also at this location the interface tensile strength is reached and the stresses are located in the softening curve of the shear and tensile behaviour of the interface. The vertical displacements that arise due to the fact that the interface strength is reached are significantly bigger than in the case of the optimal situation, as is shown in Graph 16.



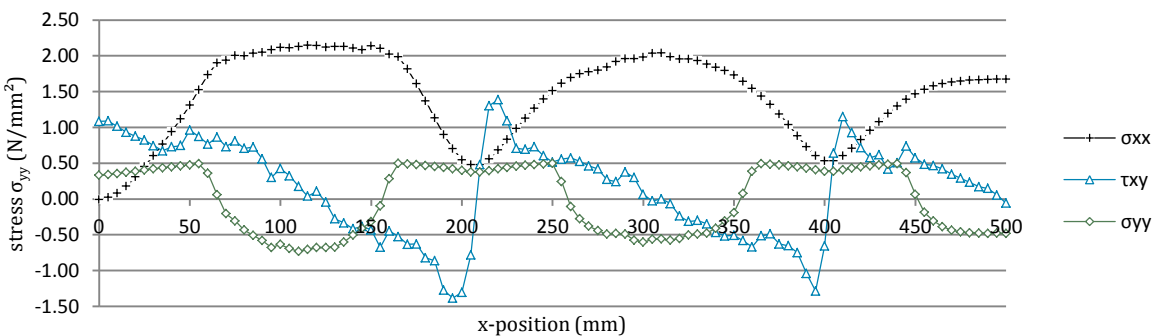
Graph 28: vertical screed deformation at 0.1 – 0.3‰ shrinkage difference, 0.5 N/mm² interface tensile strength



Graph 29: screed and interface stresses at 0.1‰ shrinkage difference, 0.5 N/mm² interface tensile strength



Graph 30: screed and interface stresses at 0.2‰ shrinkage difference, 0.5 N/mm² interface tensile strength



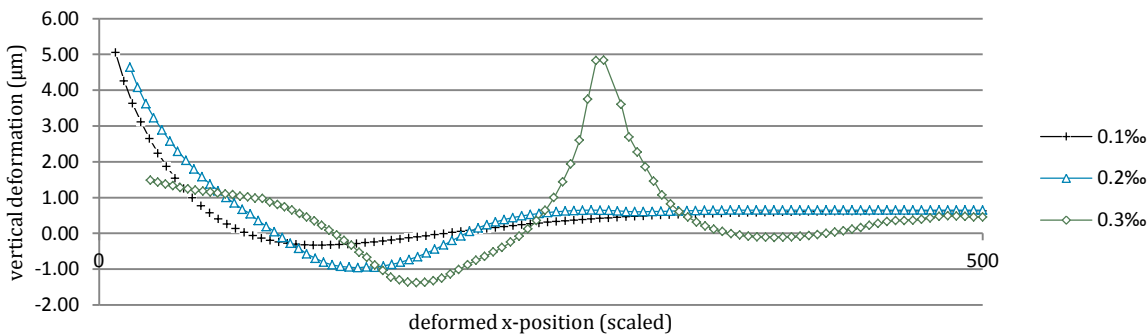
Graph 31: screed and interface stresses at 0.3‰ shrinkage difference, 0.5 N/mm² interface tensile strength

Sub-research 4: variable interface properties –shear strength

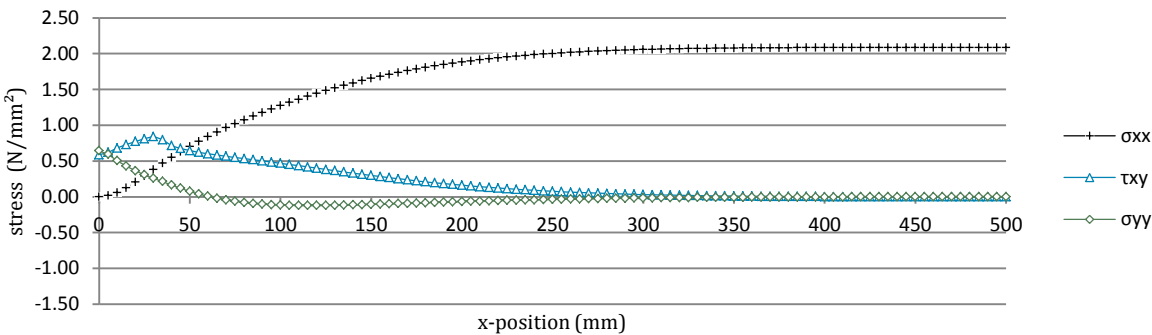
In this sub-research investigation is executed equivalent to sub-research 3. Yet the applied interface shear strength in this sub-research is 1.0 N/mm^2 with $\mu = 0.6$. For the tensile strength a value of 1.0 N/mm^2 is used. In Graph 33 the screed and interface stresses at 0.1‰ screed shrinkage are shown. By comparing this graph with Graph 17 it can be concluded that the lower interface shear strength does not influence the screed behaviour after 0.1‰ screed shrinkage while the stresses at the interface have not reached the interface strength.

At 0.2‰ screed shrinkage the influence of the lower interface shear strength becomes more prevailing. In Graph 34 it can be seen that the interface shear strength is reached at the first 120 mm from the edge of the specimen. The interface shear stresses in the first 120 mm now show the softening behaviour, where the stresses decrease almost linearly from 120 mm from the edge to the edge. Because the shear force that can be distributed by the interface is lower in this area, the amount of restraint for deformation of the screed is lower. This results in bigger horizontal screed deformations and lower stresses in the screed. By comparing the results of this situation with the optimal bond situation it can be seen that the peak value of the screed stress is reached at a bigger distance from the edge ($\pm 140 \text{ mm}$ vs. $\pm 75 \text{ mm}$).

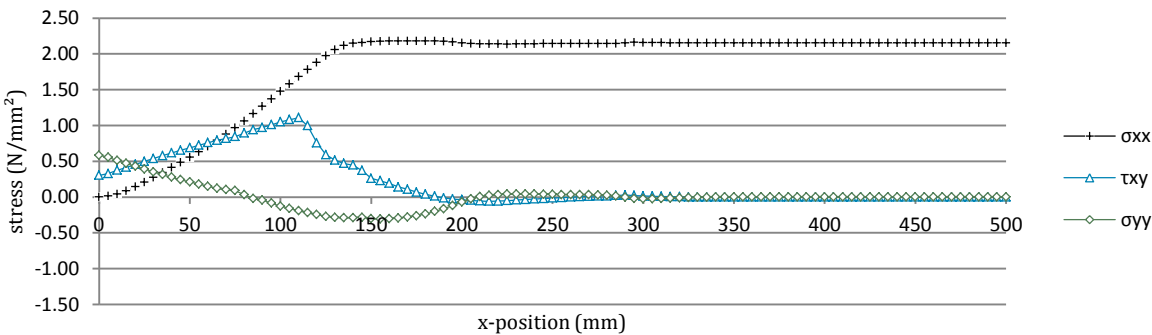
By increasing the screed shrinkage even more it can be seen that this results in the first crack in the screed at a bigger distance from the edge ($\pm 275 \text{ mm}$ vs. 200 mm). The vertical deformations at the location of the crack show no significant differences with the optimal bond situation, but the horizontal deformations increase significantly.



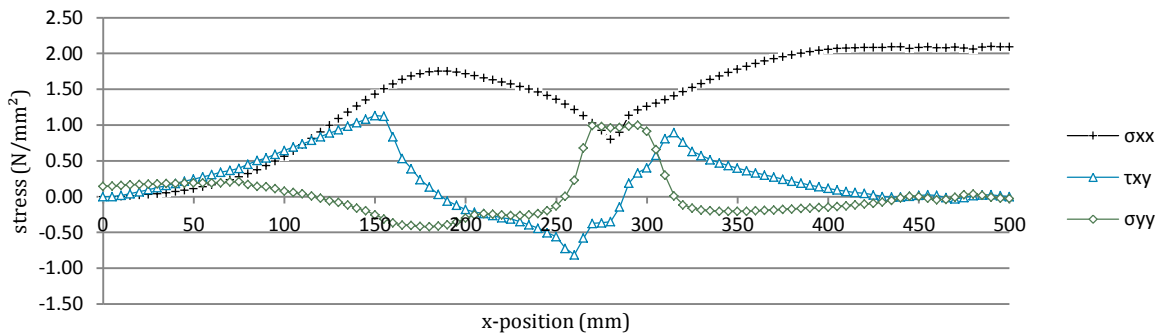
Graph 32: vertical screed deformation at 0.1 – 0.3‰ shrinkage difference, 1.0 N/mm^2 interface shear strength



Graph 33: screed and interface stresses at 0.1‰ shrinkage difference, 1.0 N/mm^2 interface shear strength



Graph 34: screed and interface stresses at 0.2‰ shrinkage difference, 1.0 N/mm^2 interface shear strength



Graph 35: screed and interface stresses at 0.3‰ shrinkage difference, 1.0 N/mm² interface shear strength

6.4 Review

In this chapter the influence of different parameters on the distribution of stresses at the interface and in the screed was studied by means of an analytical approach and a FEM study. The analytical approach consisted of a parametric study where the distribution of stresses in the screed and at the interface between screed and bearing floor was analysed with varying screed thickness, screed stiffness and interface stiffness. Hereby no values for the strength of the bond/ screed were taken into account.

In the FEM study the behaviour of the bonded screed due to shrinkage was analysed with variable screed thicknesses, concrete classes and interface properties. In this study the values for the bond/ screed strength were taken into account in order to observe the behaviour of the screed during cracking/ debonding.

When shrinkage differences occur at the interface between screed and bearing floor stresses will develop in both the screed and at the interface. The horizontal stresses that occur in the screed are tensile stresses that arise as a result of restrained deformations (the bonded surface causes the restraint). These stresses are zero at the edge of a floor and increase to its maximum at increasing distance from the edge. When the amount of shrinkage becomes that high that the tensile strength of the screed is reached cracks will occur in the screed. In the case of a crack a new 'edge' situation is formed, where the horizontal increases from zero to its maximum value at increasing distance from the crack.

The vertical and shear interface stresses due to shrinkage differences are distributed in a reversed order. Around the edge of a floor field the stresses reach their maximum and the stresses decrease to zero at increasing distance from the edge. In the case a crack is formed the stresses are again maximal at the location of the crack and decrease to zero at increasing distance from the edge.

The FEM study has pointed out that when debonding has occurred at the interface due to the fact that the shear strength / tensile strength of the bond is reached, the area and starting point over which the increase of the screed stress and the decrease of the interface stresses shifts away from the edge / crack. This causes the potential distance between two cracks to increase. Yet the vertical deformations of the screed increase significantly, causing curling of the screed. As explained in section 2.6 this can cause serious damage to the screeds.

Both the analytical approach and the FEM study have pointed out that an increase in screed height increases the stresses at the interface. According to the analytical approach an increase of 20 mm screed thickness increases the maximum shear stress with 0.15 N/mm² at 0.1‰ shrinkage difference. According to the FEM study this increase is ± 0.08 N/mm². The vertical interface stress increases with 0.10 N/mm².

An increase in concrete class increases the stresses at both the interface and in the screed. The analytical approach and the FEM study have pointed out that this increase is caused by an increase in stiffness of both the interface and the screed. According to Hooke's law of elasticity the forces due to shrinkage are bigger at increased stiffness. An increase in stresses will occur, however when it is assumed that the bond strength at the interface is increased as a result of a stronger screed strength this will not directly cause problems in debonding / cracking of the screed.

7. Practical experiments

7.1 Introduction

In addition to the theoretical researches that are discussed in chapter 5 and 6 practical experiments are performed. The first experiments that were carried out compose a research to the influence of different practical parameters to the results of Pull-Off tests. A description of the experiments along with a discussion of the results is included in section 7.2. The theoretical research to the behaviour of bonded screeds exposed to shrinkage discussed in chapter 6 has pointed out that shrinkage differences cause stresses at the interface between the screeds and bearing floors. In order to determine the maximum stresses that are permissible at the interfaces without debonding/ cracking of screeds experiments are performed. In these experiments the bond strength of cementitious layers on a concrete substrate is tested with variable surface roughness's. A description of the experiments as well as a discussion of the results is included in section 7.3.

7.2 Pull-Off testing method experiments

7.2.1 Test method

In order to execute the experiments concrete specimen were casted. The sizes of these specimens were 300x300x100mm and they were poured from a concrete mixture that was used to pour floors on a building site in Utrecht. After pouring the surface of the specimen was wetted and covered with foil. The specimen were demoulded after 24 hours of hydration and then again wetted and covered with foil to ensure that the specimen hydrated in a moisty environment.

The Pull-Off testing experiments were executed after 32 days of hydration. Per test piece 5 tests were performed. In order to perform the test 5 cylindrical cores with an internal diameter 50 mm were drilled in the specimen with a minimum depth of 15mm according to Figure 60. Subsequently the laitance was thoroughly removed from the surface by making use of a steel brush. Hereafter the surface was cleaned from dust and loose parts and finally the steel dollies with diameter 50 mm were glued to the surface with a Pleximon two component glue. After fully hardening of the glue the Pull-Off tests were executed. A minimum of 120 minutes hardening was maintained.

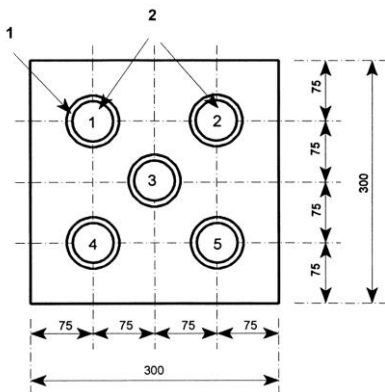


Figure 60: minimal distances between drilled cores

Figure 61: analogue device

Figure 62: digital device

For the purpose of the research different experiments were performed. The different experiments that were carried out are discussed below.

Experiment 1.1: different testing devices

In order to perform the Pull-Off tests two testing devices were available from the manufacturer Proceq. The first testing device was the Proceq SA, which is a hand driven Pull-Off tester that presents the results on an analogue display (Figure 61). The second testing device was the Proceq DY-206, which is an automatically driven Pull-Off tester with a digital display (Figure 62). Apart from the hand/ automatic controlling of the pulling force the procedure for performing the Pull-Off tests is equal for both devices. In order to compare the results of both devices 10 tests were executed with each device (so 2 test pieces were tested with each device).

Experiment 1.2: drilled core / no drilled core

In order to determine the surface tensile strength different Pull-Off testing methods are available with and without drilling a core before gluing the dolly to the surface. The influence of applying a drilled core on the test results is investigated by means of this experiment.

Practical experiments

Experiment 1.3: diagonal loading

Because of irregularities at the concrete surface it is possible that the testing device is situated in a way that the pulling force is not applied perfectly perpendicular to the surface (Figure 63). This causes the dolly to be loaded diagonally. The influence of diagonal loading is investigated in this experiment by elevating one of the legs of the Pull-Off tester.

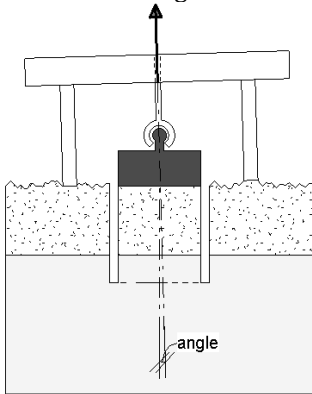


Figure 63: irregularities at the concrete surface can cause diagonal loading

Figure 64: elevated leg front view

Figure 65: elevated leg side view

Experiment 1.4: eccentric loading

As a result of roughness of the concrete surface or poor applying of the glue between the dolly and the concrete surface it is possible that the dolly is not glued to the surface for the whole area. When little parts of the dolly are not glued to the surface this can cause eccentricities when applying the load at the centre of the dolly. The influence of partly gluing of the dolly is investigated in this experiment. The experiment is executed by preventing the glue to attach at 5 mm and 10 mm from the side of the dolly (see Figure 66 - Figure 68).

Experiment 1.5: diagonal drilled core

When drilling a core with a diamond drilling machine on site without making use of an instrument that fixes the drilling machine to the concrete surfaces the possibility exists that the core is drilled in a way not perfectly perpendicular to the surface. The influence of a drilled core at a slope relative to the surface is investigated in this experiment. Slopes of 1:20 and 1:10 are included in the experiment (see Figure 69).

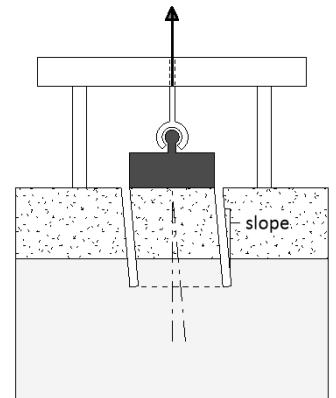
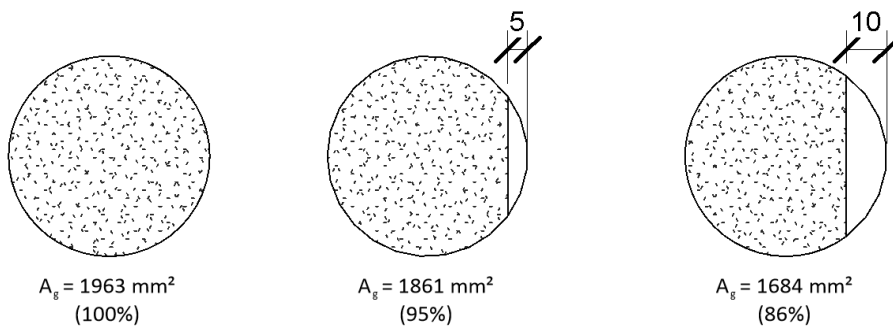


Figure 66: fully glued dolly

Figure 67: dolly 5 mm not glued

Figure 68: dolly 10 mm not glued

Figure 69: diagonal drilled core

Concrete class

Before performing the experiments the compressional and tensile strength is determined by means of compression and tensile split tests on cubes of 150x150x150mm. These tests were accomplished at 32 days after pouring the concrete. The results are given in Table 20. Given the fact that the mean cube compressive strength equals $f_{ck,mean} = 35.9 \text{ N/mm}^2$ with a minimum value of $f_{ck,min} = 32.3 = 0.9 * 35.9 \text{ N/mm}^2$ it can be stated that the concrete of the specimen after 32 days of hydration has reached the properties of concrete class C28/35.

Table 20: results compression and tensile split tests after 32 days hydration

	Cube 1 (N/mm ²)	Cube 2 (N/mm ²)	Cube 3 (N/mm ²)	Cube 4 (N/mm ²)	Cube 5 (N/mm ²)	Cube 6 (N/mm ²)	Max (N/mm ²)	Min (N/mm ²)	Mean (N/mm ²)
Compression test	39.5	33.9	36.3	32.3	35.3	38.1	39.5	32.3	35.9
Tensile split test	4.2	3.9	3.5	4.2	3.8	3.3	4.2	3.3	3.8

7.2.2 Results and discussion

In this sub-section the outcomes of the previously described experiments are presented and discussed. The results are all presented in maximal mean stresses. These stresses are obtained by dividing the maximal pull off force by the area of the dolly, according to formula (27).

$$\sigma = \frac{F_{po}}{A_d} = \frac{F_{po}}{\frac{1}{4} * \pi * d^2} \quad (27)$$

Where:

- σ maximal mean stress (N/mm²);
- F_{po} is the maximal pull of force (N);
- d is the diameter of the dolly (mm)

The results are presented in tables and graphs for the different experiments. At some of the tests no value is presented in the table. In these cases the results of the Pull-Off tests were not valid because the dolly was not perfectly glued to the surface. Furthermore some of the results are marked with an asterisk (*). This indicates that the plane of failure is located at the tip of the drilled core (Figure 76). The planes of failure of the values presented without an asterisk are located in the concrete directly below the dolly.

Experiment 1.1: different testing devices

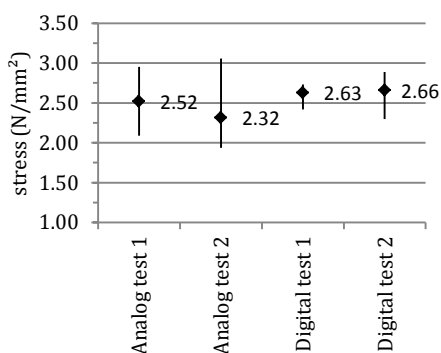
A total of 10 Pull-Off tests are executed with each device. The results of these tests are included in Table 21. The mean value of these results and their bandwidth are presented in Graph 36 per test piece. This graph shows that the bandwidth of the results that are obtained by testing with the hand driven analogue device have a bigger spread than in case of the automatically driven digital device. The big spread in the results is probably due to the fact that the increase of force per second with the hand driven device is faster than when the automatically driven device is applied. Furthermore the increase in pulling force is not perfectly regulated, resulting in less accuracy in the outcome of the test. This lower accuracy in regulating the increase in pulling force causes the mean value of the outcome to be lower. The increase in pulling force in case of the hand driven device is regulated at 100 N/s, a value that can hardly be equalised when increasing the pulling force by hand. The higher speed in case of increasing the pulling force by hand results in earlier failing of the specimen so a lower maximal pulling force is measured.

A practical problem that has occurred during executing the hand driven tests is that in the case that a high amount of energy comes free at the breaking point of the specimen the analogue pulling force indicator quickly shifts to a high value and then falls down to a lower one. This causes the observer to doubt the validity of the results what amplifies the statement of a less accuracy for the hand driven device.

Apart from differences in the way of controlling and presentation of the results per device also physical differences are present between the two devices. The legs of the digital device are located at a smaller distance relative to each other (Figure 70 - Figure 71). This increases the chance that the tripod will be perpendicular to the dolly. At bigger distances the probability increases that the tripod is placed at an angle above the dolly inducing eccentric loading. Later in this section the consequences of diagonal loading will be discussed in further detail.

Table 21: results experiment 1.1

		Dolly 1 (N/mm ²)	Dolly 2 (N/mm ²)	Dolly 3 (N/mm ²)	Dolly 4 (N/mm ²)	Dolly 5 (N/mm ²)	Max (N/mm ²)	Min (N/mm ²)	Mean (N/mm ²)
Analog device	test piece 1	2.09	2.34	-	2.95	*2.70	2.95	2.09	2.52
	test piece 2	3.06	2.14	2.14	-	1.94	3.06	1.94	2.32
Digital device	test piece 1	2.65	2.72	2.63	2.42	2.73	2.73	2.42	2.63
	test piece 2	*2.66	2.89	2.30	2.73	2.72	2.89	2.30	2.66



Graph 36: result ranges experiment 1.1



Figure 70: analogue device



Figure 71: digital device

Experiment 1.2: drilled core / no drilled core

The results of the tests without applying a drilled core are obtained by the hand driven device. The digital device could in this case not be applied considering the maximal pulling force (6 kN) is smaller than the force required to pull off the dollies of the surface without a drilled core. A total of 10 Pull-Off tests are executed for each case. The results of these tests are included in Table 22. The mean value of these results and the bandwidth are presented in Graph 37 per test piece. The pulling force that is required to pull off a dolly when no drilled core is applied is bigger than when a drilled core is applied. In the case of no drilled core the pulling force is on average > 30% percent higher than when no drilled core is applied. This higher force is due to the area that is addressed by the pulling force to distribute the stresses (Figure 72). The maximal pulling force is divided by the area of the dolly to obtain a mean stress that represents the strength of the material at the location directly below the dolly. When, in case of no drilled core, a bigger area is addressed the calculated mean stress is not representative for the situation.

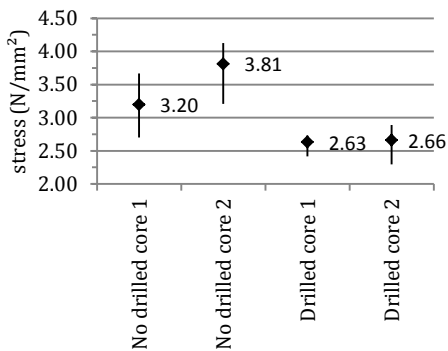


Figure 72: addressed area to distribute stresses in the situation of no drilled core (left) and a 15 mm drilled core (right)

The results of the tests with no drilled core contain a bigger spread. This can be due to the fact that the surface of the concrete is not homogenous, causing the size of the area that is addressed to distribute the pulling force to differentiate in the different situations. Another explanation for this spread is that the hand driven device is used, which contains the property of bigger spreads in the results compared to the digital device.

Table 22: results experiment 1.2

		Dolly 1 (N/mm ²)	Dolly 2 (N/mm ²)	Dolly 3 (N/mm ²)	Dolly 4 (N/mm ²)	Dolly 5 (N/mm ²)	Max (N/mm ²)	Min (N/mm ²)	Mean (N/mm ²)
No drilled core	test piece 1	-	2.70	2.95	3.67	3.46	3.67	2.70	3.20
	test piece 2	3.87	4.07	3.21	3.77	4.13	4.13	3.21	3.81
Drilled core	test piece 1	2.65	2.72	2.63	2.42	2.73	2.73	2.42	2.63
	test piece 2	*2.66	2.89	2.30	2.73	2.72	2.89	2.30	2.66



Graph 37: result ranges experiment 1.2



Figure 73: pulled off dolly without applying a drilled core

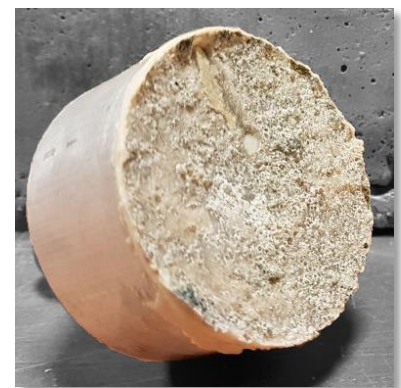


Figure 74: pulled off dolly with applying a drilled core

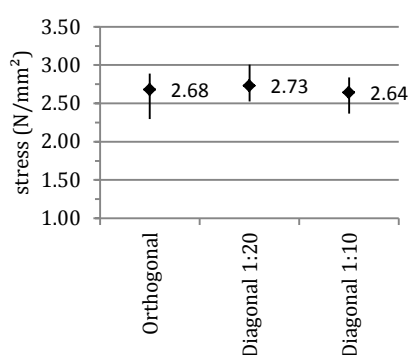
Experiment 1.3: diagonal loading

The results of the experiment are presented in Graph 38 and Table 23. For the maximal, minimal and mean value of the orthogonal situation the values of experiment 1.1 and 1.2 are used. In the graph can be seen that no significant differences in the maximal pulling force are obtained. The maximal pulling forces obtained with the diagonal loaded tests all fall within the range of the ‘normal’ orthogonal tests.

Although the values do not significantly diverge from the ‘normal’ situation, the plane of failure is consistently different in case of diagonal loading. When pulling diagonal to the surface the plane of failure is consistently at the tip of the drilled core (Figure 76). When pulling perpendicular to the surface the plane of failure is directly below the dolly (Figure 75).

Table 23: results experiment 1.3

	Dolly 1 (N/mm ²)	Dolly 2 (N/mm ²)	Dolly 3 (N/mm ²)	Dolly 4 (N/mm ²)	Dolly 5 (N/mm ²)	Max (N/mm ²)	Min (N/mm ²)	Mean (N/mm ²)
Orthogonal	-	-	-	-	-	2.89	2.30	2.68
Diagonal 1:20	*2.53	*2.85	*2.54	*2.71	*3.00	3.00	2.53	2.73
Diagonal 1:10	*2.61	*2.37	*2.80	*2.84	*2.59	2.84	2.37	2.64



Graph 38: result ranges experiment 1.3



Figure 75: pulled off dolly: concrete failure at the surface of the concrete



Figure 76: pulled off dolly: concrete failure at the tip of the drilled core

Experiment 1.4: eccentric gluing

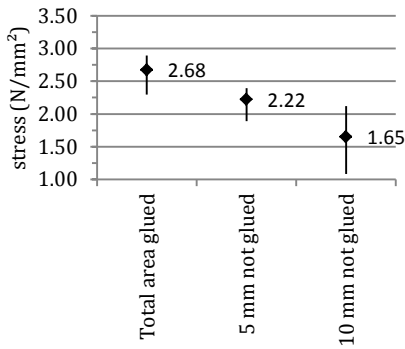
The results of the experiment are presented in Graph 39 and Table 24. For the maximal, minimal and mean value of the total glued area situation the values of experiment 1.1 and 1.2 are used. In the graph it can be seen that the maximal pulling force decreases with an increasing part of the dolly that is not glued. Furthermore a bigger spread is encountered in the case of the 10 mm not glued situation. This spread is likely due to the fact that the part of the area that is not glued is not exactly equal for every situation, causing differences in maximal pulling force. The plane of failure is consistently directly below the dolly for all the situations (Figure 77 and Figure 78).

It could be stated that the way of calculating the stress calculated is not representative only a part of the dolly is glued, which means that the area by which the pulling force is divided has to be adjusted. A dolly that is not glued for 10 mm represents a glued area of 86% (Figure 68). This should indicate the calculated stress of a 10 mm not glued dolly to be 86% of the stress in case of a totally glued dolly. In reality the stress is $(1.65/2.69) = 61\%$ so the statement is incorrect. The explanation for this is that the pulling force is distributed eccentrically to the concrete in case of a partly glued dolly, inducing no even distributed stresses.

Table 24: results experiment 1.4

	Dolly 1 (N/mm ²)	Dolly 2 (N/mm ²)	Dolly 3 (N/mm ²)	Dolly 4 (N/mm ²)	Dolly 5 (N/mm ²)	Max (N/mm ²)	Min (N/mm ²)	Mean (N/mm ²)
Total area glued	-	-	-	-	-	2.89	2.30	2.68
5 mm not glued	2.39	1.89	2.39	2.22	-	2.39	1.89	2.22
10 mm not glued	1.74	2.12	-	1.08	1.66	2.12	1.08	1.65

Practical experiments



Graph 39: result ranges experiment 1.4



Figure 77: dolly 5mm not glued

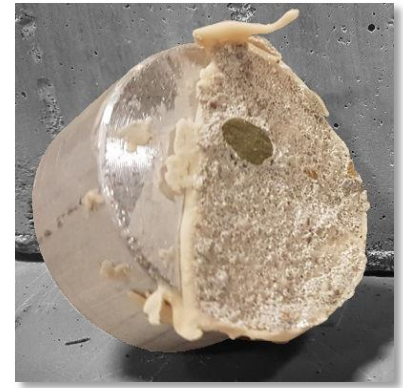


Figure 78: dolly 10mm not glued

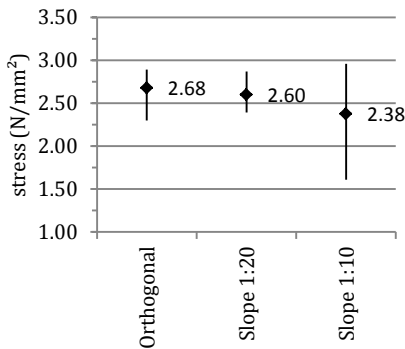
Experiment 1.5: diagonal drilled core

The results of the experiment are presented in Graph 40 and Table 25. For the maximal, minimal and mean value of the orthogonal situation the values of experiment 1.1 and 1.2 are used. In the graph can be seen that in the situation of the cores drilled at a slope of 1:20 no significant differences in the maximal pulling force are obtained. The maximal pulling forces obtained with these tests all fall within the range of the ‘normal’ orthogonal tests.

At the situation where cores are drilled at a slope of 1:10 the mean value of the maximal stress is lower than compared to the orthogonal situation. At 4 out of the 5 tests performed the plane of failure of these situations is obtained at the tip of the drilled core. The maximal force that is required to pull off the dolly is in these cases lower, caused by stress concentrations at the tip of the drilled core due to eccentric loading. More theoretical information about this phenomenon is given in section 5.

Table 25: results experiment 1.5

	Dolly 1 (N/mm ²)	Dolly 2 (N/mm ²)	Dolly 3 (N/mm ²)	Dolly 4 (N/mm ²)	Dolly 5 (N/mm ²)	Max (N/mm ²)	Min (N/mm ²)	Mean (N/mm ²)
Orthogonal	-	-	-	-	-	2.89	2.30	2.68
Slope 1:20	2.42	2.87	2.81	2.39	2.50	2.87	2.39	2.60
Slope 1:10	*2.32	*1.61	*2.48	2.96	*2.51	2.96	1.61	2.38



Graph 40: result ranges experiment 1.5



Figure 79: pulled off dolly orthogonal drilled core

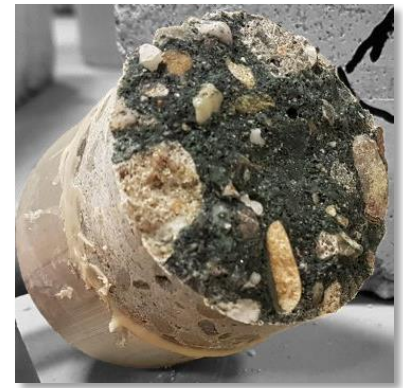


Figure 80: pulled off dolly drilled core with slope 1:10

7.3 Bond experiments

7.3.1 Test method

In order to execute the experiments concrete specimen were casted in the same way as the specimen used in the experiments of section 7.2. The sizes of these specimens were 300x300x100mm and they were poured from a concrete mixture that was used to pour floors on a building site in Utrecht. After pouring the surface of the specimen was wetted and covered with foil. The specimen were demoulded after 24 hours of hydration and then again wetted and covered with foil to ensure that the specimen could hydrate in a moisty environment. Two weeks after hydrating the surface of the specimen was subjected to different treatments, existing of:

- No treatment (Figure 81);
- Sanding (Figure 82);
- Milling (Figure 83);
- Grit blasting (Figure 84).



Figure 81: concrete surface not treated



Figure 82: concrete surface treated by sanding



Figure 83: concrete surface treated by milling



Figure 84: concrete surface treated by grit blasting

Experiment 2.1: surface tensile strength

After executing the surface treatments at the first part of the specimen 5 cores with diameter 50 mm were drilled into the surface per test piece. The surface then was cleaned from dust and loose parts and dollies with diameter 50 mm were glued to the surface with a Pleximon two component glue. After fully hardening of the glue the Pull-Off tests were performed to measure the surface tensile strength per surface treatment. A minimum of 120 minutes hardening was maintained. The Proceq DY-206 Pull-Off tester was used to perform the Pull-Off tests.

Experiment 2.2: bond strength at a second layer of sand cement

The second part of the specimen was used for experiment 2.2. In this experiment the specimen were placed in formwork after performing the surface treatments. Hereafter the surface of the specimen was cleaned from dust and loose parts and moistened with water. Subsequently a second layer of 30 mm thick was poured on the specimen existing of an earth dry sand cement mixture. After five days of drying the specimens were demoulded. During demoulding it appeared that the sand cement layer was detached from the concrete specimen, thus no Pull-Off tests could be performed to measure the bond strength.

Experiment 2.3: bond strength at a second layer of a liquid cementitious mixture

The third part of the specimen was used for experiment 2.3. The specimen were placed in formwork after performing the surface treatments and cleaned from dust and loose parts. Hereafter 2 test pieces per surface treatment were

provided with a Cobra primer DPM 820. One piece per surface treatment was not provided with a primer. After 2 hours of drying of the primer a layer of 10 mm was poured on the specimen existing of a liquid cementitious mixture (UZIN NC 170 LevelStar). Three days later the specimens were demoulded.

Cores with an inner diameter of 50 mm were drilled in the specimen 14 days after pouring the cementitious layer. Hereafter the surface was roughened with a steel brush and steel dollies were glued to the top layer. Subsequently pull of tests were performed with the Proceq DY-206 Pull-Off tester to measure the bond strength.

Concrete class

Before performing the experiments the compressional and tensile strength is determined by means of compression and tensile split tests on cubes of 150x150x150mm. These tests were accomplished at 45 days after pouring the concrete. The results are given in Table 20. Given the fact that the mean cube compressive strength equals $f_{ck,mean} = 37.5 \text{ N/mm}^2$ with a minimum value of $f_{ck,min} = 35.6 = 0.95 * 37.5 \text{ N/mm}^2$ it can be stated that the concrete of the specimen after 45 days of hydration has reached the properties of concrete class C30/37.

Table 26: results compression and tensile split tests after 45 days hydration

	Cube 1 (N/mm ²)	Cube 2 (N/mm ²)	Cube 3 (N/mm ²)	Cube 4 (N/mm ²)	Cube 5 (N/mm ²)	Cube 6 (N/mm ²)	Max (N/mm ²)	Min (N/mm ²)	Mean (N/mm ²)
Compression test	38.4	38.3	36.2	35.6	40.8	35.8	40.8	35.6	37.5
Tensile split test	3.7	3.3	3.3	3.8	3.2	4.7	4.7	3.2	3.7

7.3.2 Results and discussion

The results of the previously described experiments are presented and discussed in this sub-section per experiment.

Experiment 2.1: surface tensile strength

The surface of the concrete specimen was treated before the surface tensile strength was measured per surface treatment. Ordered in surface roughness the order of the surface treatments is:

1. Sanded surface
2. No surface treatment
3. Milled surface
4. Grit blasted surface

The results of the experiment are given in Table 27. The mean values of the results per surface treatment are shown in Graph 41, including the range between the maximal and minimal measured value. From the results it is concluded that the surface roughness does not directly influence the surface tensile strength.

Applying no surface treatment gave the lowest surface strength. A mean value of 0.68 N/mm^2 was found for this. Due to the fact that when no surface treatment is applied there still is laitance present at the concrete surface (section 3.4.1), existing of a very weak cement layer at the concrete surface. This layer can be pulled off from the concrete surface very low force. In Figure 85 a dolly is shown that is pulled off from the surface that did not have a treatment. In this figure it is clear to see that a very thin cement skin was pulled off from the concrete. The glue was still even visible at the surface of the dolly.

The milled surface, which has the second roughest surface, appears to have the second lowest surface tensile strength. A mean value of 0.98 N/mm^2 was found for the surface tensile strength. In the case of milling, a thin layer of laitance was removed from the surface, but the clashes of the small hammers against the surface also weakened the surface below the laitance. In Figure 87 it can be seen that a somewhat thicker layer of cement was pulled off from the concrete during the Pull-Off test and even some broken parts of the aggregates were present on the dolly. Important is to note that the parts of the aggregates were broken, so they were not pulled off as a whole from the concrete. This breaking of the aggregates was caused by the clashes of the small hammers on the surface during milling.

The sanded surface has the second highest surface tensile strength. For the sanded surface a mean value of 1.30 N/mm^2 was found. In the case of sanding the laitance was scrubbed off the surface until the aggregates were visible at the surface. Even little parts of the aggregates were sanded, creating a surface with a low amount of weak spots. Because a very smooth surface was created it was relatively easy to glue to dolly to the surface. In Figure 86 it can be seen that bigger parts of the concrete are pulled off during the pull of test. Not only cement parts, but also aggregates are pulled off as a whole from the surface. The force to pull off these aggregates was relatively big, inducing a strong surface tensile strength.

Grit blasting the concrete surface had the biggest influence on the surface tensile strength. For the grit blasted surface a mean value of 1.57 N/mm^2 was found for the surface tensile strength. The blasted grit removed a big part of the weak parts at the surface, until the aggregates became visible as a whole. This induced that all the weak parts were removed from the surface. In Figure 88 it can be seen that relatively big parts of the concrete are pulled off, with even whole aggregates stuck on it.

After comparing the results of the sanded surface to the results of the grit blasted surface it is concluded that the grit blasted surface gave a bigger spread. This spread is probably due to the fact that it is harder to glue the whole area of the dolly to the rough grit blasted surface. This induces little parts of the glue not to connect to the surface, so the

pulling force has to be distributed by a smaller area of the concrete surface. In Figure 88 it can also be seen that some parts of the glue are still visible in yellow.

Table 27: results experiment 2.1

	Dolly 1 (N/mm ²)	Dolly 2 (N/mm ²)	Dolly 3 (N/mm ²)	Dolly 4 (N/mm ²)	Dolly 5 (N/mm ²)	Max (N/mm ²)	Min (N/mm ²)	Mean (N/mm ²)
No surface treatment	0.71 0.42	1.04 0.35	0.97 0.58	0.77 0.71	0.63 0.67	1.04	0.35	0.68
Sanded surface	1.72 1.39	1.38 1.38	1.40 0.95	1.53 0.90	1.49 0.83	1.72	0.83	1.30
Milled surface	0.93 0.80	1.35 1.04	0.65 0.87	1.06 1.02	1.32 0.80	1.35	0.65	0.98
Grit blasted surface	1.74 1.74	1.61 2.17	1.29 1.72	1.21 1.25	1.63 1.34	2.17	1.21	1.57



Figure 85: pulled off dolly no surface treatment



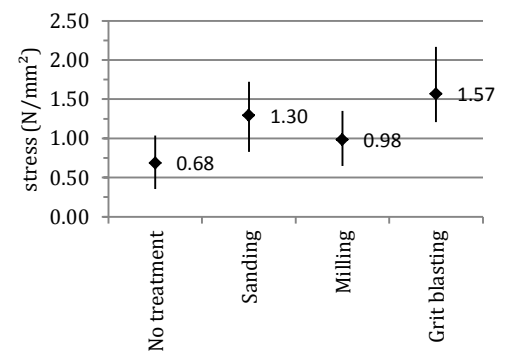
Figure 86: pulled off dolly sanded surface



Figure 87: pulled off dolly milled surface



Figure 88: pulled off dolly grit blasted surface



Graph 41: result ranges experiment 2.1

Experiment 2.2: bond strength at a second layer of sand cement

Five days after pouring the sand cement layer on the concrete specimen the moulds were removed. During demoulding it appeared that the sand cement layer was detached from the concrete specimen, so no bond was created between the two layers. When removing the sand cement layer a dry and little sandy surface was found at the surface of the specimen. This implies that there was probably not enough water present at the adhesion area to hydrate all the mixture of the second layer. Due to the fact that the concrete of the specimen was only two weeks old it is expected that the surface still showed a lot of suction. This caused the water from the sand cement mixture to be sucked into the concrete specimen, creating a dry area between the two concrete layers.

From this experiment it is concluded that no matter how rough the surface is made, it still is very important to treat/cure the concrete surface to achieve a good bond. A better bond could have been achieved by making use of a primer before applying the sand cement layer that reduces suction of the concrete specimen.

Practical experiments

Experiment 2.3: bond strength at a second layer of a liquid cementitious mixture

Before pouring the liquid cementitious layer the concrete surface was treated in the same four ways as is done in experiment 2.1. The bond strength tests were performed after 14 days of hydrating of the liquid cementitious layer. The results of the experiment are given in Table 28. The mean values including the maximal and minimal measured value of the results are shown in Graph 41 per surface treatment.

Table 28: results experiment 2.3

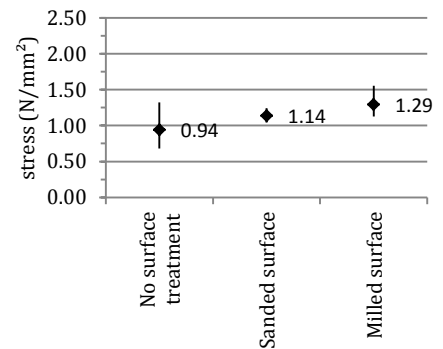
	Dolly 1 (N/mm ²)	Dolly 2 (N/mm ²)	Dolly 3 (N/mm ²)	Dolly 4 (N/mm ²)	Dolly 5 (N/mm ²)	Max (N/mm ²)	Min (N/mm ²)	Mean (N/mm ²)
No surface treatment	0.92	1.32	0.68	-	0.85	1.32	0.68	0.94
Sanded surface	1.24	1.04	1.15	1.04	1.22	1.24	1.04	1.14
Milled surface	-	1.55	1.34	1.16	1.12	1.55	1.12	1.29
Grit blasted surface	-	-	-	-	-	-	-	-



Figure 89: pulled off dolly no surface treatment



Figure 90: pulled off dolly sanded surface



Graph 42: result ranges experiment 2.3



Figure 91: pulled off dolly milled surface



Figure 92: pulled off dolly grit blasted surface

Table 28 shows no measured results for the grit blasted surface. During testing the plane of failure was consistently directly below the dolly (Figure 92). In this way only the surface tensile strength of the top layer was measured, what means that no exact value could be given to the bond strength. Stress values between 1.1 – 1.6 N/mm² were found in these tests. It could be stated that the bond strength then should be even stronger than the measured results. However, the plane of failure directly below the dolly could also be caused by incorrect testing. Experiments in section 0 showed that eccentric loading can cause the plane of failure to shift from the tip of the drilled core to the plane directly below the dolly.

The milled surface gave with a mean value of 1.29 N/mm² the best results for the bond strength. The sanded surface had with a mean value of 1.14 the second best results and the surfaces that were not treated induced the lowest bond strength. For these surfaces a mean value of 0.94 N/mm² was found. In Figure 89 - Figure 91 the pulled off cores are given for the different surface treatments.

In Figure 89 it can be seen by the grey colour that laitance was still present at the substrate surface that did not undergo a surface treatment. The laitance is a weak layer that can be pulled off from the substrate very easily, resulting in weak bond strength. Graph 42 shows a big spread in the results of the Pull-Off tests. Because the surface of the substrate differs in roughness and amount of laitance per location big differences are found in bond strength per location.

The sanded surface gave the smallest spread in the results. Because of the sanding the surface of the substrate is smooth and a big amount of laitance is removed. In Figure 86 a pulled off core is shown. In this figure it can be seen that the surface where the bond was formed was very smooth. Because the surface roughness of the substrate was almost equal at every location the results in bond strength do not show a big spread. The grey parts at the surface show that a small amount of cement is pulled off from the substrate. This indicates that the amount of laitance was reduced, compared to the situation where no treatment was applied to the surface.

A pulled off core of the milled surface is presented in Figure 91. In this figure it is clear to see that the roughness of the substrate surface is rougher than in the other situations. In the figure no light grey parts are visible at the surface of the drilled core, what means that the milling did successfully remove the laitance. At the surface darker and lighter parts are visible. The lighter parts contain cement parts of the substrate, the darker parts indicate the cementitious mixture of the second layer. As the darker parts are visible this implies that the strength properties of the substrate are optimal at these locations. This induces the bond to fail at the maximal tensile strength of the second layer. Nevertheless, not the whole bond failed at the maximal tensile strength of the second layer, so the substrate still contained weaker parts.

7.4 Review

In this chapter a description and presentation of the results of two practical experiments was given. The first experiment included a research to the influence of several practical parameters on the results of Pull-Off tests. The second experiment included a research to the influence of substrate surface roughness on the bond strength of cementitious screed layers on a concrete substrate. The results of the experiments are consecutively discussed in this review.

Pull-Off testing

The parameters that were varied in the research consisted of the application of different testing devices, the application of a drilled core / no drilled core, diagonal loading, eccentric gluing and diagonal drilling of the cores. From the experiments it is concluded that the manually driven analogue device has a lower accuracy and a bigger spread than the automatically driven digital device. This is due to the fact that the increase in pulling force is generally faster and not constant at the manually driven device. In the continuation of the experiments the digital device was maintained.

Applying no drilled core caused the results of the Pull-Off test to be >30% bigger than in the situation where a drilled core was applied. The increase is due to the fact that a bigger surface is used to distribute the tensile forces to the concrete. This explanation is proven by the fact that the area that stuck to the dolly after pulling off was bigger than the surface of the dolly itself.

Diagonal loading did not directly lead to a deviation of the maximum pulling force. However the plane of failure shifted from directly below the dolly to the tip of the drilled core in all the situations. Eccentric gluing did significantly influence the results of the Pull-Off tests. A dolly 5 mm from the side of the dolly not glued to the surface of the concrete already caused the results to be on average 18% lower.

Applying a diagonal drilled core induced stress concentrations at the tip of the drilled core. This caused the maximal pulling force to be lower. Furthermore the plane of failure shifted from directly below the dolly to the tip of the drilled core. Applying a diagonal load with slope 1:10 results on average led to a decrease of $\pm 10\%$ from the maximal pull off force.

Bond strength

In order to get insight in the values that are achievable for the bond strength of cementitious screeds on concrete bearing floors three experiments were performed. For the purpose of the entire experiments concrete specimen were casted and after hydrating the surfaces of these specimens were treated in order to remove laitance and roughen the surface. In the end there were four types of surfaces, consisting of a not treated surface, a sanded surface, a milled surface and a grit blasted surface.

In the first experiment the surface tensile strength of the surfaces of the specimen was tested with help of the Pull-Off test. In section 2.7 it was explained that in the regulations for screeds it is prescribed that the substrate surface requires to have a minimum tensile strength that is equal to the required bond strength in order to achieve a good bond. The experiments have shown that the order of mean surface tensile strength per surface treatment is: 'no treatment (0.68 N/mm^2)' - 'milling (0.98 N/mm^2)' - 'sanding (1.30 N/mm^2)' - 'grit blasting (1.57 N/mm^2)'.

The specimens that were used for the second experiment were after performing the surface treatments provided with a sand cement screed layer. Before applying the screed layer the substrate surface was pre-wetted in order to reduce suction of the substrate. However, after hardening of the screed layer the sand cement appeared to be not bonded to the substrate. As the interface was very dry and a little sandy this implied that there was not enough water present at the adhesion area to hydrate all the mixture of the second layer, presumably due to suction of the two weeks young substrate. From this experiment it was concluded that no matter how rough the surface is made, it still is very important to treat/ cure the concrete surface to achieve a good bond. A better bond could have been achieved by making use of a primer before applying the sand cement layer that reduces suction of the concrete specimen.

In the third experiment the specimen were provided with a liquid cementitious layer. From this experiment it was concluded that the order of mean bond strength per surface treatment is: 'no treatment (0.94 N/mm^2)' - 'sanding (1.14

Practical experiments

N/mm²)' - 'milling (1.29 N/mm²)'. No measured results were found for the grit blasted surface. During testing the plane of failure was consistently directly below the dolly, instead of at the bonded interface. Stress values between 1.1 – 1.6 N/mm² were found in these tests. It could be stated that the bond strength then should be even stronger than the measured results. However, incorrect testing could be a cause of the shift in plane of failure as well.

By comparing the results of the bond strength tests with the results of the substrate surface tensile tests it is concluded that a rougher substrate surface does not directly indicate a stronger substrate surface tensile strength or stronger bond strength. Furthermore it is concluded that it is possible for the bond strength to be stronger than the original substrate surface tensile strength.

8. Conclusions and recommendations

8.1 Conclusions

This study evaluated the causes and mechanism of cracking and debonding of cementitious screeds, the formation of the bond between screeds and concrete bearing floors and the method to determine the bond strength. The main conclusions of this study are summarized in this chapter. The objective of the study was to:

Obtain insight in the cracking and debonding behaviour of screed and provide a guideline which describes in what way the properties of bonded screeds can be controlled and which requirements must be met to control debonding/cracking of screeds.

Concerning the cracking and debonding behaviour the following conclusions are drawn:

1. Stresses in screeds are in most cases induced by imposed deformations (due to shrinkage, temperature deformations, moisture changes) which arise as a result of restraint in movement of the screeds. Cracking of screeds occurs when stresses in the screed have reached the tensile strength of the material;
2. The stresses are influenced by the amount of strain difference between the screed and bearing floor. The most relevant stresses that arise in the screed are horizontal tensile stresses (σ_{xx}). These stresses are zero at the edge of a floor and increase to its maximum at increasing distance from the edge. When the amount of shrinkage becomes that high that the tensile strength of the screed is reached cracks will occur in the screed. In the case of a crack a new 'edge' situation is formed, where the horizontal stress increases from zero to its maximum value at increasing distance from the crack;
3. Besides stresses in the screed strain differences cause stresses at the interface as well, existing of vertical (σ_{yy}) and shear (τ_{xy}) interface stresses. When the tensile / shear strength of the bond between screed and bearing floor is reached debonding will occur;
4. The vertical and shear interface stresses that arise due to strain differences are maximal at the edge of a floor field, decreasing to zero at increasing distance from the edge. In the case a crack is formed the stresses are again maximal at the location of the crack and decrease to zero at increasing distance from the edge;
5. The main influencer of strain differences is screed shrinkage. In the case that for the hydration shrinkage of cementitious screeds a value can be assumed equally to concrete, the shrinkage is $\varepsilon_{s,max} = 0.3\%$. According to the FEM study this shrinkage results in a cracked screed (with properties equal to C20/25 concrete, thickness 50 mm), with maximal values for the interface stresses of $\sigma_{yy} = \pm 1.8 \text{ N/mm}^2$ and $\tau_{xy} = \pm 1.3 \text{ N/mm}^2$ were obtained;
6. In the standards for screeds the requirement of a value of 1.5 N/mm^2 is drafted for the substrate surface tensile strength, in order to achieve a good bond;
7. An increase in screed height increases the stresses at the interface. According to the analytical approach an increase of 20 mm screed thickness increases the maximum shear stress with 0.15 N/mm . According to the FEM study this increase is $\pm 0.08 \text{ N/mm}^2$. The vertical interface stress increases with 0.10 N/mm^2 ;
8. An increase in concrete class increases the stresses at both the interface and in the screed due to an increase of stiffness. However when it is assumed that the bond strength at the interface is increased as a result of a stronger screed strength this will not directly cause problems in debonding / cracking of the screed;
9. When debonding has occurred at the interface due to the fact that the shear strength / tensile strength of the bond is reached, the area and starting point over which the increase of the screed stress and the decrease of the interface stresses shifts away from the edge / crack. This causes the potential distance between two cracks to increase;
10. Debonding of the screed enables the screed to curl, causing serious damage to the screed in the form of fully debonded broken screed parts.

With respect to the formation of the bond and controlling the bond strength properties of screeds on concrete bearing floors the following conclusions are drawn:

1. The bond between screed and bearing floor is based on a combination of Van der Waals forces and mechanical interlocking;
2. Van der Waals forces are electromagnetic forces that work between two molecules and can be positively influenced by decreasing the distance between molecules. In practice this means that liquid mixtures for screeds will obtain stronger Van der Waals forces than earth dry mixtures;
3. Mechanical interlocking contains a mechanical anchorage that is created by mortar that covers the roughness of the substrate. The contact surface is essential in creating a good bond. The bigger the contact area, the bigger the potential of creating a good bond. Interlocking can be improved by improving the surface roughness and improving the absorption capacity of the substrate;
4. Caution is required with improving the absorption of the substrate, as a too large absorption can extract moisture from the adhesive interface, resulting in a lower quality of the screed at interface;

Conclusions and recommendations

5. Factors that influence the adhesion of screeds to concrete bearing floors concerning the concrete surface are surface cleanliness, laitance, surface moisture, surface roughness and substrate porosity. Factors concerning the overlay include the application of a bonding agent, overlay compaction and overlay curing;
6. From the practical experiment is concluded that the order of mean surface tensile strength of the concrete substrate per surface treatment is: 'no treatment (0.68 N/mm²)' - 'milling (0.98 N/mm²)' - 'sanding (1.30 N/mm²)' - 'grit blasting (1.57 N/mm²)';
7. Provided with a liquid cementitious layer the order of mean bond strength per surface treatment is: 'no treatment (0.94 N/mm²)' - 'sanding (1.14 N/mm²)' - 'milling (1.29 N/mm²)'. No valid results were found for the bond strength of the grit blasted situation;
8. No measurable bond was developed in the situation where the specimen were provided with a sand cement layer after wetting the roughened surfaces, indicating that no matter how rough the surface is made, it still is very important to treat/ cure the concrete surface to achieve a good bond;
9. A rougher substrate surface does not directly indicate a stronger substrate surface tensile strength or stronger bond strength;
10. It is possible for the bond strength to be stronger than the original substrate surface tensile strength;
11. In no situation a mean bond strength was measured above 1.29 N/mm². For a screed with properties equal to C20/25 concrete, thickness 50 mm it was given that a strain of 0.3‰ leads to an maximal interface stress of $\sigma_{yy} = \pm 1.8 \text{ N/mm}^2$. This indicates that none of the situations would be strong enough to prevent debonding.

Regarding the method with which the bond strength properties can be measured in order to validate if the requirements on the bond strength are met the following conclusions are drawn:

1. The best applicable test to determine the bond strength of screeds bonded to concrete bearing floors till so far is the Pull-Off test, mostly due to its possibility to perform the test in situ;
2. The Pull-Off test is very sensitive to give results that do not represent the actual surface tensile / bond strength:
 - a. When the pulling force is applied with eccentricities to the specimen, the maximal force that can be distributed by the concrete decreases with respect to the perfectly orthogonal situation with $\pm 6\%$ per millimetre eccentricity according to the analytical study;
 - b. The decrease of maximum force has a small increase when applying a higher concrete class or if the concrete contains smaller fracture energy;
 - c. A decrease of the dolly size results in an increase in the influence of the eccentricities, especially at dolly sizes with diameter <40 mm. The difference in results of dollies with diameter >50 mm are relatively small (2% at an eccentricity of 2 mm) according to the FEM study;
 - d. Applying no drilled core when performing the Pull-Off test results in 5.8% - 16% higher maximal pulling forces compared to the theoretical concrete strength according to the FEM study. The theoretical value is closely approached when drilled cores of >15 mm are applied;
 - e. The mean value of the results of Pull-Off tests with no drilled core were >30% higher than when a drilled core of 15mm was applied in the practical experiment;
 - f. Diagonal loading does not directly lead to a decrease of the maximal pulling force, but it does lead to stress concentrations at the tip of the drilled cores in an early stadium. This results in a shift of the plane of failure from directly below the dolly to the tip of the drilled core;
 - g. Partly, eccentric gluing causes the plane of failure to be at the glued surface instead of the tip of the drilled core. The decrease in maximal pull off force according to the FEM study gets up to 8% for a 5 mm not-glued dolly, increasing to maximal 22% for a 10 mm not glued dolly. According to the practical experiments the results of a 10 mm not glued dolly are on average 18% lower;
 - h. Diagonal drilling causes an increased stress concentration at the tip of the diagonal drilled core, resulting in lower pull off forces. The deviation according to the FEM study can get up to 11.9% for a drilled core with a deviated angle of 7.6°. By increasing the angle the deviation increases almost linearly. According to the practical experiment applying a diagonal load with slope 1:10 results on average leads to a decrease of $\pm 10\%$ from the maximal pulling force;
3. Manually driven devices which are used to perform Pull-Off tests are less accurate and give a bigger spread than automatically devices, due to its not perfectly regulated (high) speed in increasing the pulling force.

8.2 Discussion

In this study theoretical as well as practical research is carried out to several subjects in order to answer the main issue of the thesis. In the theoretical study the behaviour of screeds during shrinkage and the influence of eccentricities on the results of Pull-Off tests is analysed by means of an analytical and FEM study. In these studies the screed material is assumed to have properties equal to concrete. In current literature barely any data is available about the material properties of screeds. As there are different types of screed mixtures used in practice (such as sand cement mixtures and self-levelling liquid mixtures) the properties of these mixtures are expected to deviate. This can influence the strength properties of the screed / the bond between screed and bearing floor and the shrinkage behaviour.

The amount of screed shrinkage is assumed to be $\varepsilon_{s,max} = 0.3\%$, equal to concrete. Yet since there are different types of mixtures applied in practice with big differences in w/c factor, porosity and cohesion, the maximal amount of shrinkage is expected to deviate per mixture. Screed shrinkage is a major influencer in the development of stresses in screeds and at the interface between screeds and bearing floors. As it is expected that the maximal amount of screed shrinkage will deviate from the value that is assumed, the values of the stresses will deviate as well. This causes that a fully-founded statement about the minimal bond strength properties could not yet be carried out.

The concrete of the bearing floors and the screed materials are modelled in the theoretical studies as homogeneous materials. However in reality this is not the case. Concrete (screeds are assumed to be equal to concrete) is in reality a heterogeneous material, meaning that the properties are not equal in every direction. Concrete is dependent on the individual properties of (hydrated) cement, sand and coarse aggregates. The deviation of strength and stiffness properties in each direction may have influence on the behaviour and development in the screed and at the bonding interface during screed shrinkage and the cracking / failure behaviour of the concrete during Pull-Off tests.

In the theoretical analysis of the Pull-Off test the shape of the dolly was schematised as square instead of cylindrical to simplify the calculations. In section 5.2 a note was made what the influence of this different shape was on the behaviour of the concrete during eccentric performed Pull-Off tests. It is expected that the influence of eccentricities on the result of the Pull-Off test will be slightly less in the case of a cylindrical dolly.

For the purpose of the practical research concrete specimens were casted at a building site in Utrecht. In order to pour a concrete specimen with properties that approach the concrete of bearing floors that are fabricated in practice a mixture was used that came directly out of the truck mixers at site. However, concrete was used from several truckmixers at one day. It was assumed that the properties of the mixtures per truck were equal, but in reality the mixtures could be slightly different. This could cause the properties per specimen to be slightly different, what could induce in deviating results during testing.

During casting of the specimens intensive attention was payed to finishing of the concrete, in the form of wetting the surface and covering the surface with foil. As the specimens had a small surface it was relatively easy to ensure a good finishing. Yet in reality the surfaces of concrete floors can be large. This induces the accuracy of finishing to be less, causing the quality of the surfaces to be different at various locations. In practice the measured bond strengths and surface tensile strengths could be lower than in obtained in the experiments.

Per situation a minimum of 5 tests were performed to obtain the results, deviating per test situation. As this is a low amount of tests no scientifically grounded verdict could be made about the obtained results. However an indication of the direction where the results will end is made by these experiments.

By comparing the results of the theoretical and practical study concerning the influence of eccentricities on the results of Pull-Off tests it is concluded that the theoretical study gives a correct view of the behaviour of the concrete during the tests. The planes of failure from the practical experiments matched the predicted planes of failure from the FEM study. Furthermore a good insight is given in the FEM study in what parameter has the greatest influence in the results of the Pull-Off tests, although the percentages in deviations show differences between the experiments and the FEM study.

8.3 Recommendations

To conclude this report in this section recommendations are given for the implementation of the information given in this study in practice as well as recommendations for further research.

Surface tensile strength

In the study practical research is carried out to the influence of surface roughness treatments on the surface tensile strength. From this study it is concluded that the order of mean surface tensile strength of the concrete per surface treatment is: no treatment – milling – sanding – grit blasting. In the standards for screeds the requirement is drafted that the substrate surface tensile strength must be at least 1.5 N/mm^2 to provide a good bond between screed and substrate. Grit blasting is the only method with which a mean value of at least 1.5 N/mm^2 is achieved. Yet some of the results were still below 1.5 N/mm^2 so this method does not ensure the surface tensile strength to be minimal 1.5 N/mm^2 at every location. Furthermore it is expected that other factors such as the intensity of grit blasting, the amount of laitance at the concrete surface and more will influence the surface tensile strength. Further research is recommended to make clear in what way the minimum value at every location of the concrete surface can be achieved.

Conclusions and recommendations

Tensile bond strength

Practical research is performed in this study to the influence of surface roughness treatments on the tensile bond strength of screeds on concrete bearing floors. From this study it is concluded that the order of mean bond strength per surface treatment is: no treatment – sanding – milling. For the grit blasted surfaces no values are obtained during the test. This could be an effect of wrongly executed Pull-Off tests, what induced the plane of failure to shift from the tip of the drilled core to the plane directly below the dolly. Yet this could also mean that the bond strength is stronger than the screed material and that as a result of this the plane of failure during the Pull-Off tests was not at the bonded interface. Further research is recommended with stronger screed properties to obtain values of the bond strength at grit blasted substrate surfaces.

Besides the substrate roughening treatments other factors influence the bond strength as well. To give a good insight in how different values for the bond strength can be achieved it is recommended to study the influence of factors such as substrate porosity, substrate surface moisture content, application of a bonding agent, screed mixture cohesion and screed curing on the bond strength.

Screed strain

In the FEM study analyses is done on the screed behaviour at strain differences between screed and bearing floor of maximal 0.3‰. This value represents the shrinkage of the screed, where a value for shrinkage is assumed to be equal to concrete. However in the discussion it is already mentioned that it is expected that this value will be different in reality. Furthermore no strain differences due to temperature changes are included in the analyses. In order to make a clear statement about the maximal stress values that will rise in the screed and at the interface further research is recommended to be performed to the amount of screed strain due to shrinkage and temperature differences.

Shear bond strength

The tensile bond strength of screeds on concrete bearing floors was the main subject that was studied in this research. Yet from the study it is concluded that besides tensile stresses, bonded interfaces will be subjected to shear stresses as well. The Pull-Off test method with which the bond strength is determined in this study only tests the tensile bond strength. In the practical experiments no values were obtained of the shear bond strength and the influence of factors such as substrate roughness on the shear bond strength. In chapter 4 it is mentioned that the shear strength overall is a factor 2.04 higher than the tensile strength. However more research is recommended to the development and the values of the shear bond strength to get insight in the relation between the shear and tensile strength. With that data a more complete view can be given in the bond between screeds and bearing floors and its debonding behaviour.

Screed cracking behaviour

This study was mainly focussed on the bond strength of screeds on bearing floors during screed shrinkages and how to increase the bond strength. However from the theoretical analysis it is concluded that strain differences can cause besides debonding also cracking of the screeds. At the location of a crack the stresses of interfaces are high, what means that there will be more places with high interface stresses if more cracks are present in a screed. In the study no research is done to the tensile strength properties of screeds, the application of reinforcement and the way in which cracking can be prevented / reduced. Further research on this subject is advised.

Test method

The Pull-Off test is in this study handled to test the bond strength of screeds on bearing floors and the surface tensile strength. This method is preferred to be used mostly because its possibility to perform tests on site. From the study it is concluded that it is recommended to always use an automatically driven Pull-Off tester to increase the accuracy of the results. To obtain the right values the test should always be performing with drilling a core of minimal 15 in the substrate (in both the bond as the surface tensile strength test). Furthermore a dolly has to be used with a minimum diameter of 50 mm.

The Pull-Off test method only tests the tensile bond strength. In order to have a complete view of the bond strength between screeds and bearing floors it is of importance to have information about the shear bond strength as well. Further research to methods with which the shear bond strength can be tested is advised. Here it is preferred to do study to a test method which can be executed on site.

Lists of figures and tables

Figures

Figure 1: the automatic motorized Pull-Off bond strength tester [2].....	7
Figure 2: fracture surface after executing the Pull-Off test [2].....	7
Figure 3: fracture surface on the substrate [2].....	7
Figure 4: bonded screed.....	9
Figure 5: unbonded screed on a separation layer.....	9
Figure 6: floating screed on an insulation layer.....	9
Figure 7: floating screed with floor heating.....	9
Figure 8: bonded Terrazzo.....	10
Figure 9: floating Terrazzo on an insulation layer.....	10
Figure 10: stress-strain diagram concrete.....	10
Figure 11: cementitious screed casted on a concrete bearing floor.....	11
Figure 12: local heating can cause eigenstresses in sections.....	11
Figure 13: difference in stress distribution in screed applied with bond, without bond and on an insulation layer.....	12
Figure 14: interface shear stresses as a result of deflection of a multiple layered floor.....	13
Figure 15: shear distribution and shear stress in a single span floor.....	13
Figure 16: development of shear and tensile stresses in a screed [3].....	15
Figure 17: schematic representation of curving leading to cracking.....	15
Figure 18: mechanical interlocking.....	17
Figure 19: contact area of solid materials applied on a concrete substrate.....	17
Figure 20: rough hydrated cement grains with small contact points (left) versus polymer modified mortar (right) [8].....	18
Figure 21: the sand patch method is used to determine the Average Texture Depth (ATD).....	19
Figure 22: degree of influence of different factors influencing bond strength.....	19
Figure 23: three bond strength measuring categories.....	21
Figure 24: failure envelope of the different measuring categories presented in Mohr's circles.....	21
Figure 25: different methods to determine the tensional bond strength of two concrete layers.....	22
Figure 26: eccentric loading as a result of not-centric placing of the tripod or drilling the core under an angle.....	22
Figure 27: shear bond test methods.....	23
Figure 28: compressive-shear bond test methods.....	24
Figure 29: setup pull off test with eccentric tensile force.....	25
Figure 30: deformation after applying eccentric tensile force.....	25
Figure 31: stress- deformation relation concrete specimen.....	25
Figure 32: distribution of tensile stresses along the width of the dolly.....	26
Figure 33: to obtain stability the outer forces have to equal the inner forces.....	26
Figure 34: shift of centreline as a result of a not glued surface at 5 mm from the edge for a cylindrical and a square dolly.....	30
Figure 35: schematisation pull off test used for the FEM approach.....	31
Figure 36: principal total strain and crack formation for specimen with low G_f at maximal tensile force ($u_y = 10 \mu\text{m}$), plane surface.....	33
Figure 37: principal total strain and crack formation for specimen with low G_f at maximal tensile force ($u_y = 10 \mu\text{m}$), 15 mm drilled core.....	33
Figure 38: principal total strain and crack formation for specimen with high G_f at maximal tensile force ($u_y = 14 \mu\text{m}$), plane surface.....	33
Figure 39: principal total strain and crack formation for specimen with high G_f at maximal tensile force ($u_y = 10 \mu\text{m}$), 15 mm drilled core.....	33
Figure 40: principal total strain and crack formation for a diagonal loaded specimen ($s = 2:10$) at $u_y = 6 \mu\text{m}$	35
Figure 41: principal total strain and crack formation for a diagonal loaded specimen ($s = 2:10$) at maximal pulling force ($u_y = 12 \mu\text{m}$).....	35
Figure 42: principal total strain and crack formation for a partly glued specimen ($g = 5 \text{ mm}$) at $u_y = 6 \mu\text{m}$	36
Figure 43: principal total strain and crack formation for a partly glued specimen ($g = 5 \text{ mm}$) at $u_y = 12 \mu\text{m}$	36
Figure 44: principal total strain and crack formation for a partly glued specimen ($g = 5 \text{ mm}$) at $u_y = 6 \mu\text{m}$, x-supported.....	37
Figure 45: principal total strain and crack formation for a partly glued specimen ($g = 5 \text{ mm}$) at $u_y = 20 \mu\text{m}$, x-supported.....	37
Figure 46: principal total strain and crack formation at maximal tensile force for a 2 mm diagonal, 15 mm drilled core, no support in x-direction.....	38
Figure 47: principal total strain and crack formation at maximal tensile force for a 2 mm diagonal, 15 mm drilled core, supported in x-direction.....	39
Figure 48: schematisation shrinkage model used for the analytical approach.....	41
Figure 49: schematisation screed shrinkage model used for the FEM approach.....	45
Figure 50: curving of the screed at the edge of the specimen causes vertical tensile stresses at the interface.....	46
Figure 51: analogue device.....	55
Figure 52: digital device.....	55
Figure 53: minimal distances between drilled cores.....	55
Figure 54: irregularities at the concrete surface can cause diagonal loading.....	56
Figure 55: elevated leg front view.....	56
Figure 56: elevated leg side view.....	56
Figure 57: fully glued dolly.....	56
Figure 58: dolly 5 mm not glued.....	56
Figure 59: dolly 10 mm not glued.....	56
Figure 60: eccentric drilled core.....	56

Lists of figures and tables

Figure 61: analogue device.....	57
Figure 62: digital device.....	57
Figure 63: pulled off dolly without applying a drilled core	58
Figure 64: pulled off dolly with applying a drilled core	58
Figure 65: pulled off dolly: concrete failure at the surface of the concrete	59
Figure 66: pulled off dolly: concrete failure at the tip of the drilled core.....	59
Figure 67: dolly 5mm not glued.....	60
Figure 68: dolly 10mm not glued	60
Figure 69: pulled off dolly orthogonal drilled core.....	60
Figure 70: pulled off dolly drilled core with slope 1:10	60
Figure 71: concrete surface not treated.....	61
Figure 72: concrete surface treated by sanding.....	61
Figure 73: concrete surface treated by milling.....	61
Figure 74: concrete surface treated by grit blasting.....	61
Figure 75: pulled off dolly no surface treatment.....	63
Figure 76: pulled off dolly sanded surface.....	63
Figure 77: pulled off dolly milled surface.....	63
Figure 78: pulled off dolly grit blasted surface.....	63
Figure 79: pulled off dolly no surface treatment.....	64
Figure 80: pulled off dolly sanded surface.....	64
Figure 81: pulled off dolly milled surface.....	64
Figure 82: pulled off dolly grit blasted surface.....	64
Figure 83: Terrazzo floor detail Erasmus MC.....	75
Figure 84: crack initiation at the location of the prefab concrete blocks	75
Figure 85: concrete tensile strength types in a terrazzo floor section.....	76

Tables

Table 1: four types of concrete shrinkage.....	11
Table 2: Coefficients of Thermal Expansion for common Portland Cement Concrete components [5]	13
Table 3: Dutch standards concerning screeds	15
Table 4: German and British standards concerning screeds	16
Table 5: methods to roughen the substrate surface, ranked in increasing roughness.....	18
Table 6: overview of the available standardisation of pull-off tests	22
Table 7: material parameters according to MC 2010	27
Table 8: geometry parameters	27
Table 9: deviation of maximal tensile force at 1 mm eccentricity of various concrete classes.....	29
Table 10: material properties concrete elements	31
Table 11: maximal tensile force at various core drilling depths and their deviation from the theoretical force.....	32
Table 12: comparison of results FEM and Analytical approach	34
Table 13: maximal tensile force per diagonal loading slope.....	35
Table 14: maximal mean tensile stress with partly glued dollies.....	36
Table 15: maximal mean tensile stress with partly glued dollies, supported in x-direction	37
Table 16: maximal tensile force pull off test with eccentric drilled cores.....	38
Table 17: parameters applied in analytical approach.....	41
Table 18: material properties concrete elements	45
Table 19: Coefficients for the determination of interface shear strength according to the MC 2010 [35]	50
Table 20: results compression and tensile split tests after 32 days hydration.....	56
Table 21: results experiment 1.1.....	57
Table 22: results experiment 1.2	58
Table 23: results experiment 1.3.....	59
Table 24: results experiment 1.4.....	59
Table 25: results experiment 1.5.....	60
Table 26: results compression and tensile split tests after 45 days hydration.....	62
Table 27: results experiment 2.1	63
Table 28: Linear Expansion Coefficient of aggregates and concrete [4].....	77
Table 29: requirements given in the Dutch standards concerning bond strength	77
Table 30: requirements given in the Dutch standards concerning cracking of screeds.....	77

References

- [1] Ir. C. A. van der Steen, "brief tcb150626/dki/cst: Trekproeven op vloeren Erasmus MC 08.12.2015," Technoconsult, Heeswijk, 9 december 2015.
- [2] Ir. C. A. van der Steen, "brief tcb150615/cst: Resultaten metingen huidtreksterkte diverse projecten," Technoconsult, Heeswijk, 15 december 2015.
- [3] NEN-EN 1542, "Products and systems for the protection and repair of concrete structures - Test methods - Measurement of bond strength by pull-off," 1999.
- [4] NEN-EN 13892-8, "Determination of bond strength of screed materials," 1990.
- [5] Dr. Ir. D. A. Hordijk, "Local approach to fatigue of concrete," Delft, 1991.
- [6] Ir. C. A. van der Steen, *Het (Dek)vloerenboek*, Bedrijfschap Afbouw, 2010.
- [7] K. van Breugel, C. R. Braam, E. A. B. Koenders, *Concrete Structures under Imposed Thermal and Shrinkage Deformations*, Delft, 2013.
- [8] Wetenschappelijk en technisch centrum voor het bouwbedrijf, "Dekvloeren deel 2: uitvoering," Carlo De Pauw, 1994.
- [9] Ir. H. Borsje, "Scheurvorming en onthechting van afwerkklagen op beton," in *Special Betondag 1996*, 1996.
- [10] Stichting CUR, "CUR/Betonvereniging-publicatie 172 "Duurzaamheid en onderhoud van betonconstructies"," Gouda, januari 1998.
- [11] prof. dr. J. Bijen, dr. ir. P. E. Roelfstra and dr. ir. T. Salet, "Hechting van jong beton aan oud beton," *Cement*, vol. 11, pp. 76-83, 1993.
- [12] J. Silfwerbrand and J. Paulsson, "Better Bonding of Bridge Deck Overlays," *Concrete International*, vol. October, pp. 56-61, 1998.
- [13] J. Silfwerbrand, "Improving Concrete Bond in Repaired Bridge Decks," *Concrete International*, vol. September, pp. 61-66, 1990.
- [14] S. Austin, P. Robins and Y. Pan, "Tensile bond testing of concrete repairs," *Materials and Structures*, vol. 28, pp. 249-259, 1995.
- [15] J. Silfwerbrand, "Bonded concrete overlays - bond strength issues," in *Concrete Repair, Rehabilitation and Retrofitting*, London, ICCRRR, 2006, pp. 19-21.
- [16] P.M.D. Santos and E.N.B.S. Júlio, "Factors affecting Bond between New and Old Concrete," *ACI Materials Journal*, vol. 48, no. 108, pp. 449-456, 2011.
- [17] P.M.D. Santos, E.N.B.S. Júlio and V. D. Silva, "Correlation between concrete-to-concrete bond strength and roughness of the substrate surface," *Construction and Building Materials*, no. 21, pp. 1688-1695, 2007.
- [18] L. Courard, A. Garbacz and T. Piotrowski, "Effect of concrete substrate texture on the adhesion properties of PCC repair mortar," ResearchGate, 2014.
- [19] A. Garbacz, M. Górka and L. Courard, "Effect of concrete surface treatment in repair systems," *Magazine of Concrete Research*, vol. 0, no. 56, pp. 1-12, 2014.
- [20] E.N.B.S. Júlio, F. Branco and V. D. Silva, "Concrete-to-concrete bond strength. Influence of the roughness of the substrate surface," *Construction and Building Materials*, pp. 675-681, 17 June 2004.
- [21] NEN-EN 1504-3, "Products and systems for the protection and repair of concrete structures - Definitions, requirements, quality control and evaluation of conformity - Part 3: Structural and non-structural repair," 2005.
- [22] M.M. Sprinkel, "Bond strength between shotcrete overlay and reinforced concrete base," *Concrete repair bulletin*, vol. January/February, pp. 8-13, 2016.
- [23] K. R. Hindo, "In-place Bond Testing and Surface Preparation of Concrete," *ACI*.
- [24] A. Momayez, M.R. Ehsani, A.A. Ramezani pour and H. Rajaie, "Comparison of methods for evaluating bond strength between concrete substrate and repair materials," *Cement and Concrete Research*, vol. 35, pp. 748-757, 2005.
- [25] A.I. Abu-tair, S.R. Rigden and E. Burley, "Testing the bond between repair materials and concrete substrate," *ACI Mater*, vol. 6, no. 93, pp. 553-558, 1996.
- [26] R. Yamashita, M. Okano, Y. Horoi, T. Yamamoto and T. Miyagawa, "Flexural Bond Strength and Fracture Energy Tests of Concrete Joint Using Simple Beam Specimen Connected with Concrete Adhesives," in *Third International Conference on Sustainable Construction Materials and Technologies*, Kyoto, 2013.
- [27] L.I. Knab and C.B. Spring, *Evaluation of Test Methods for Measuring the Bond Strength of Portland-Cement Based Repair Materials to Concrete*, Gaithersburg: US Department of commerce, 1988.
- [28] A. Momayez, A.A. Ramezani pour, H. Rajaie and M.R.Ehsani, "Bi-Surface Shear Test for Evaluating Bond between Existing and New Concrete," *ACI Materials Journal*, Vols. 101-M11, pp. 99-106, 2004.
- [29] J. Silfwerbrand, "Shear bond strength in repaired concrete structures," *Materials and Structures*, vol. 36, pp. 419-424, 2003.
- [30] J.L. Granju, B. Bissonnette, L. Courard and L. Fowler, "Bonded Cement-Based Material Overlays for the Repair, the Lining or the Strengthening of Slabs or Pavements," State-of-the-Art Report of the RILEM Technical Committee 193-RLS, 2011.
- [31] F. Saucier, J. Bastien, M. Pigeon and M. Fafard, "A combined shear-compression device to measure concrete-to-concrete bonding," *Experimental Techniques*, vol. September/ October, pp. 50-55, 1991.
- [32] S. Austin, P. Robins and Y. Pan, "Shear bond testing of concrete repairs," *Cement and Concrete Research*, vol. 29, pp. 1067-1076, 1999.
- [33] British Standard, "BS 6319-4:1984 Testing of resin and polymer/cement compositions for use in construction. Method for measurement of bond strength (slant shear method)," BSI, 1984.

References

- [34] ASTM International, "ASTM C882-99 Standard Test Method for Bond Strength of Epoxy-Resin Systems Used With Concrete By Slant Shear," ASTM, West Consohocken, 1999.
- [35] N.J. Delatte, M.S. Williamson and D.W. Fowler, "Bons Strength Development with Maturity of High-Early-Strength Bonded Concrete Overlays," *ACI Materials Journal*, Vols. 96-M26, pp. 201-207, 2000.
- [36] fib, "Model Code 2010 First complete draft Volume 1," International Federation for Structural Concrete (fib), Lausanne, Switzerland, 2010.
- [37] Office of Research, Development and Technology, RDT, "Portland Cement Concrete Pavements Research," U.S. Departement of Transportation, 3 August 2016. [Online]. Available: <https://www.fhwa.dot.gov/publications/research/infrastructure/pavements/pccp/thermal.cfm>. [Accessed 22 Februari 2017].
- [38] Stufib studiecel 9, "Losse toplagen in monoliet afgewerkte betonvloeren," Stufib, Nieuwegein, oktober 2006.
- [39] Mapei, "Technical Notebook - Laying floor screeds".
- [40] WTCB, "Technische voorlichting 189 - Dekvloeren," Brussel, September 1993.
- [41] Ir. C.A. van der Steen, "Communicatie of Confrontatie - spanningen door de complexiteit van vloeren," *VTM*, vol. 2, pp. 4-7, 2011.
- [42] Ir. C.A. van der Steen, "Samenhang dekvloer bepaalt de kwaliteit," *VTM*, vol. 3, pp. 12-15, 2013.
- [43] Ir. P. D. Steijaert, "Niet-constructieve schade aan bedrijfsvloeren," *Cement*, vol. 2, 1994.
- [44] K.N. Bakhsh, "Evaluation of Bond Strength between Overlay and Substrate Repairs - Master Degree Thesis," KTH Architecture and the Built Environment, 2010.
- [45] NEN 1042, "In-situ floorings - Quality and execution of cement bonded terrazzo wearing surfaces," 2001.
- [46] NEN 2741, "In-situ floorings - Quality and execution of cementitious screed," 2001.
- [47] NEN 2742, "In-situ floorings - Floating screed - Terms, construction and quality control," 2007.
- [48] NEN-EN 13813, "Screed material and floor screeds - Screed material - Properties and requirements," 2002.
- [49] CUR-Aanbeveling 92, "Floor heating in Terrazzo flooring," 2002.
- [50] CUR-Aanbeveling 110, "Cementitious self-levelling screeds," 2012.
- [51] NEN 2741/A1, "In-situ floorings - Quality and execution of cementitious screed," 2008.
- [52] DIN 18353, "Allgemeine Technische Vertragsbedingungen für Bauleistungen - Estricharbeiten," 2016.
- [53] DIN 18560, "Estriche im Bauwesen," 2015.
- [54] BS 8204-1, "Screeds, bases and in situ floorings. Concrete bases and cementitious levelling screeds to receive floorings. Code of practice," 2009.
- [55] BS 8204-2, "Screeds, bases and in situ floorings. Concrete wearing surfaces. Code of practice," 2011.
- [56] BS 8204-4, "Screeds, bases and in situ floorings. Cementitious terrazzo wearing surfaces. Code of practice," 2011.
- [57] fib, "Model Code 2010 First complete draft Volume 2," International Federation for Structural Concrete, Lausanne, Switzerland, 2010.

Appendix

A.1 Background information

A.1.1 Terrazzo floors Erasmus MC

Terrazzo floors are concrete floors existing of multiple layers, where a concrete interlayer (possibly provided with shrinkage reinforcement and/or underfloor heating) is casted on a structural floor. On this layer a cementitious top layer is casted which serves as finishing layer. This top layer is provided with aggregates and surface treatment consisting of polishing/ sanding/ impregnating/ crystallising ensures that the correct aesthetic requirement is achieved.

At the Erasmus MC terrazzo floors were adhesively casted on constructive concrete floors. The total thickness of the screed was 80 mm, existing of a 60 mm interlayer (concrete quality C28/35) and a 20 mm top layer Eterno Terrazzo. The interlayer was provided with heating pipes with a diameter of 15mm and $\phi 5-75$ net reinforcement (Figure 30). Before casting the interlayer the concrete floor was cleaned and provided with a Cugla primer. The first 24 hours after casting the interlayer the concrete was kept wet and afterwards it was covered by a felt cloth provided with foil for a period of minimal 14 days. When the foil was removed, the floor was cleaned from dirt and dust and steel strips mounted on concrete cubes were placed in boxes of 1,2 m x 2,4 m. Subsequently the Cugla primer was applied and the top layer was casted, kept wet for 24 hours and covered with the felt cloth.

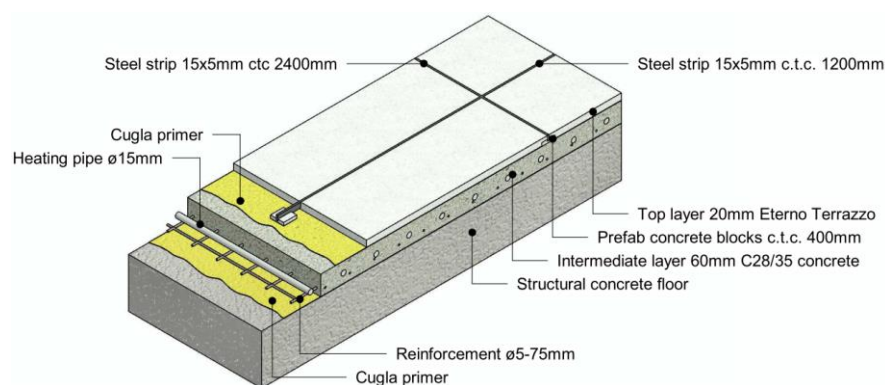


Figure 93: Terrazzo floor detail Erasmus MC

After a period of at least one month the felt cloth was removed. When the floor became visible it appeared that the floor was provided with a lot of cracks. In Figure 31 the cracks in the terrazzo floor are visualised in a plan view. This drawing makes clear that the cracks start at the location of the prefab blocks that are used to support the steel strips. Besides the cracks that appeared on the floor it was also found by knocking that the terrazzo was debonded from the intermediate layer at several places.

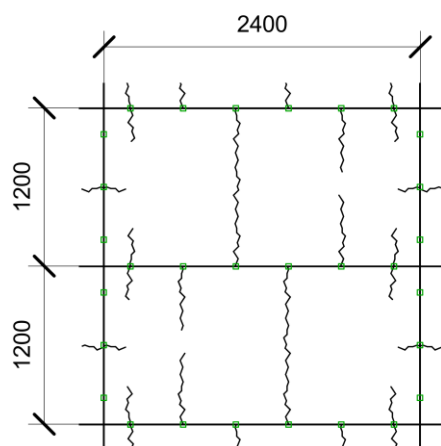


Figure 94: crack initiation at the location of the prefab concrete blocks

A.1.2 Different types of tensile strength

The central subject discussed in this report is the bond between two layers of concrete. A way to classify the bond strength of two layers of concrete is by determining the tensile bond strength. This tensile bond strength is dependent on the tensile strength at different layers of the bonding materials. To clarify the different types of tensile (bond) strength an overview is included in Figure 95, where a section of a terrazzo floor casted with bond to the bearing structure is used as guidance.

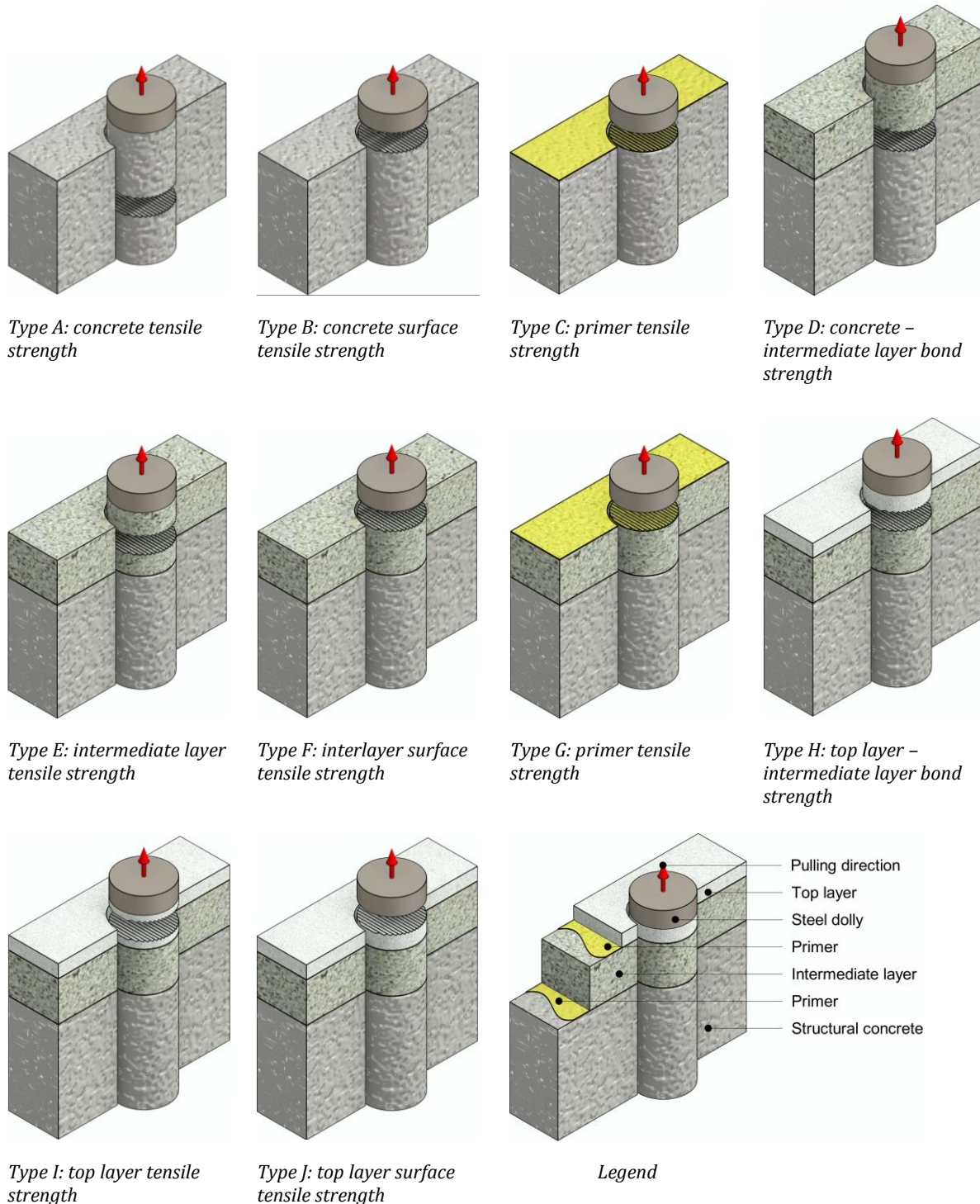


Figure 95: concrete tensile strength types in a terrazzo floor section

A.2 Tables

Table 29: Linear Expansion Coefficient of aggregates and concrete [7]

Aggregate type (silica weight content)	Linear Expansion Coefficient α ($\cdot 10^{-6} K^{-1}$)			
	aggregate (α_{agg})		concrete (α_c)	
	range	average	range	average
Quartzite (94%)	7,0 – 13,2	10,3	11,7 – 14,6	12,1
Quartz (94%)	-	-	9,0 – 13,2	-
Sandstone (84%)	4,3 – 12,1	9,3	9,2 – 13,3	11,4
Granite (66%)	1,8 – 11,9	6,8	8,1 – 10,3	9,6
Dolomite (50%)	4,5 – 8,5	6,8	-	9,6
Basalt (51%)	4,0 – 9,7	6,4	7,9 – 10,4	9,3
Limestone (0%)	1,8 – 11,7	5,5	4,3 – 10,3	8,6
Moraine aggr. (5-95%)	-	-	9,0 – 13,5	-
Fly ash (0%)	5,1 – 7,5	-	-	-

Table 30: requirements given in the Dutch standards concerning bond strength

Code	Requirement
NEN 1042	<ul style="list-style-type: none"> - The thickness of the intermediate layer of terrazzo floors bonded to the bearing floor has to be at least 30mm, for terrazzo floors without bond to the bearing floor this has to be at least 50mm; - In case of terrazzo bonded to the bearing floor the substrate needs to have a 'slightly roughened surface' to improve bond strength; - To provide good adhesion between bearing floor and terrazzo the substrate needs to be free of dust and loose components, furthermore the substrate may not show excessive suction; - Quantitative requirements to the roughness, suction and bond strength of the bearing floor are not drafted in this standard; - The texture depth of the intermediate layer has to be at least 3 mm to provide a good bond between intermediate and top layer; - To improve adhesion between screed and substrate a slurry coat has to be applied; - It is advised to limit the amount of dilatations to the minimum when applying bonded terrazzo floors because debonding is very likely to occur at the place of dilatations.
NEN 2741 + A1	<ul style="list-style-type: none"> - Local debonding of screeds with a diameter of maximal 6 times screed thickness is permissible. For debonded parts at the edge of the floor the diameter is maximal 3 times screed thickness; - To provide good adhesion between bearing floor and terrazzo the substrate needs to be free of dust and loose components, furthermore the substrate may not show excessive suction; - The minimal bonding capacity of the substrate needs to be $1,5 N/mm^2$; - To improve adhesion between screed and substrate a slurry coat has to be applied; - The average screed surface tensile strength must be at least $0,5 N/mm^2$, with a minimal value of $0,3 N/mm^2$ for the lowest strength.
NEN 2742	- No bond is present at this floor type
NEN-EN 13813	- This standard classifies mortars in bond strength classes: B0,2/ B0,5/ B1,0/ B1,5/ B2,0.
CUR 92	- A reference is made to NEN 1042.
CUR 110	<ul style="list-style-type: none"> - The requirements with respect to bonding in the CUR are equal to the NEN 2741+A1; - In addition to the requirements of the NEN 2741+A1 the CUR 110 indicates that deformations of the bearing floor have to be taken into account when looking at the adhesion between the screed and bearing floor. Deformations can cause serious shear stresses in the interface which can cause debonding; - The average surface tensile strength of self-levelling screeds has to be at least $1,0 N/mm^2$, with a minimal value of $0,6 N/mm^2$

Table 31: requirements given in the Dutch standards concerning cracking of screeds

Code	Requirement
NEN 1042	<ul style="list-style-type: none"> - To control cracking induced by shrinkage reinforcement can be applied in the intermediate layer. The maximal mesh size is 150 mm, the minimal cover has to be 10 mm; - Other requirements are equal to the requirements drafted in NEN 2741 + A1.
NEN 2741 + A1	<ul style="list-style-type: none"> - To prevent the onset of cracking dilatations can be applied in screeds. The standard advises only to apply dilatations at places where the bearing structure is dilated as well, to prevent debonding of the screed; - In order to control shrinkage after pouring a foil has to be applied on the screed to prevent evaporation; - Reinforcement can be applied if cracking as a result of shrinkage/ temperature changes is expected. It is also recommended to apply reinforcement if cracks are already present in the bearing floor.
NEN 2742	<ul style="list-style-type: none"> - To control cracking reinforcement can be applied, however reinforcement will not prevent the screed from cracking; - Other requirements are not drafted in this standard.
NEN-EN 13813	- A manufacturer of a screed material may declare the shrinkage and swelling value of the screed material in accordance with prEN 13454-2.

Appendix

CUR 92	- A reference is made to NEN 1042.
CUR 110	- Cracks with a width of 0,3mm are acceptable if no other agreements are made on beforehand.

A.3 Calculations

A.3.1 Maple file analytical approach Pull-Off testing method

```

> restart;
Input
> Ec := 30303; ft := 2.21; Gf := 0.075; wc := 5.14*Gf/ft; h := 30; b := 50; d := 50;
      Ec := 30303
      ft := 2.21
      Gf := 0.075
      wc := 0.1744343891
      h := 30
      b := 50
      d := 50
(1)

> step := 5·10-6; phi0 := 0; phi1 := 1·step; phi2 := 2·step; phi3 := 3·step; phi4 := 4·step; phi5 := 5·step; phi6 := 6
·step; phi7 := 7·step; phi8 := 8·step; phi9 := 9·step; phi10 := 10·step;
Step 1: determination of the specimen properties
> fcrack(x) := ft·exp(-x·a); Gfrac := int(fcrack(x), x=0..wc) = Gf; a := solve(Gfrac, a, maxsols=1); d1 :=  $\frac{ft}{Ec} \cdot h$ ;
      sigma(delta) := convert(piecewise(delta < d1,  $\frac{ft}{d1} \cdot delta$ , d1 ≤ delta, fcrack(delta - d1)), Heaviside);
      fcrack := x → ft e-x·a
      Gfrac :=  $-\frac{2.210000000(-1. + e^{-0.1744343891a})}{a} = 0.075$ 
      a := 29.28861509
      d1 := 0.002187902188
      sigma := delta → convert(piecewise(delta < d1,  $\frac{ft \delta}{d1}$ , d1 ≤ delta, fcrack(delta - d1)), Heaviside)
(2)

> plot(sigma(delta), delta=-0.005..wc, y=-0.3..(ft+0.2), title="Stress-deformation relation concrete", axesfont
= ["CALIBRI", 8], titlefont= ["CALIBRI", 10, bold], labelfont= ["CALIBRI", 8], labels= ["deformation delta(mm)",
"stress sigma (MPa)"], labeldirections= ["horizontal", "vertical"], size=[300, 200]);
Stress-deformation relation concrete

Step 2: determination of the inner force – mean deformation relation
> delta(x, phi, deltamean) := phi·x + (deltamean -  $\frac{phi \cdot d}{2}$ ); F(phi, deltamean) := piecewise(deltamean <  $\frac{phi \cdot d}{2}$ , 0,
      deltamean ≥  $\frac{phi \cdot d}{2}$ , b·int(sigma(delta(x, phi, deltamean)), x=0..d));
      delta := (x, phi, deltamean) → phi x + deltamean -  $\frac{1}{2} \phi d$ 
(3)

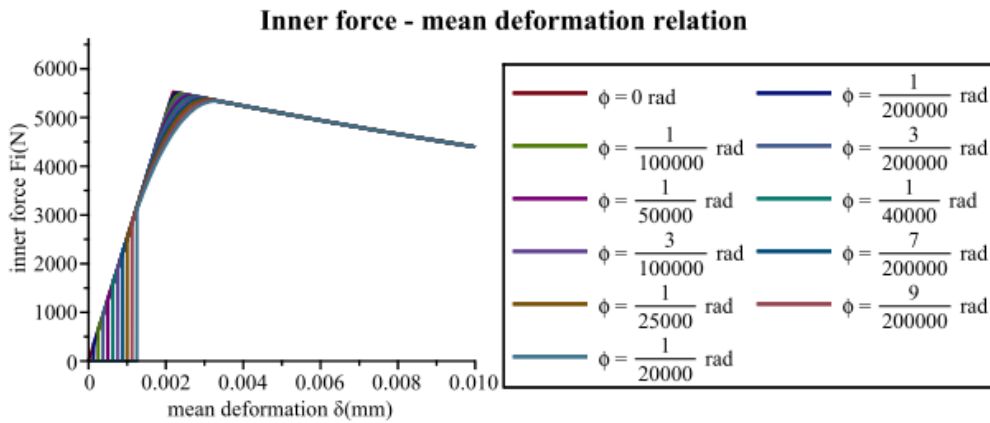
```

$$F := (\phi, \text{deltamean}) \rightarrow \text{piecewise} \left(\text{deltamean} < \frac{1}{2} \phi d, 0, \frac{1}{2} \phi d \leq \text{deltamean}, b \left(\int_0^d \sigma(\delta(x, \phi, \text{deltamean})) dx \right) \right) \quad (3)$$

```

> plot([F(phi0, deltamean), F(phi1, deltamean), F(phi2, deltamean), F(phi3, deltamean), F(phi4, deltamean), F(phi5,
deltamean), F(phi6, deltamean), F(phi7, deltamean), F(phi8, deltamean), F(phi9, deltamean), F(phi10,
deltamean)], deltamean=0..(0.01), y=0..(1.2·ft·d·b), title="Inner force - mean deformation relation", axesfont
=["CALIBRI", 8], titlefont=["CALIBRI", 10, bold], labelfont=["CALIBRI", 8], labels=[
"mean deformation δ(mm)", "innerforce Fi(N)", labeldirections=["horizontal", "vertical"], legend
=[typeset("φ = ", eval[1](phi0), " rad"), typeset("φ = ", eval[1](phi1), " rad"), typeset("φ = ", eval[1](phi2),
" rad"), typeset("φ = ", eval[1](phi3), " rad"), typeset("φ = ", eval[1](phi4), " rad"), typeset("φ = ", eval[1](phi5),
" rad"), typeset("φ = ", eval[1](phi6), " rad"), typeset("φ = ", eval[1](phi7), " rad"), typeset("φ = ", eval[1](phi8),
" rad"), typeset("φ = ", eval[1](phi9), " rad"), typeset("φ = ", eval[1](phi10), " rad")], legendstyle=[location
=right, font=["CALIBRI", 8], size=[600, 200]]];

```



Step 3: determination of the eccentricity - mean deformation relation

```

> c(phi, deltamean) := int(x·sigma(delta(x, phi, deltamean)), x=0..d) / int(sigma(delta(x, phi, deltamean)), x=0..d); e(phi, deltamean) := d/2 - c(phi, deltamean);
M(phi, deltamean) := e(phi, deltamean)·F(phi, deltamean);

```

$$c := (\phi, \text{deltamean}) \rightarrow \frac{\int_0^d x \sigma(\delta(x, \phi, \text{deltamean})) dx}{\int_0^d \sigma(\delta(x, \phi, \text{deltamean})) dx}$$

$$e := (\phi, \text{deltamean}) \rightarrow \frac{1}{2} d - c(\phi, \text{deltamean})$$

$$M := (\phi, \text{deltamean}) \rightarrow e(\phi, \text{deltamean}) F(\phi, \text{deltamean}) \quad (4)$$

```

> ecc(phi, deltamean) := convert(piecewise(deltamean < phi·d/2, 0, deltamean ≤ 0.01, e(phi, deltamean), deltamean
> 0.01, 0), Heaviside);

```

$$\text{ecc} := (\phi, \text{deltamean}) \rightarrow \text{convert} \left(\text{piecewise} \left(\text{deltamean} < \frac{1}{2} \phi d, 0, \text{deltamean} \leq 0.01, e(\phi, \text{deltamean}), 0.01 < \text{deltamean}, 0 \right), \text{Heaviside} \right) \quad (5)$$

```

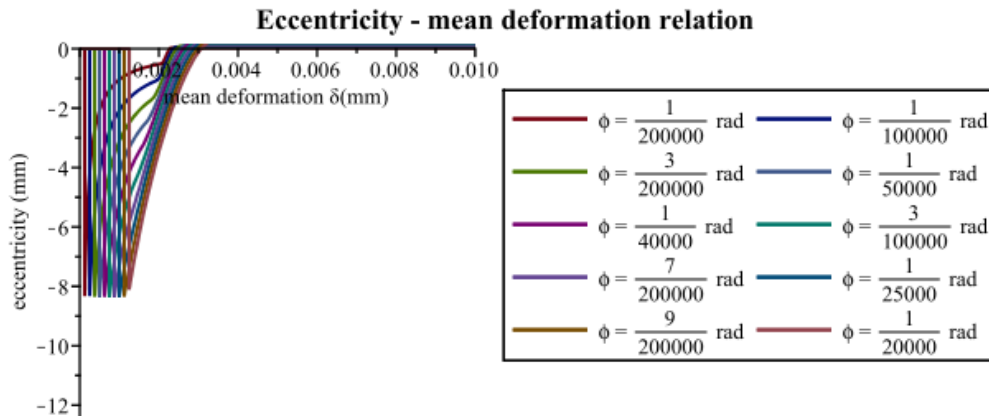
> plot([ecc(phi1, deltamean), ecc(phi2, deltamean), ecc(phi3, deltamean), ecc(phi4, deltamean), ecc(phi5, deltamean),
ecc(phi6, deltamean), ecc(phi7, deltamean), ecc(phi8, deltamean), ecc(phi9, deltamean), ecc(phi10, deltamean)],

```

```

deltamean=0..(0.01), y=- $\frac{d}{4}$ ..0, title="Eccentricity - mean deformation relation", axesfont=["CALIBRI", 8],
titlefont=["CALIBRI", 10, bold], labelfont=["CALIBRI", 8], labels=["mean deformation  $\delta$ (mm)", "eccentricity (mm)"],
labeldirections=["horizontal", "vertical"], legend=[typeset("phi = ", eval[1](phi1), " rad"), typeset("phi = ",
eval[1](phi2), " rad"), typeset("phi = ", eval[1](phi3), " rad"), typeset("phi = ", eval[1](phi4), " rad"), typeset("phi = ",
eval[1](phi5), " rad"), typeset("phi = ", eval[1](phi6), " rad"), typeset("phi = ", eval[1](phi7), " rad"), typeset("phi = ",
eval[1](phi8), " rad"), typeset("phi = ", eval[1](phi9), " rad"), typeset("phi = ", eval[1](phi10), " rad")], legendstyle
=[location=right, font=["CALIBRI", 8], size=[600, 200]];

```



Step 4: Determination of the maximal force per eccentricity

```

> s(phi, ec) := fsolve(ecc(phi, deltamean) = ec, deltamean =  $\frac{\phi \cdot d}{2}$  ..1.8·d1);

```

$$s := (\phi, ec) \rightarrow \text{fsolve}\left(\text{ecc}(\phi, \text{deltamean}) = ec, \text{deltamean} = \frac{1}{2} \phi d \cdot 1.8 d1\right) \quad (6)$$

```

> Fmax(phi) := maximize(F(phi, deltamean), location);

```

$$Fmax := \phi \rightarrow \text{maximize}(F(\phi, \text{deltamean}), \text{location}) \quad (7)$$

```

> locmax0 := Fmax(phi0) : assign(locmax0[2][1][1]); F0 := locmax0[1]; u0 := deltamean; e0 := 0; M0 := 0;
deltamean := 'deltamean';

```

$$F0 := 5525.$$

$$u0 := 0.002187902188$$

$$e0 := 0$$

$$M0 := 0$$

(8)

```

> data(phi) := Vector([s(phi, -4), s(phi, -3.5), s(phi, -3), s(phi, -2.5), s(phi, -2), s(phi, -1.5), s(phi, -1), s(phi, -0.5), s(phi, 0),
F(phi, s(phi, -4)), F(phi, s(phi, -3.5)), F(phi, s(phi, -3)), F(phi, s(phi, -2.5)), F(phi, s(phi, -2)), F(phi, s(phi, -1.5)),
F(phi, s(phi, -1)), F(phi, s(phi, -0.5)), F(phi, s(phi, 0))]);

```

Output

```

> Ec; ft; convert(Gf, float); h; b; d; phi := evalf(phi0); u0; F0; phi := evalf(phi1); data(phi)[1]; data(phi)[2]; data(phi)[3];
data(phi)[4]; data(phi)[5]; data(phi)[6]; data(phi)[7]; data(phi)[8]; data(phi)[9]; data(phi)[10]; data(phi)[11];
data(phi)[12]; data(phi)[13]; data(phi)[14]; data(phi)[15]; data(phi)[16]; data(phi)[17]; data(phi)[18]; phi :=
evalf(phi2); data(phi)[1]; data(phi)[2]; data(phi)[3]; data(phi)[4]; data(phi)[5]; data(phi)[6]; data(phi)[7];
data(phi)[8]; data(phi)[9]; data(phi)[10]; data(phi)[11]; data(phi)[12]; data(phi)[13]; data(phi)[14];
data(phi)[15]; data(phi)[16]; data(phi)[17]; data(phi)[18]; phi := evalf(phi3); data(phi)[1]; data(phi)[2];
data(phi)[3]; data(phi)[4]; data(phi)[5]; data(phi)[6]; data(phi)[7]; data(phi)[8]; data(phi)[9]; data(phi)[10];
data(phi)[11]; data(phi)[12]; data(phi)[13]; data(phi)[14]; data(phi)[15]; data(phi)[16]; data(phi)[17];
data(phi)[18]; phi := evalf(phi4); data(phi)[1]; data(phi)[2]; data(phi)[3]; data(phi)[4]; data(phi)[5];
data(phi)[6]; data(phi)[7]; data(phi)[8]; data(phi)[9]; data(phi)[10]; data(phi)[11]; data(phi)[12]; data(phi)[13];
data(phi)[14]; data(phi)[15]; data(phi)[16]; data(phi)[17]; data(phi)[18]; phi := evalf(phi5); data(phi)[1];
data(phi)[2]; data(phi)[3]; data(phi)[4]; data(phi)[5]; data(phi)[6]; data(phi)[7]; data(phi)[8]; data(phi)[9];
data(phi)[10]; data(phi)[11]; data(phi)[12]; data(phi)[13]; data(phi)[14]; data(phi)[15]; data(phi)[16];
data(phi)[17]; data(phi)[18]; phi := evalf(phi6); data(phi)[1]; data(phi)[2]; data(phi)[3]; data(phi)[4];
data(phi)[5]; data(phi)[6]; data(phi)[7]; data(phi)[8]; data(phi)[9]; data(phi)[10]; data(phi)[11]; data(phi)[12];

```

```

data(phi)[13]; data(phi)[14]; data(phi)[15]; data(phi)[16]; data(phi)[17]; data(phi)[18]; phi := evalf(phi7);
data(phi)[1]; data(phi)[2]; data(phi)[3]; data(phi)[4]; data(phi)[5]; data(phi)[6]; data(phi)[7]; data(phi)[8];
data(phi)[9]; data(phi)[10]; data(phi)[11]; data(phi)[12]; data(phi)[13]; data(phi)[14]; data(phi)[15];
data(phi)[16]; data(phi)[17]; data(phi)[18]; phi := evalf(phi8); data(phi)[1]; data(phi)[2]; data(phi)[3];
data(phi)[4]; data(phi)[5]; data(phi)[6]; data(phi)[7]; data(phi)[8]; data(phi)[9]; data(phi)[10]; data(phi)[11];
data(phi)[12]; data(phi)[13]; data(phi)[14]; data(phi)[15]; data(phi)[16]; data(phi)[17]; data(phi)[18]; phi :=
evalf(phi9); data(phi)[1]; data(phi)[2]; data(phi)[3]; data(phi)[4]; data(phi)[5]; data(phi)[6]; data(phi)[7];
data(phi)[8]; data(phi)[9]; data(phi)[10]; data(phi)[11]; data(phi)[12]; data(phi)[13]; data(phi)[14];
data(phi)[15]; data(phi)[16]; data(phi)[17]; data(phi)[18]; phi := evalf(phi10); data(phi)[1]; data(phi)[2];
data(phi)[3]; data(phi)[4]; data(phi)[5]; data(phi)[6]; data(phi)[7]; data(phi)[8]; data(phi)[9]; data(phi)[10];
data(phi)[11]; data(phi)[12]; data(phi)[13]; data(phi)[14]; data(phi)[15]; data(phi)[16]; data(phi)[17];
data(phi)[18];

```

30303

2.21

0.075

30

50

50

0.002187902188

5525.

$\phi := 0.000005000000000$

0.0002604166667

0.0002976190477

0.0003472222223

0.0004166666668

0.0005208333335

0.0006944444447

0.001041666667

0.002074254980

0.002276213372

657.6171875

751.5625000

876.8229170

1052.187500

1315.234376

1753.645834

2630.468751

5237.319740

5503.506175

$\phi := 0.000010000000000$

0.0005208333332

0.0005952380951

0.0006944444443

0.0008333333332

0.001041666666

0.001388888889

0.001998182455

0.002175448527

0.002363416987

1315.234375

1503.125000

```
1753.645833
2104.375000
2630.468748
3507.291668
5036.146560
5341.945860
5481.811620
 $\phi := 0.00001500000000$ 
0.000781250000
0.0008928571429
0.001041666667
0.001250000000
0.001562500000
0.001935596338
0.002099292781
0.002249511363
0.002451445275
1972.851562
2254.687500
2630.468751
3156.562500
3945.703125
4860.899426
5154.335585
5339.179580
5460.372825
 $\phi := 0.00002000000000$ 
0.001041666667
0.001190476191
0.001388888889
0.001666666667
0.001883133952
0.002031968559
0.002173243284
0.002326222916
0.002539407514
2630.468751
3006.250001
3507.291667
4208.750000
4704.180460
4972.210806
5171.594935
5327.071150
5438.978370
 $\phi := 0.00002500000000$ 
0.001302083333
0.001488095238
```

0.001689754046
0.001839055355
0.001974071224
0.002107213971
0.002246857635
0.002405394924
0.002627546189
3288.085937
3757.812500
4249.757216
4562.120831
4803.356784
5002.898625
5171.279275
5311.692740
5417.685955

$\phi := 0.00003000000000$

0.001543057766
0.001676764348
0.001801995144
0.001924987564
0.002049758039
0.002180241087
0.002322008631
0.002486388377
0.002715776720
3886.702970
4183.152631
4431.777642
4648.631126
4840.954324
5012.282900
5163.903075
5294.701870
5396.475145

$\phi := 0.00003500000000$

0.001660500989
0.001771015704
0.001883757411
0.002000318074
0.002122699060
0.002253838798
0.002398825696
0.002568774072
0.002804108322
4100.437607
4311.177828
4506.856122

4688.663538
4857.126303
5012.157445
5152.872975
5276.801415
5375.347905
 $\phi := 0.00004000000000$
0.001745404866
0.001849423135
0.001958272923
0.002073099541
0.002195624394
0.002328629160
0.002477145687
0.002652251657
0.002892543379
4198.860284
4376.397448
4546.633738
4708.987092
4862.719201
5006.809470
5139.673195
5258.341640
5354.304570
 $\phi := 0.00004500000000$
0.001821151688
0.001922940634
0.002030724493
0.002145621875
0.002269347853
0.002404704162
0.002556768145
0.002736604379
0.002981077208
4255.702174
4414.453464
4569.086513
4718.673038
4862.157352
4998.232926
5125.067590
5239.518080
5333.343790
 $\phi := 0.00005000000000$
0.001893663132
0.001994942835
0.002102900904



0.002218703448
0.002344118286
0.002482009245
0.002637518697
0.002821681310
0.003069716560
4291.330442
4437.628356
4581.455867
4721.836906
4857.648560
4987.505995
5109.500670
5220.454265
5312.466940

(9)